REPORT DOCUMENTATION PAGE

Form Approved
OMB No. 0704-0188

1. AGENCY USE ONLY *(Leave blank)*	2. REPORT DATE	3. REPORT TYPE AND DATES COVERED
	3/31/2000	Final Technical Report, 1/27/97-3/31/00

4. TITLE AND SUBTITLE

Dispersed Liquid Agent Fire Suppression Screen 3A/1/789

5. FUNDING NUMBERS

6. AUTHOR(S)

Jiann C. Yang, Michelle K. Donnelly, Nikki Prive, and William L. Grosshandler

7. PERFORMING ORGANIZATION NAME(S) AND ADDRESS(ES)

National Institute of Standards and Technology
Building and Fire Research Laboratory
100 Bureau Drive, Gaithersburg, MD 20899

8. PERFORMING ORGANIZATION REPORT NUMBER

NISTIR 6319

9. SPONSORING/MONITORING AGENCY NAME(S) AND ADDRESS(ES)

The Strategic Environmental Research & Development Program (SERDP)

10. SPONSORING/MONITORING AGENCY REPORT NUMBER

11. SUPPLEMENTARY NOTES

12a. DISTRIBUTION/AVAILABILITY STATEMENT

Unlimited

DISTRIBUTION STATEMENT A
Approved for Public Release
Distribution Unlimited

20031121 112

13. ABSTRACT *(Maximum 200 words)*

The design, construction, demonstration, and operation of a bench-scale device capable of screening the fire suppression efficiency of liquid agents are described in detail in this report. The apparatus is based on a well-characterized flame, a means to facilitate the introduction of liquid agents, and a way to generate liquid droplets. The performance of the apparatus has been characterized using fluids with different thermophysical properties and fire suppression effectiveness. The apparatus is robust and easy to operate. A step-by-step test procedure is provided to facilitate the use of the apparatus. The droplet delivery system is designed to handle small quantity of liquid sample. The apparatus can also be used to screen gaseous agents. When a powder delivery system is integrated into the current apparatus, the facility, in principle, can be employed to screen powder agents.

14. SUBJECT TERMS	15. NUMBER OF PAGES
Apparatus, droplets, fire suppression, halon replacement, sprays, testing	93
	16. PRICE CODE

17. SECURITY CLASSIFICATION OF THIS REPORT	18. SECURITY CLASSIFICATION OF THIS PAGE	19. SECURITY CLASSIFICATION OF ABSTRACT	20. LIMITATION OF ABSTRACT
Unclassified	Unclassified	Unclassified	Unlimited

DISPERSED LIQUID AGENT FIRE SUPPRESSION SCREEN

FINAL TECHNICAL REPORT

March 31, 2000

Jiann C. Yang, Michelle K. Donnelly, Nikki Privé, William L. Grosshandler

Building and Fire Research Laboratory

National Institute of Standards and Technology

Building 224, Room B356, Mail Stop 8651, Gaithersburg, MD 20899

Sponsored by:

The Department of Defense

Strategic Environmental Research and Development Program

TABLE OF CONTENTS

SUMMARY

Task Objective

The objective is to develop a bench-scale suppression screen (or multiple screens) for comparing the flame extinction performance of dispersed gases and liquids.

Technical Problems

Halon 1301 (CF_3Br) has properties that make it particularly effective as a fire extinguishing agent. In addition to the chemical activity attributable to the bromine atom, halon 1301 is a gas at room temperature and pressure. It is stored as a liquid under high pressure making it superheated at atmospheric conditions. When discharged, halon 1301 flashes to a gas and quickly disperses throughout the volume being protected. Replacements are sought which perform equally well in applications critical to the Department of Defense. This project will contribute to the overall goal of attaining effective, environmentally responsible alternatives to the ozone depleting substance, halon 1301.

Water is particularly attractive as an alternative to halon because it is environmentally benign, and if introduced in some fires under idealized conditions can extinguish the flames at mass loadings not much greater than those required of CF_3Br. However, droplets greater than a few micrometers in diameter do not flow as the surrounding gas, and they require a much longer time to evaporate at room temperature than superheated halon 1301.

Water mist systems currently under development produce different droplet size distributions. Additives have been suggested to increase the effectiveness of water as an extinguishing agent. Non-aqueous fluids with excellent flame inhibition qualities will be proposed in other tasks of the DoD Next Generation Fire Suppression System Technology Program.

How can the performance of these many agents be compared to one another in a small-scale laboratory setting? The equivalent standardized screen for gaseous agents, the cup burner apparatus, was not developed for condensed phase suppressants. This is the problem we propose to remedy. Basic research is needed to design an apparatus that is flexible enough to handle the variety of liquid agents coming down the pike and that has the precision necessary for discriminating the performance among the different agents.

General Methodology

The methodology is to adapt a porous cylindrical burner, using propane as a fuel for the diffusion flame. Design a laminar flow tunnel for the suppressant transport to the flame; investigate aerosol generation techniques and design one capable of generating 25-250 μm droplets. Calibrate the performance of the burner with gaseous agents. Select test fluids (*e.g.*, water; water with an additive; a low viscosity fluorocarbon; a high viscosity compound with low volatility) to span a variety of anticipated operating conditions; generate a database using these fluids. Prepare fabrication drawings and an operations manual and distribute them to participating laboratories.

Technical Results

The design, construction, demonstration, and operation of a bench-scale device capable of screening the fire suppression efficiency of liquid agents are described in detail in this report. Two techniques of generating droplets have been examined: (1) a piezoelectric droplet generator and (2) a small glass nebulizer. The piezoelectric droplet generator was found incapable of handling fluids with high loading of dissolved solid due to frequent clogging of the orifice opening. The nebulizer is used in the current liquid screen apparatus. The performance of the screen apparatus has been demonstrated using both inert gases and aqueous solutions. A test protocol has been established.

Important Findings and Conclusions

The performances of the burner and the flow facility have also been extensively characterized by examining various operational parameters. Day-to day and burner variations also did not affect critical blow-off limits. The facility is not difficult to operate.

For generation of liquid droplets, a commercially available ICP (Inductively Coupled Plasma) nebulizer, in lieu of a piezoelectric droplet generator, is better suited for screening liquid agents with high loading of dissolved salt. Clogging of orifice opening in the piezoelectric droplet generator becomes unavoidable when fluids with dissolved salts are used due to salt-out effects at the small orifice opening. The application of an ICP nebulizer alleviates the clogging problems because the opening of the capillary is larger; however, the spray generated is

polydispersed. The performance of the nebulizer does not change significantly when fluids with different thermophyscial properties are used within the range of conditions encountered in the screening procedure. The nebulizer coupled with a small syringe pump can be used to perform screening tests with small quantities (~ 10 ml or less) of liquid agents.

The relative suppression ranking of the three inert gases (argon, helium, and nitrogen) from the screen apparatus is similar to those from cup-burner tests; argon requires the most amount added to the oxidizer stream to cause blow-off, whereas helium requires the least.

The performance of the screening apparatus has been demonstrated using several aqueous solutions with different thermophysical properties. For all the fluids tested, potassium acetate or lactate with a mass fraction of 0.6 is the most effective. In particular, for a given application rate, the potassium acetate or lactate solution is more effective in suppressing the flame than pure water. Blow-off velocity decreases as the fluid application rate increases, that is, when the application rate is high, only low speed air is needed to blow-off the flame. High loading (60 % mass fraction) of potassium acetate or lactate performs better than low loading (30 %).

Significant Hardware Developments

A screen apparatus for liquid agents delivered in droplet form has been developed. The apparatus can also be used for gaseous agent screen and can, in principle, be extended to screen powder agents. One of the attributes of the apparatus is the ability to utilize small amount of liquid sample to perform a test.

Special Comments

None.

Implications for Future Research

The liquid agent screen apparatus is a useful tool for other principal investigators to facilitate their search for new fire suppressants because it can provide rapid screens with minimum effort. It is currently being used to evaluate high-boiling point compounds and other liquid agents. The apparatus may also be suitable for evaluating powder agents when a powder delivery system is integrated into the current system.

BIBLIOGRAPHY OF PAPERS AND ARTICLES PUBLISHED

- Yang, J.C., Donnelly, M.K., Prive, N., and Grosshandler, W.L., "An Apparatus for Evaluating Liquid Fire Suppressants," *Proceedings of Halon Options Technical Working Conference*, 12-14 May 1998, Albuquerque, New Mexico.

- Yang, J.C., Donnelly, M.K., Prive, N., and Grosshandler, W.L., "A Dispersed Liquid Agent Fire Suppression Screening Method," *Annual Conference on Fire Research*, November 2-5, 1998, Gaithersburg, Maryland.

- Yang, J.C., Prive, N., Donnelly, M.K., and Grosshandler, W.L., "Spade-Shaped Flame," Photographic Poster presented at the Gallery of Fluid Motion, 51st Annual Meeting of the Division of Fluid Dynamics, The American Physical Society, 22-24 November 1998, Philadelphia, Pennsylvania.

- Yang, J.C., Donnelly, M.K., Prive, N.C., and Grosshandler, W.L., "Fire Suppression Efficiency Screening using a Counterflow Cylindrical Burner," *Proceedings of the 5th ASME/JSME Joint Thermal Engineering Conference*, March 15-19, 1999, San Diego, California.

- Yang, J.C., Prive,N.C., Donnelly, M.K., Grosshandler, W.L., "Recent Results from the Dispersed Liquid Agent Fire Suppression Screen," Proceedings of the Halon Options Technical Working Conference, April 27-29, 1999, Albuquerque, New Mexico.

- Yang, J.C., Donnelly, M.K., Prive, N.C., and Grosshandler, W.L., "On the Design of an Apparatus for Screening Liquid Fire Suppressants," Proceedings of the 8th International Fire Science and Engineering Conference, Vol. 2, pp. 1343-1348, June 29-July 1, 1999, Edinburgh, Scotland.

- Yang, J.C., Donnelly, M.K., Prive, N.C., and Grosshandler, W.L., "Dispersed Liquid Agent Fire Suppression Screen Apparatus," NISTIR 6319, July 1999, U.S. Department of Commerce, Washington, DC.

- Yang, J.C., Donnelly, M.K., Prive, N.C., and Grosshandler, W.L., "An Apparatus for Screening Fire Suppression Efficiency of Dispersed Liquid Agents," submitted to *Fire Safety Journal*.

DETAILED DESCRIPTION OF THE PROJECT

Introduction

The recent ban on halon 1301 (CF_3Br) production (as a result of its ozone depleting potential) has resulted in extensive search for its replacements and alternatives. The applications of fire suppression efficiency screening methods constitute an important aspect of this search process because good screening methods can facilitate the identification, comparison, and selection of potential candidates for halon replacement. Most of the current methods for fire suppression efficiency screening (*e.g.*, cup burners) are designed for evaluating fire suppressants that can be delivered in the form of vapor. Potential uses of liquid agents as replacements have been recently proposed in several applications (*e.g.*, shipboard machinery spaces, engine compartments in armored vehicles). Therefore, there is a need for the development of a reliable screening method for liquid agents that can be delivered in droplet form. The objective of this work is to design, construct, and demonstrate a laboratory-scale apparatus that can perform the screening of liquid agents in a well-controlled experimental setting. This report describes the design and the operational procedure of the NIST dispersed liquid fire suppression screening apparatus. Detailed component drawings are documented in the Appendices. The design of the apparatus is based on a well-characterized flame, a means to facilitate the introduction of small amounts of liquid agents, and a way to generate liquid droplets that can be entrained into the flame. The device can also be used to screen gaseous fire suppressants. In principle, the apparatus can be employed to screen powders by incorporating a powder delivery system in lieu of a liquid droplet generator.

In the literature, three experimental configurations have been used for agent screening applications: (1) counterflow cylindrical burners, (2) counterflow flat-flame burners, and (3) cup burners.

A porous cylindrical burner in a counterflow configuration, wherein a diffusion flame is formed in the forward stagnation region of the burner placed in a uniform oxidizer flow, with fuel being ejected uniformly from the burner surface, has been extensively used to study flame structure [1,2,3,4] and flame extinction using inert gases [5], halons [6], and powders [6]. There are many advantages associated with the use of a counterflow cylindrical burner. The fuel and the oxidizer flows can be independently adjusted, if required. The flame is laminar, two-dimensional, and very stable in the forward stagnation region. The geometry of the burner and the flow field allow for relatively simple analysis of the forward stagnation region [7,8,9,10,11,12,13]. Both wake and enveloped flames can be easily maintained over a wide range of fuel and oxidizer flows. The flame is easily observed, and critical stages such as the blow-off limit (abrupt transition from an enveloped flame to a wake flame) can be ascertained with ease and high reproducibility. The flame front can be easily accessed by intrusive [2,3] or non-intrusive [8,13] probing techniques, thus enabling detailed studies of flame structure, if desired. However, clogging of the porous burner surface due to soot deposition and/or condensed-phase suppressant may be a disadvantage if the burner is operated for a long period of time; cleaning or replacing the clogged burner may be required [6].

Another counterflow geometry, which involves the use of two opposed vertical ducts separating at a distance with fuel and oxidizer counterflowing toward each another to establish a flat flame, has recently been used for extinction studies with solid aerosols [14,15] and two-phase droplet spray flames [16, and references therein]. Although counterflow flat-flame burners possess all the operational merits of a counterflow cylindrical burner mentioned above, the operation of these burners is elaborate.

Cup burners, which are widely used for screening gaseous agents, have also been employed recently to study the suppression efficiencies of condensed-phase agents [17,18]; however, the presence of the cup makes the introduction and characterization of liquid agents difficult. In addition, the global strain rate of a pool flame established at the cup is not well defined.

Table 1 lists a comparison of the various operational characteristics among the three screening apparatus: the cup burner, the counterflow flat flame burner, and the counterflow cylindrical burner. Since the operation of a counterflow cylindrical burner is less complicated than that of a counterflow flat-flame burner and the experimental configuration facilitates the introduction of condensed-phase agents into the oxidizer stream, we make use of such a burner in our liquid agent screening apparatus.

Experimental Design

There are three major elements in the apparatus: (1) the wind tunnel, (2) the porous cylindrical burner, and (3) the droplet generator. The wind tunnel is used to provide uniform oxidizer flow to the porous cylindrical burner at low turbulence intensity and to facilitate the delivery of liquid agent droplets to the flame for testing.

Wind Tunnel

The wind tunnel is open-circuit and is oriented vertically upwards. A schematic and a photograph of the tunnel are shown in Figures 1 and 2 respectively. There are five major components in the wind tunnel: (1) a blower, (2) a diffuser, (3) flow straightener, (4) a contraction section, and (5) a test section. The total length of the tunnel from the entrance of the diffuser to the exit of the test section is approximately 1.2 m. The tunnel, except the test section, is made of clear polycarbonate or polymethyl methacrylate for visual observation of droplet transport toward the burner. This section describes the design of each component and the operation of the wind tunnel in detail. Precise drawings of all component parts of the wind tunnel and a list of vendors for the components used can be found in the Appendices.

Blower

The air flow in the tunnel is provided by a variable-speed (frequency controlled) blower, whose outlet is connected to the main part of the wind tunnel via an expandable, flexible 10 cm aluminum ductwork and a coupling to convert a circular cross section to a square (see **Appendix I**). The blower is driven by a 1.5 kW frame motor which is controlled by an inverter drive.

Since the blower has a capacity greater than is needed, a slide gate damper is installed at the blower inlet to reduce the air intake. The damper plate dimensions are provided in **Appendix II**.

Table 1. Comparison of the operational characteristics of the three screening apparatus

	Co-flow cup burner	Counterflow flat-flame burner	Counterflow cylindrical burner
Gaseous agent screening applications	x	x	x
Introduction of condense-phase agent to flame for evaluation	xxx	xx	x
Characterization of condensed-phase agent in flame	xxx	xx	xx
Attainment of stable and repeatable flame	xxx	x	x
Adjustment of strain rate and composition	xxx	x	x
Accessibility for flame diagnostics	x	x	x
Observation of flame extinction	x	x	x
Flame structure analysis	xxx	xx	xx
Amenability to modeling (with chemical reactions)	xxx	x	x
Attainment of adiabaticity	xxx	xx	xx
Facility design	x	xxx	xx
Interpretation of results	x	xx	xx
Elimination of burner clogging	xx	x	xxx
Facility operation	x	xx	x
Simulation of flame behind bluff body	impossible	impossible	x

Degree of difficulty: x – simple; xx – difficult; xxx – very difficult

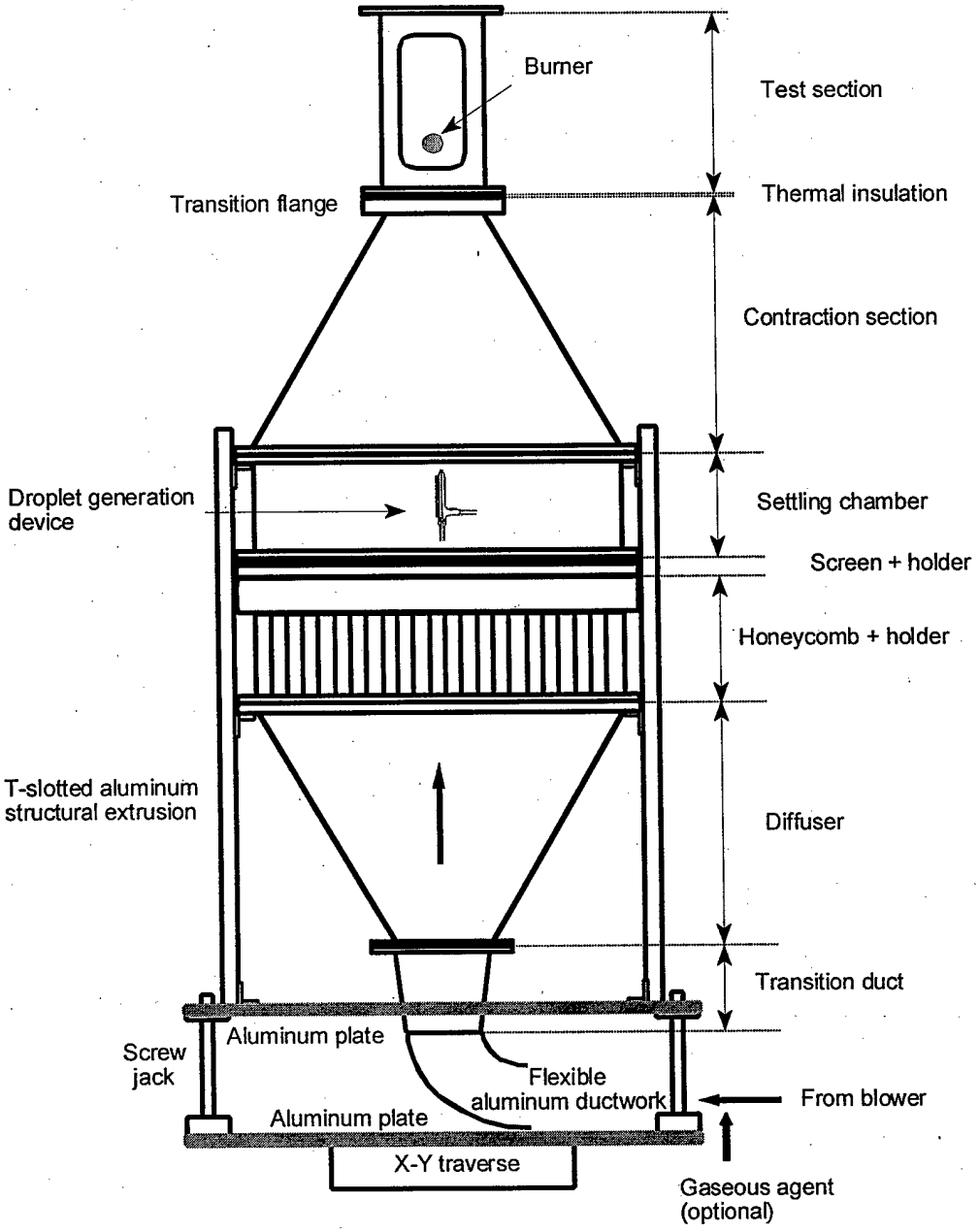

Figure 1. Schematic of the wind tunnel.

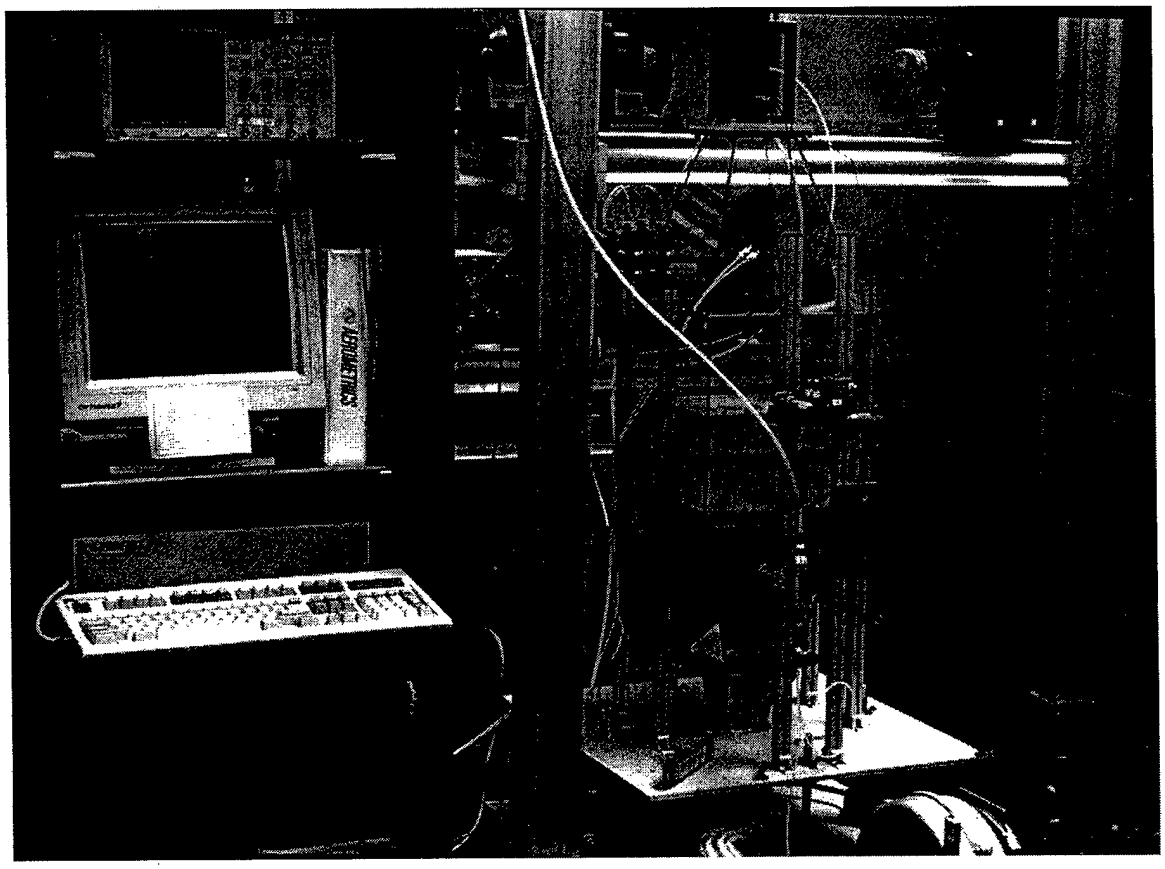

Figure 2. Photograph of the wind tunnel.

Diffuser

The 30 cm long diffuser has an inlet cross sectional area of 10 cm x 10 cm and an expansion ratio (based on areas) of 1:9. Detailed drawings of the diffuser can be found in **Appendix III**.

Flow Straightener

The flow straightener section, which serves to insure that the flow to the test section is laminar and uniform over the entire cross-section, consists of a honeycomb and a screen. The honeycomb is made of polycarbonate with cell diameter of 3.2 mm. Detailed drawings of the honeycomb housing are given in **Appendix IV**. A 50-mesh center-to-center stainless steel screen with 30 % open area and with wire diameter of 0.23 mm is used. The screen is tautly sandwiched between two square flanges (see **Appendix V**).

Settling Chamber

A constant cross-section settling chamber is placed between the screen and the inlet of the contraction section. **Appendix VI** lists detailed schematics of the chamber.

Contraction Section

The contraction section with a contraction ratio (based on areas) of 9:1 has an inlet cross sectional area of 30 cm x 30 cm and is 30 cm long. A square flange, which was machined to have a smooth transition passage to minimize flow separation, is placed between the outlet of the contraction section and the inlet of the test section. Drawings of contraction section and the transition flange are provided in **Appendices VII and VIII** respectively.

Test Section

The test section has a cross sectional area of 10 cm x 10 cm and a length of 20 cm. It is made of black-anodized aluminum with three Pyrex®[1] observation windows (12 cm x 7 cm x 0.64 cm) mounted flush against the three walls of the test section using high-temperature silicone. A hole is machined in one of the windows to allow mounting of an aluminum insert which is used to hold a brass cylindrical extension (see **Porous Cylindrical Burner**). The burner is inserted through the fourth wall. The combustion products from the burner are vented to an exhaust hood. **Appendix IX** contains detailed drawings of the test section. A thermal insulation gasket is placed between the inlet of the test section and the outlet of the contraction section.

Mounting of the Wind Tunnel

The wind tunnel is mounted on an aluminum base plate with four T-slotted aluminum structural extrusion beams fastened by corner brackets. The aluminum plate is placed on four worm-gear screw jacks coupled together via flexible shafts. The jacks are mounted on a second

[1] Certain commercial products are identified in this report in order to specify adequately the equipment used. Such identification does not imply recommendation by the National Institute of Standards and Technology, nor does it imply that this equipment is the best available for the purpose.

aluminum plate and are driven by a stepping motor and a computer controlled microstepping indexer drive to raise and lower the tunnel (a BASIC program is provided in **Appendix X**). The horizontal X-Y movement of the wind tunnel is provided by mounting the whole wind tunnel assembly on a milling machine index table. Alternatively, the wind tunnel can be mounted on other X-Y-Z traverse mechanisms. The X-Y-Z traverse mechanism is used to position the burner with respect to the stationary optical set-up for droplet characterization at various locations near the burner.

Porous Cylindrical Burner

The design of the burner is based on several important criteria. The burner has to be robust, easily built, installed, and operated, and able to generate reliable screen test data.

The burner is a replaceable porous (20 μm pores) sintered stainless steel standard ½" UNF threaded cup filter with a length L of 3.18 cm, an inner diameter of 1.12 cm, and an outer diameter D of 1.58 cm. The advantage of this burner design over those used in the past is that burner replacement can be easily performed if partial or complete clogging of the porous burner surface occurs due to the deposition of soot particles or residue from liquid agents containing dissolved solids. The burner is screwed onto an extended water-cooled insert through which fuel is injected. The water is used to cool the burner (to prevent damage to the porous surface structure) and the fuel (to prevent fuel pyrolysis prior to its ejection through the porous surface). A cut-away view of the burner interior is shown in Figure 3.

The burner, together with the insert, does not span the entire test section of the wind tunnel. A cylindrical brass rod (same diameter as the burner) with internal water cooling is inserted from the opposite wall and is used as an extension so that the burner assembly can be treated as a single cylinder across the test section. Figure 4 is a photograph of the burner assembly. Detailed diagrams of the burner assembly can be found in **Appendix XI**.

The side and downstream 180° portions of the burner surface are coated with a thin layer of high-temperature resistant black paint in order to prevent fuel ejection into the wake region. The high pressure drop across the porous sintered surface assures a very uniform fuel flow over the burner surface.

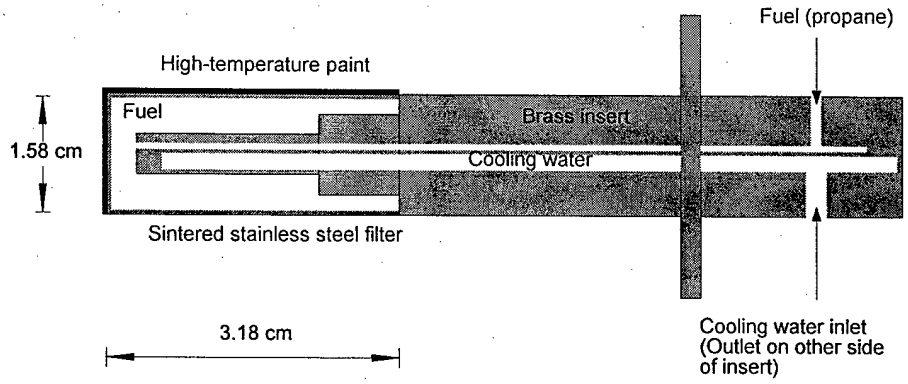

Figure 3. Cut-away view of the burner insert.

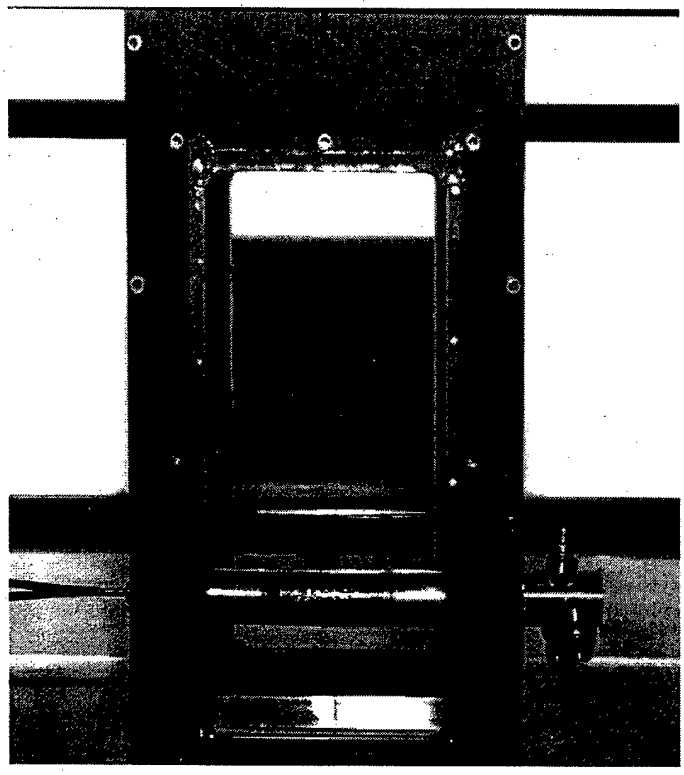

Figure 4. A photograph of the burner assembly.

Propane, which is moderately sooting, is used as fuel, and its flow is regulated by a mass-flow controller (with a range of 0 to 4 L/min), which is controlled by a personal computer using a

data acquisition board and software. A bubble flow meter was used to calibrate the mass-flow controller. The overall uncertainty of the linear calibration curve is 0.01 L/min.

Droplet Generation Device

In the course of the development of the apparatus, two droplet generation techniques have been examined: one utilizes a piezoelectric transducer and the other uses a small nebulizer.

Piezoelectric Droplet Generator

According to Rayleigh's analysis of the instability of capillary jets, the frequency f for maximum instability is given by the following equation [19]:

$$f = \frac{u_j}{4.508\, d_j} \qquad (1)$$

where u_j is the jet velocity and d_j is the jet diameter. When the jet is perturbed at this frequency, uniform sized droplets with uniform spacing are formed. Rayleigh's analysis is based on an inviscid liquid jet. Experimentally, monodispersed droplets can be generated within a range of frequencies [20]:

$$\frac{u_j}{7\, d_j} < f < \frac{u_j}{3.5\, d_j} \qquad (2)$$

Depending on the droplet generator design, an extension of the above frequency range has been reported [21].

In our experimental apparatus, a piezoelectric droplet generator is used to create uniform liquid droplets (< 100 ☞m). The design of the droplet generator is similar to that described in [22]. The operating principle of the droplet generator is based on the break-up of a jet ejecting from an orifice as a result of controlled vibration from a piezoelectric transducer driven at a fixed frequency.

The droplet generator consists of a liquid chamber which is connected to a 40 ml stainless steel reservoir, a bleed port (for eliminating any air bubbles trapped inside the chamber during priming), an orifice plate, and a piezoelectric transducer. The transducer is bonded with conductive epoxy to a circular disc stamped from a flat stainless steel (0.38 mm thick) shim stock. Detailed drawings of the droplet generator are given in **Appendix XII**.

The initial jet emanating from the orifice plate can be obtained by pressurizing the liquid reservoir with nitrogen. Jetting from the orifice can be achieved with very low nitrogen pressurization ($\approx$ 30 kPa gauge). A 0.5 μm filter is used in the liquid feedline to minimize clogging of the orifice openings due to potential foreign particulates in the liquid.

Several approaches for fabricating the orifice plate have been attempted which include using sapphire orifices, laser drilled holes, and holes from photochemical machining (commercially available printhead). In our current set-up, sapphire orifices are used because they are well fabricated to a tight tolerance, are not expensive, are readily available, and come in different size openings. Individual sapphire orifices, which are press-fitted at the end of a bored out 6-32 set-screw or inside a plastic housing, are obtained directly from vendors. The orifice can be easily attached to a plate to form an orifice plate.

The droplet generator is located in the settling chamber and is approximately 42 cm upstream of the burner. The presence of the droplet generator in the wind tunnel does not create any significant perturbation or blockage effect on the oxidizer flow field near the burner because the flame characteristics do not change with or without the presence of the droplet generator in the flow stream. Although uniform size droplets with uniform spacing are observed several centimeters ($\approx$ 10 cm) from the orifice as a result of controlled jet break-up, the droplet behavior becomes random further downstream, which may be due to the wake and drag effects on the droplets in the stream. The air stream in the wind tunnel also facilitates the dispersion of the single droplet stream into a small droplet cloud. By adjusting the location of the droplet generator with respect to the burner, droplet loss to the wind tunnel walls can be minimized because the resulting dispersed droplet cloud is confined to a very narrow region near the burner.

Although distilled and de-ionized water and a few very dilute aqueous solutions have been successfully tested with this droplet generator [23], clogging of the orifice opening constantly plagued the continuous operation of the piezoelectric droplet generator, aggravated by

liquids with high loading of dissolved salts. This approach was subsequently not considered for further development.

Nebulizer

A small glass nebulizer is currently employed in the screening apparatus to generate a fine mist of droplets. This type of nebulizer has found applications in inductively-coupled plasma (ICP) atomic emission spectroscopy and is commercially available. The nebulizer is mounted at the same location (in the settling chamber of the wind tunnel) as the piezoelectric droplet generator. A schematic of the nebulizer is shown in Figure 5.

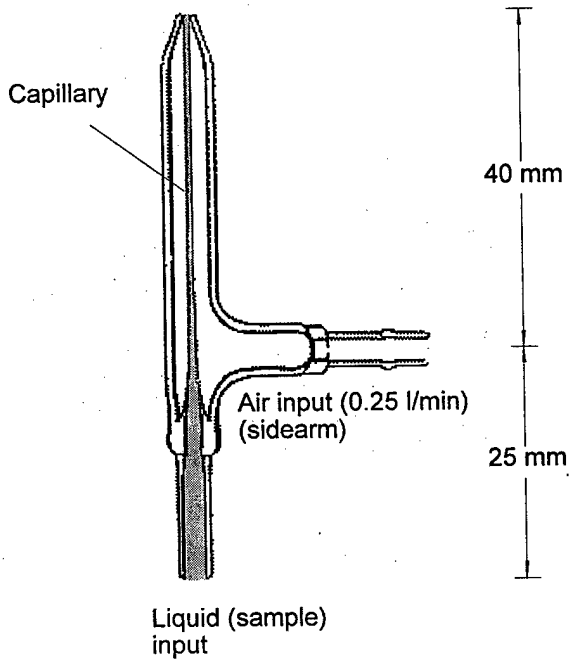

Figure 5. A schematic of the nebulizer.

The aerodynamic break-up of a liquid stream issued from the capillary by high-velocity air causes the formation of a fine mist of droplets. Because of the differences in the droplet formation mechanisms, a relatively large opening ($\approx$ 100 μm) of the capillary in the nebulizer, compared to the sapphire orifice ($\approx$ 30 μm), can be used with a wide range of liquids, including

those with a relatively high salt concentration. The large capillary opening makes the nebulizer less prone to clogging. Fluid is fed to the nebulizer by a small, programmable syringe pump. Air is supplied to the shell of the nebulizer by a mass-flow controller. The resulting mist is entrained upwards toward the flame by the air flowing in the tunnel. The atomizing air flow is set at 0.25 L/min, which is the highest flow that can be used without disturbing the flame at the burner. Because of this limit, the atomization efficiency of the nebulizer drops when the liquid delivery rate is increased beyond 1.3 ml/min; that is, larger droplets are generated that may not be entrained upward by the air flow in the tunnel.

Calibration and Characterization of the Test Facility

Characterization of the Wind Tunnel

A pitot probe equipped with a differential pressure transducer capable of measuring up to 133 Pa was used to obtain velocity data at the cross section and to calibrate the blower. Figure 6 shows the velocity measurements (error bars are expressed as $\pm 1\sigma$) across the test section at two locations (without the presence of the burner) downstream from the test section inlet with and without the damper plate at the blower intake. In the case of no damper plate, the blower was operated at the maximum setting of 60 Hz. The standard uncertainty (u) associated with the resolution of the readout of the frequency controller is 0.003 Hz [24]. In the presence of the damper plate, the blower was running at 30 Hz. Each data point represents the average of 1500 readings from the pitot probe output (sampling at 50 Hz for 30 s). The velocity profile obtained was relatively flat (< 0.5 % variation) except in the region near the walls (boundary layers). The coefficient of variation in the measurement is less than 2.5 %. The combined standard uncertainty (u_c) in the velocity measurement is 2 cm/s. Due to the limited frequency response of the pitot tube, the turbulence intensity level was not measured; however, the observation of a very stable laminar flame zone in the forward stagnation region of the burner provided a qualitative indication of low turbulence intensity.

Since the velocity profile is relatively flat in the region near the centerline of the test section, the blower was calibrated by placing the pitot probe at the centerline of the test section where the burner is located. Figure 7 is the calibration curve of the blower with the damper plate in place. Each data point represents the average of 1500 readings from the pitot probe output

(sampling at 50 Hz for 30 s). The overall uncertainty of the fit is 0.9 cm/s. The volumetric flow rates are calculated using the measured average air velocities (V_o) from the calibration curve and the cross sectional area of the test section.

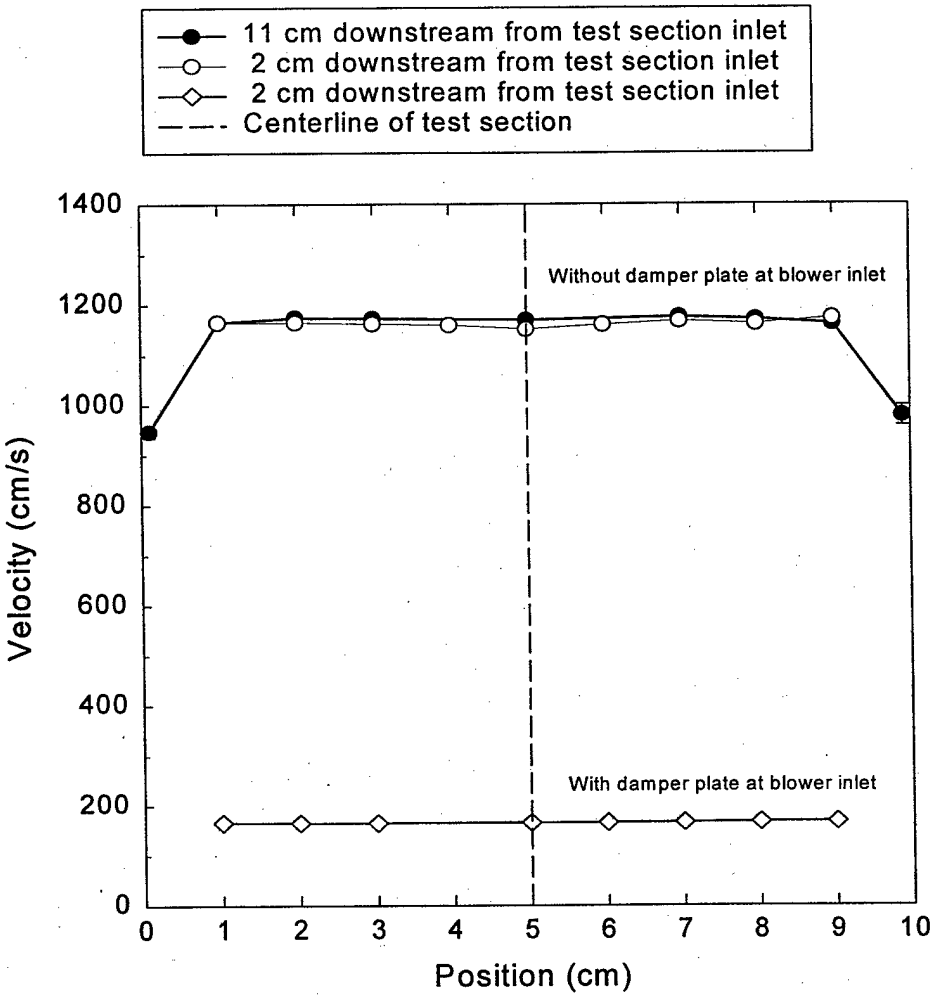

Figure 6. Velocity measurements across the test section at two locations downstream from the test section inlet with and without the damper plate at the blower inlet.

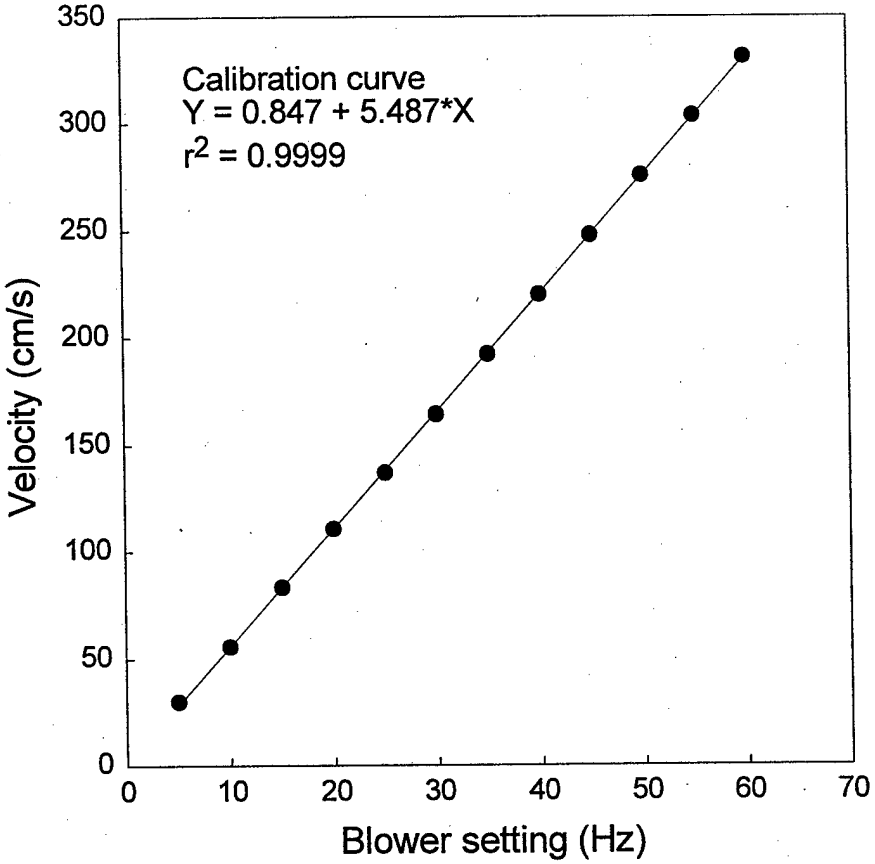

Figure 7. Calibration curve of the blower with slide-gate damper.

Characterization of the Burner

For a given burner diameter, there are only two important parameters, fuel ejection velocity (V_f) and air velocity (V_o) in the wind tunnel, that govern the performance of the burner [1,2].

Under certain flow conditions, a thin, laminar, two-dimensional blue flame is established at a distance in front of the cylinder surface. An example is given in Figure 8(a). As the fuel ejection velocity is decreased or the air velocity is increased, the flame slowly approaches the cylinder surface, and eventually the flame is abruptly blown off from the stagnation region, and a wake flame, an example of which is shown in Figure 8(b), is established. Conversely, with increasing

fuel velocity or decreasing air velocity, the flame zone gradually moves away from the cylinder surface, and eventually a laminar two-dimensional flame can no longer be sustained.

When the air velocity is very small and the fuel velocity is large, the flame zone becomes thicker, and an inner luminous yellow zone and an outer blue zone appear. When the air velocity is very large and reaches a critical value, the flame can never be stabilized, irrespective of the fuel ejection velocity.

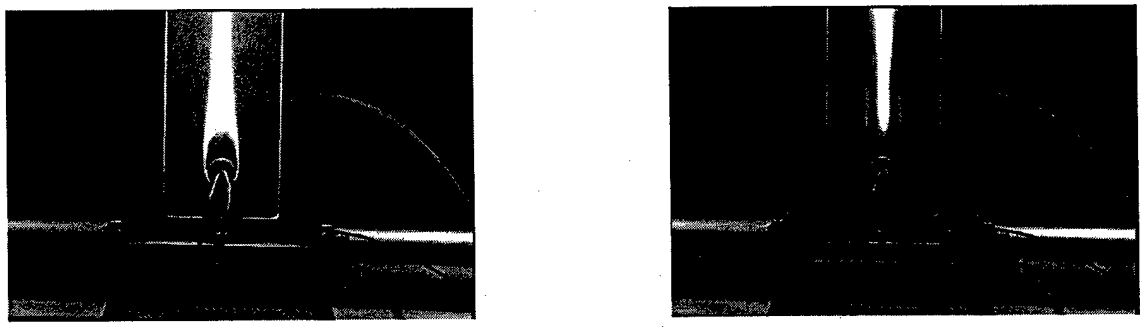

(a) (b)

Figure 8. (a) An enveloped flame and (b) a wake flame.

Figure 9 shows the various flame stability regions of the burner obtained from the test facility. Each data point on the upper curve was obtained by maintaining a fixed fuel flow and increasing the air flow until blow-off occurred. The fuel ejection velocity is calculated by dividing the fuel volumetric flow by the available fuel ejection area of the burner surface, which is equal to $\pi DL/2$. The combined uncertainty (u_c) in the estimation of the fuel ejection velocity is 0.02 cm/s. The regions below and above the curve correspond to the existence of a stable enveloped blue flame and a wake flame, respectively. There is a critical air velocity above which a stable enveloped flame can no longer be established, irrespective of the fuel flow. This critical blow-off velocity depends on fuel type and burner diameter [1]. Each data point on the lower curve was obtained by increasing the fuel ejection rate at a fixed oxidizer flow until a luminous yellow zone appeared. The conditions below this curve represent the existence of a yellow luminous zone.

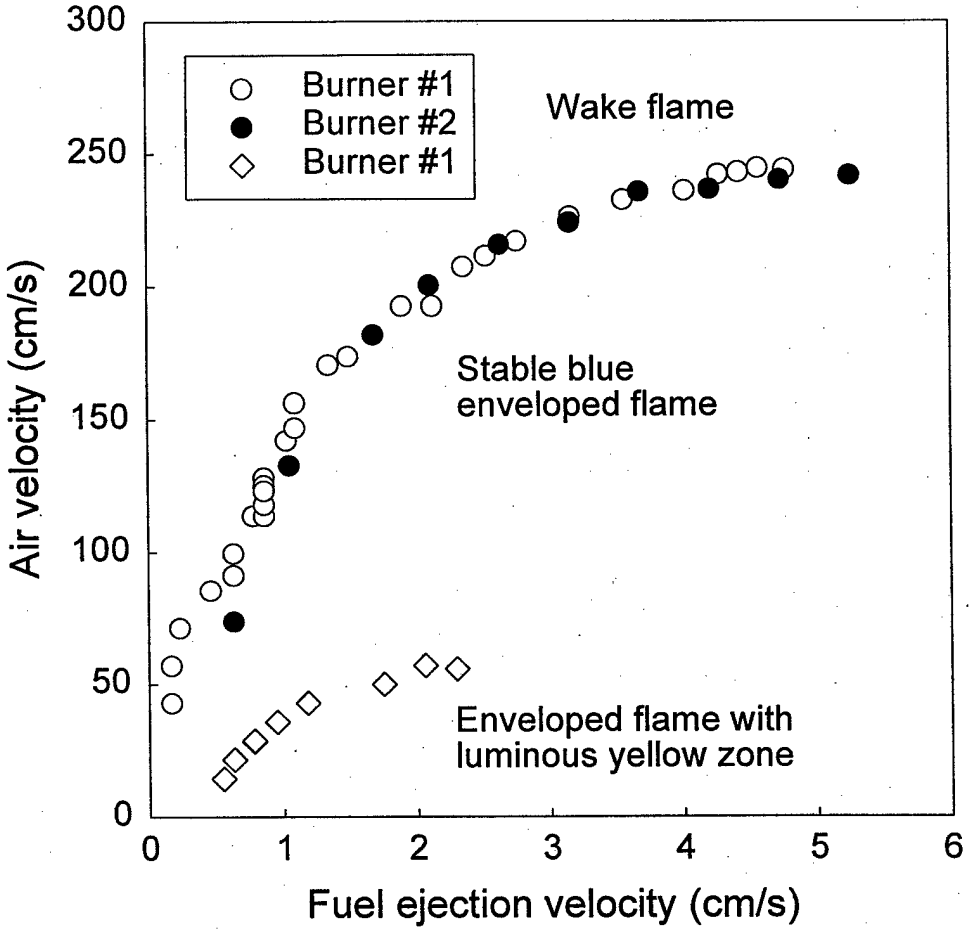

Figure 9. Flame stability (blow-off) curve.

For our proposed *liquid* screening applications, the fuel flow is always fixed at 2 L/min, which corresponds to an ejection velocity of 4.2 cm/s. The rationale for choosing this value will be elucidated in subsequent sections. The transition from a stable enveloped blue flame to a wake flame, that is the air velocity at blow-off, is used as a criterion for screening the fire suppression effectiveness of various fire suppressants; the higher the air blow-off velocity, the less effective the fire suppressant.

To assess the burner performance due to burner-to-burner variation, blow-off experiments were performed using four different burners. Based on two independent repeated observations, the overall coefficient of variation in the measurements of the air velocities at blow-off is 2 %; there is a statistically significant burner-to-burner effect at the 5 % level of significance. With the burner-to-burner effect being considered, the combined uncertainty (u_c) in the air velocity at blow-off is 3 cm/s with a degree of freedom of 7.

Screening Inert Gaseous Agents

To evaluate its applicability to fire suppression screening of gaseous agents, the apparatus was also tested with propane and three inert gases: argon, helium, and nitrogen. At a predetermined air flow and a fixed fuel flow, the inert gas was metered into the oxidizer stream at the blower outlet via a dry-test meter and a metering valve. Extinction tests were performed by gradually adding the inert inhibitor to the oxidizer (air) stream until blow-off occurred (abrupt transition from enveloped to wake flame). The volumetric flows of inhibitor at blow-off were recorded. The experiments were then repeated with a different air flow.

Figure 10 shows the amount of nitrogen added as a function of $2V_o / R$ at blow-off at different fuel injection rates; V_o is the velocity based on the total volumetric flow rate of air and inert gas at blow-off and R is the burner radius. The term, $2V_o / R$, represents the stagnation velocity gradient [1] and has the unit of strain rate (s^{-1}). Each data point represents the average of at least two runs. The standard deviations (1σ) are also plotted as error bars. The combined uncertainty in the calculated mass fraction of inert gas added is 0.005. Note that the scatter of the data reflects date-to-date variations, the use of different replaceable burners, and the initial instability of the flame at low $2V_o / R$ (see discussion below). The overall coefficient of variation is better than 10 % for higher strain rates ($2V_o / R > 100$). For a fixed $2V_o / R$, more nitrogen is needed to blow-off an enveloped flame as the fuel injection rate increases. For the same amount of nitrogen in the oxidizer stream, $2V_o / R$ at blow-off increases as the fuel injection rate increases.

It should be noted that in order to attain a low blow-off velocity gradient, the initial conditions of the flame were in the luminous yellow zone region (see Figure 9) before the inert gas was added to the air stream. Since the flame was pulsating and not very stable in this region,

the scatter of the data due to this initial flame instability is also apparent at small $2V_o / R$ in Figures 10 and 11.

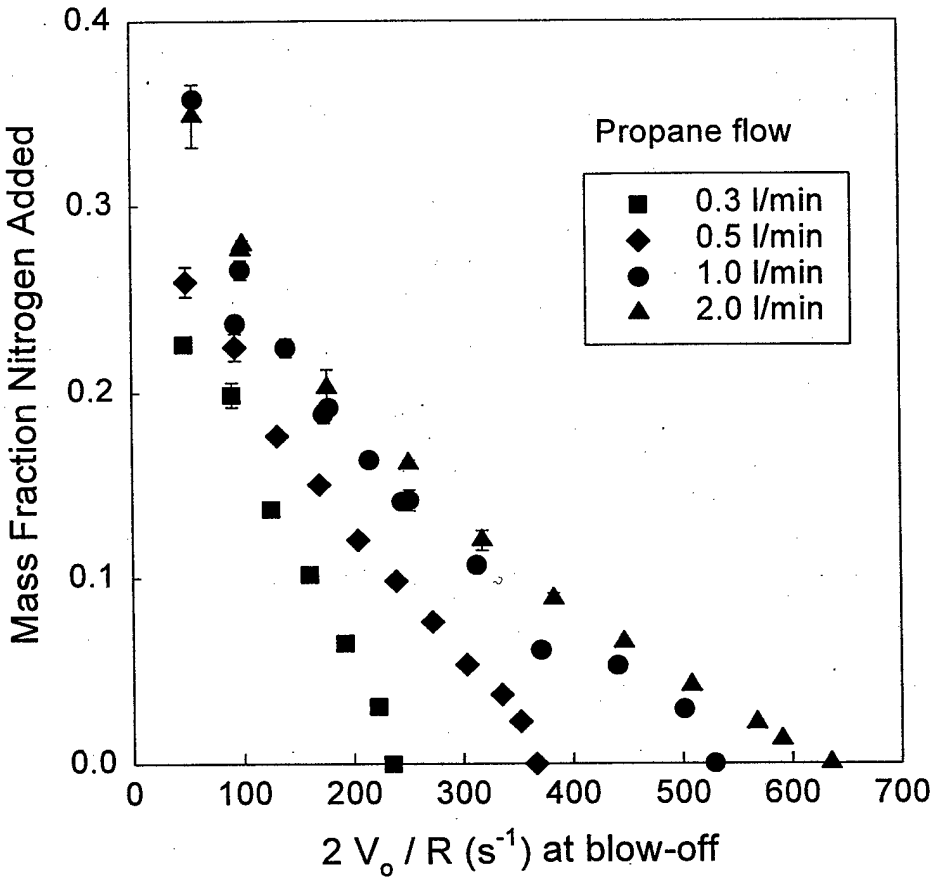

Figure 10. Mass fraction of nitrogen added in air as a function of stagnation velocity gradient at blow-off at different fuel flows.

As shown in Figure 10, there is an effect of fuel flow on the nitrogen concentration at blow-off. However, as the fuel flow increases, all the curves approach a limiting curve, that is, there is a critical fuel flow above which there is no effect of fuel flow on the blow-off concentration. This critical value should correspond to that from the stability curve (Figure 9). For the burner used, this value is close to 2 L/min (which corresponds to a fuel ejection velocity of 4.2 cm/s). The selection of 2 L/min is partly to eliminate the effect of fuel flow on blow-off

velocity. In addition, higher fuel injection velocity reduces heat loss to the burner [1]. However, a higher fuel injection velocity requires higher air velocity to achieve a stable blue flame (see Figure 9). The advantage of having a higher operating air flow is that it facilitates the droplet transport to the flame. It also enables the use of larger droplets without having them settled out by gravity. The disadvantage is that a higher air flow results in a higher global strain rate of the flame, which may not be representative of a fire and may lead to lower agent concentrations for suppression.

The results for the three inert gases (argon, helium, and nitrogen) at one fuel injection rate are shown in Figure 11. For a given $2V_o / R$, argon requires the most amount added to the oxidizer stream to cause blow-off, whereas helium requires the least. The relative ranking of these three gases is comparable to those from cup-burner tests [17]. Although there is an effect of fuel injection rate on blow-off concentration (as noted above), the relative ranking of these agents were found to be similar, for a given fuel injection rate.

Characterization of the Droplet Generation Device

Droplet Size Calculations

Since the droplets are propelled upwards, there are several limitations to the droplet sizes that can be used in the experiments. The first limitation is that for a given burner size, there is a maximum (critical) air flow (as discussed previously) above which the experiments cannot be performed because an enveloped flame cannot be initially established. However, this limitation can be easily alleviated by using a larger burner which results in a higher critical blow-off velocity [1]. The second limitation is that the droplet generator is located in the settling chamber where the air velocity is low because of the large cross sectional area of the chamber. If the initial droplet velocity is small, it is likely that the droplet (depending on its initial size) will not be entrained upwards by the low-speed air, and the droplet will eventually fall down due to gravity. The desirable droplet size for the experiments can be estimated by using the equation of motion for a droplet.

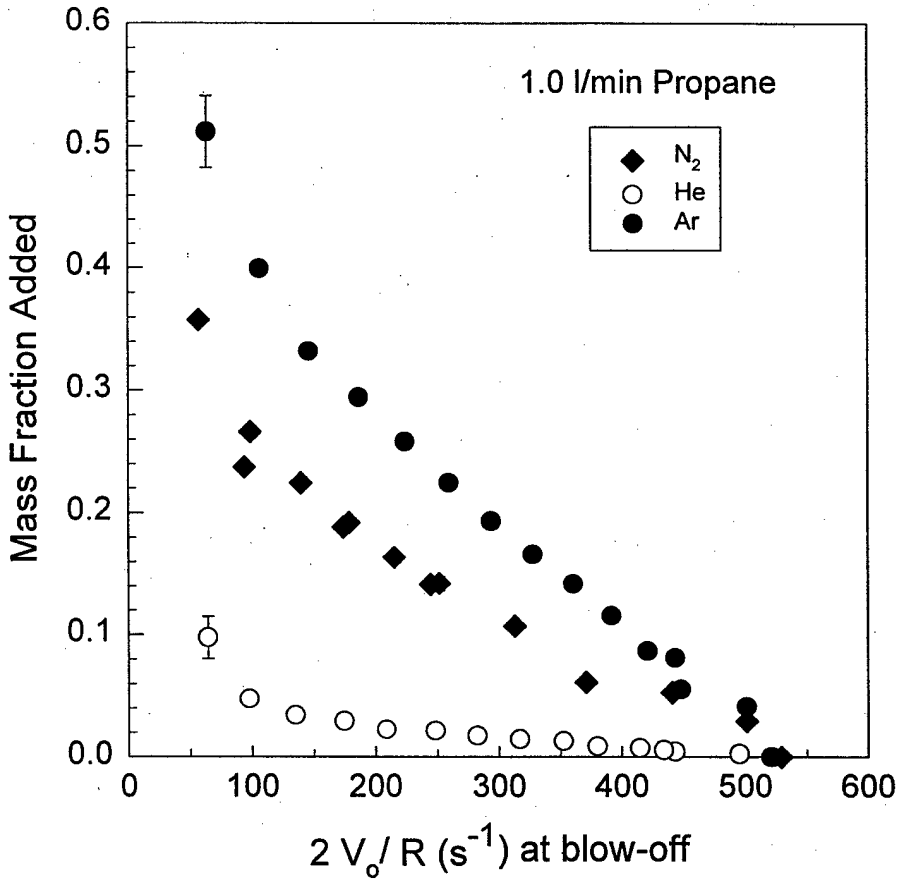

Figure 11. Mass fraction of inert gases added in air as a function of stagnation velocity gradient at blow-off.

$$m\frac{dV_d}{dt} = 3\pi\mu_O D_d f_d (V_O - V_d) + mg - \frac{\rho_O g m}{\rho_d} \qquad (3)$$

where m is the droplet mass, V_d is the droplet velocity, t is the time, μ_O is air viscosity, f_d is the drag factor, g is the gravitational acceleration, ρ_O is air density, and ρ_d is droplet density. For $Re_r \leq 10^5$, the drag factor can be obtained from [25]

$$f_d = 1 + 0.15\,Re_r^{0.687} + \frac{0.0175}{(1 + 4.25\times10^4\,Re_r^{-1.16})} \qquad (4)$$

where $Re_r = \frac{D_d |V_O - V_d| \rho_O}{\mu_O}$.

A FORTRAN computer program for solving Equations (3) and (4) using the Runge-Kutta-Verner fifth-order method is given in **Appendix XIII**. Using the above two equations, various droplet sizes under the operating conditions commensurate with the experiments are examined. A droplet with an initial velocity of 1 m/s is introduced from a droplet generator into the air stream at the settling chamber. Based on the droplet velocity measurements (see Phase Doppler Particle Analyzer Measurements), an initial droplet velocity of 1 m/s is reasonable. The burner is assumed to be operating at half of the critical velocity. Since the air velocity at the settling chamber is one-ninth of that at the test section (based on the 9:1 contraction area ratio), the initial air velocity which the droplet is exposed to is equal to $0.5\, V_{o,critical} \times (1/9)$. Figure 12 shows the calculated droplet travel distance from the droplet generator as a function of time for two water droplet sizes. The calculations were obtained by using $V_{o,critical} = 2.4$ m/s (from Figure 9). The continuous increase in air velocity through the contraction section has been taken into account in the calculations. The results in Figure 12 demonstrate that a 60 μm droplet can easily be entrained upwards by the existing air flow. However, under the same flow conditions, a 70 μm droplet will eventually be settled down due to gravity.

Phase Doppler Particle Analyzer Measurements

An Aerometrics two-component Phase Doppler Particle Analyzer (PDPA) with a Doppler Signal Analyzer (DSA) was used to measure droplet size and velocity distributions. The measurements were made at several positions near the droplet generation device and near the burner to assess the uniformity of the small dispersed droplet spray.

Droplet Size Distribution from Piezoelectric Droplet Generator

Figure 13 shows the results from the PDPA measurements taken on the centerline and 2.5 cm downstream of the orifice exit. The generator was pointed downward in the same direction as the vertical velocity prescribed by the orientation of the PDPA transmitter. The velocity components in Channels 1 and 2 represents the vertical and horizontal components, respectively.

The orifice has a nominal opening of 40 μm, and the droplet generator was pulsed at a frequency of 15 kHz with an amplitude of 50 V and a pulse duration of 10 μs. Water was used for the droplet generator characterization. The droplet size distribution is very narrow, an indication of the mono-dispersity of the droplet stream near the orifice. The Sauter mean diameter is 47.5 μm with a standard uncertainty (based on repeated measurements) of 1 μm.

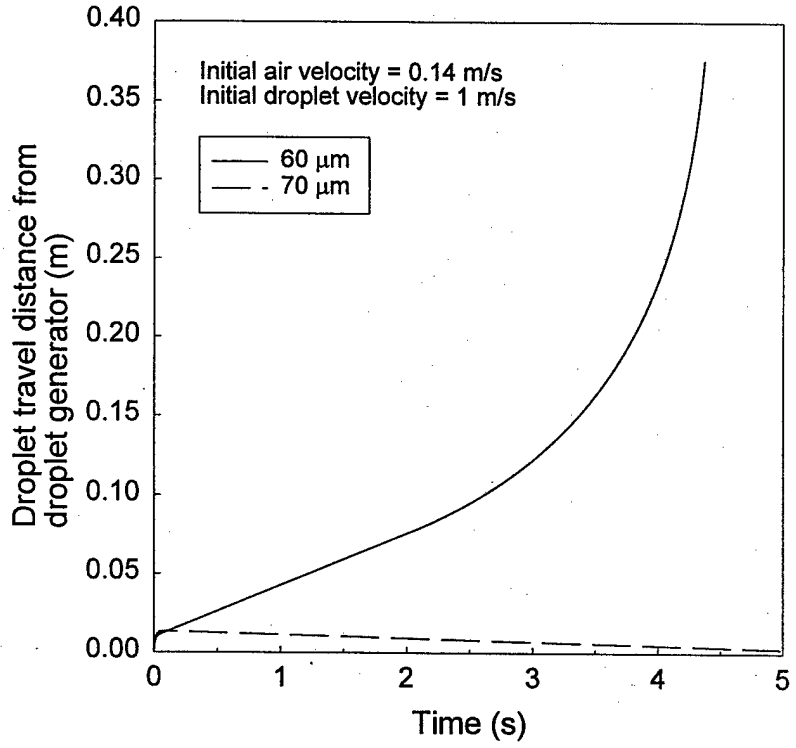

Figure 12. Droplet travel distance from a droplet generator as a function of time for two water droplet sizes.

Droplet Size Distribution from Nebulizer

PDPA measurements of the nebulizer spray were taken on the centerline, 2 cm downstream of the nebulizer exit. Air was supplied to the nebulizer at 0.25 L/min, and de-ionized water was used as the calibration liquid. The liquid flow was varied from 0.3 ml/min to 1.2 ml/min. Figure 14 is an example of one set of results taken at a liquid flow of 0.5 ml/min.

Unlike the piezoelectric droplet generator, the nebulizer creates droplets with a range of diameters, as evident in the diameter histogram in the figure. In the measurements, the nebulizer was pointed upward in the opposite direction of the vertical velocity prescribed by the orientation of the PDPA transmitter.

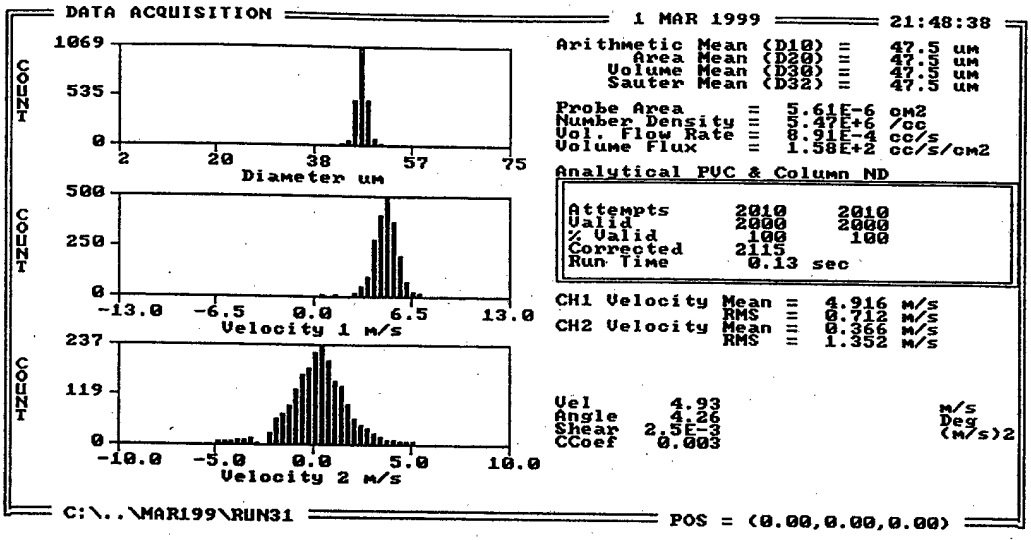

Figure 13. Measurement of piezoelectric droplet generator from the two-component PDPA at a location, 2.5 cm downstream of the orifice exit. Velocity 1 is the vertical component; velocity 2 is the horizontal component.

PDPA measurements were also taken on the centerline at the burner location. Since the experiment protocol requires the blower air speed to increase until blow-off occurs, it is necessary to determine if such an increase could result in secondary disintegration of the droplets due to increasing aerodynamic forces on the droplets. Droplet size measurements were taken at blower air speeds of 111 cm/s and 179 cm/s. The change in blower air speed within the range for the experiments was found to have a negligible effect on the diameter of the droplets which reached the burner. The Sauter mean diameter, defined as the ratio of spray droplet volume to droplet surface area, is in the range of 25 μm to 35 μm for all air velocities and water application rates. There is a slight tendency for the droplet diameter to increase with liquid delivery rate. The standard uncertainty (based on repeated measurements) is 2 μm.

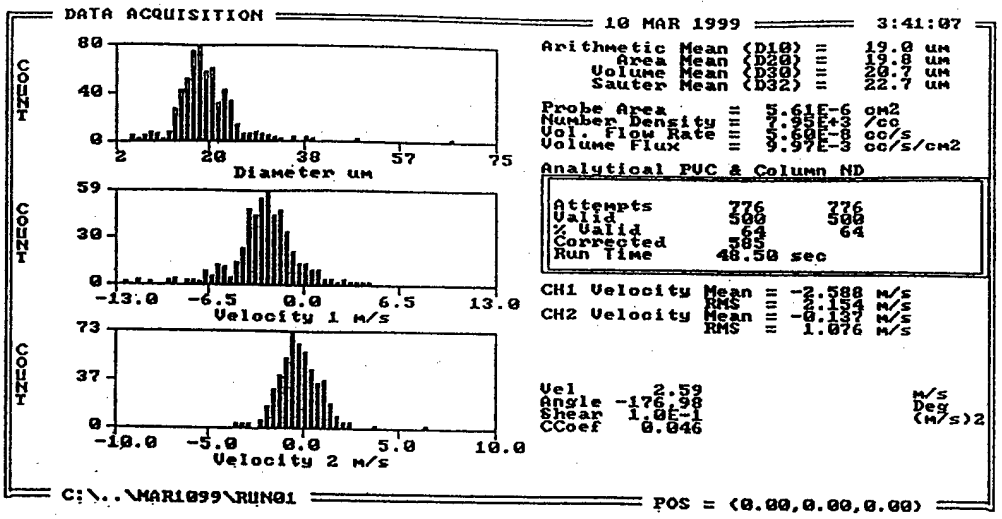

Figure 14. Measurement of the nebulizer spray using the two-component PDPA at the centerline location, 2 cm downstream of the nebulizer exit.

Droplet size measurements were also performed by moving the nebulizer to different off-center locations in the settling chamber to account for possible misalignments, and this was found to have no effect on the droplet size near the burner.

Since the atomizing characteristics of the nebulizer depend on the physical properties of the fluids [19], different droplet size distributions may result when different test fluids are used; this could complicate the interpretation of the screening results by introducing the additional effect of droplet diameter. A series of measurements was performed using the PDPA to determine the dependence of droplet size on the physical properties of the test fluids. Several surrogate fluids (water, 30 % and 45 % (mass fraction) potassium lactate, and 1000 mg/L and 2000 mg/L sodium dodecyl sulfate (SDS)) were used to simulate variations in densities, viscosities, and surface tensions. Table 2 lists some of their physical properties. Figure 15 shows the PDPA measurement results on the centerline, 2 cm downstream of the nebulizer exit for liquid flows between 0.3 ml/min and 0.9 ml/min. In all cases, the Sauter mean diameters only vary between 20 μm and 30 μm.

Table 2. Physical properties of surrogate fluids @ 20 °C

Fluid	Density (g/cm^3) ± 0.01	Viscosity* (g/s cm) ± 0.001	Surface tension¶ (dyne/cm) ± 1
Distilled water	1.00	0.010	72
30 % potassium lactate	1.15	0.025	66
45 % potassium lactate	1.23	0.038	68
1000 mg/L SDS	0.98	0.0095	52
2000 mg/L SDS	0.96	0.0093	38

*measured using a Cannon® Glass Capillary Viscometer

¶measured using a DuNouy® Tensiometer (Model No. 70535, CSC-Scientific Co., Inc.)

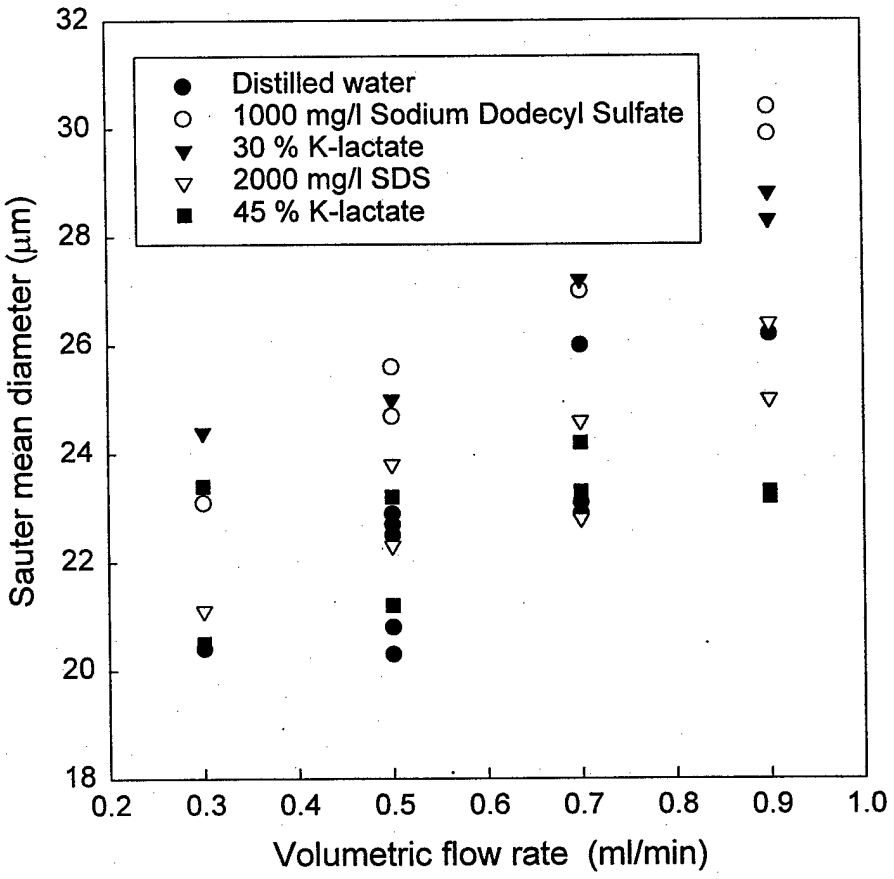

Figure 15. Droplet diameter measurements of various fluids using the PDPA at the centerline location, 2 cm downstream of the nebulizer exit.

Experimental Procedure

The operation of the dispersed liquid agent screening apparatus is described in detail in this chapter. The procedure includes the setup of the porous cylindrical burner, the preparation of the droplet generator, the establishment of a stable blue enveloped flame, and the execution of the suppression experiments.

There are two ways to perform the screen experiments: (1) increasing the air flow at a fixed liquid agent application rate until blow-off occurs, and (2) increasing liquid agent application rate at a fixed air flow until blow-off occurs. The former was selected because the procedure requires less agent and there is no need to correct for the lag time from changing the syringe pump setting (to increase the liquid flow) to attaining a steady liquid delivery rate.

Burner Set-up

- For a new burner, apply several thin coats of high temperature paint on half and the end of the porous burner surface (see Figure 3). Let the painted surface dry or cure in an oven overnight.
- Screw the burner into the insert. Mount the burner assembly to the wall of test section. Adjust the burner so that the unpainted burner surface is facing the direction of the oxidizer flow. Connect the cooling water and fuel lines to the burner assembly.
- Mount the brass cylindrical extension to the opposite observation window. Connect the cooling water lines to the cylindrical extension.

Note: To test whether there is any leakage from the paint portion of the porous surface, screw the burner into the insert, connect the fuel port to a compressed air or nitrogen line. Initiate gas flow and immerse the burner assembly into a container of water. Observe if there is bubbling from the painted surface. If leakage occurs, apply another thin layer of paint to the surface.

Preparation of Droplet Delivery System

Although a nebulizer is used in the current liquid screen apparatus, the procedure for using the piezoelectric droplet generator is also described for completeness because the droplet generator can still be used for test fluids that do not clog the orifice opening.

Piezoelectric Droplet Generator

- Place the orifice plate in an ultrasonic cleaner for 5 to 10 minutes.
- Remove the orifice plate from the cleaner, and apply pressurized air or nitrogen (at approximately 0.14 MPa gauge) to the orifice to dislodge residual cleaning solution and any foreign particles that may have adhered to the orifice opening.
- Attach the orifice plate to the droplet generator body (liquid chamber with the piezoelectric transducer). Fill the liquid reservoir with the test agent. Connect it to the droplet generator. Set the nitrogen pressure to obtain the desired liquid volumetric flow. Prior calibration of the orifice may be required to ensure the correct volumetric flow by measuring the volume of the liquid ejected over a given time interval. Alternatively, a variable drive syringe pump can also be used to supply liquid to the droplet generator.
- Prime the droplet generator with the test liquid with the bleed port open in order to expel air bubbles from the liquid chamber. Tilting and tapping the chamber facilitates the process. Recap the bleed port after priming.
- Connect the piezoelectric transducer to the pulse generator. Insert the droplet generator into the wind tunnel through the access hole on the sidewall of the settling chamber. Secure the droplet generator mount to the X-Y translation stage. Position the droplet generator. Seal the access port.
- Turn on the pulse generator, and adjust the output voltage to 50 V and a pulse duration of 5 μs to 10 μs. Set the frequency to the desired setting, between 10 kHz and 15 kHz.

Nebulizer

- Remove the test section and the contraction section from wind tunnel.
- Insert the delivery tubing through the access hole on the sidewall of the settling chamber and connect the delivery tubing to the liquid input port of the nebulizer.
- Connect the sidearm of the nebulizer to a stainless steel tubing which is mounted on a X-Y translation stage and is inserted through the access hole of the settling chamber. In addition to mounting the nebulizer, the stainless steel tubing is used to supply atomizing air to the nebulizer. Position the nebulizer to the center of the settling chamber using the X-Y stage. Seal the access hole.

- Install the contraction section and the test section.
- Fill the syringe and connect it to the delivery tubing. Set the syringe pump to the desired liquid delivery rate.

Establishment of a Stable Enveloped Flame

- With the slide-damper plate in place, set the blower to a low speed (≈ 7 Hz), and turn it on. The low blower speed is needed to facilitate the establishment of an enveloped rather than a wake flame.
- Turn on the flow of cooling water to the burner insert and cylindrical extension prior to igniting the burner.
- Turn on the mass-flow controller. It should be warmed up at least one hour prior to the experiments to ensure a stable fuel flow. Start the computer program used to control the mass-flow controller, and set the fuel flow rate to the desired amount in liters per minute (2 L/min was used in all the liquid screen tests reported herein).
- Turn on the fuel supply and the mass flow controller. Use a hand-held flexible tip butane lighter to ignite the burner. Once the flame is established, allow several minutes for the flame to stabilize. Adjust the blower speed, if necessary.

Testing

- To ensure that the burner (new or old) is functioning properly, perform a check by increasing the blower air speed (without liquid application) until blow-off occurs. The increase in blower speed should be done gradually from an initial coarse increment of 2 Hz to a final fine increment of 0.01 Hz as blow-off conditions are approached. The blower reading at blow-off should not vary more than 1.5 Hz from day-to-day, run-to-run, or burner-to-burner. Water should also be used as a baseline fluid to check the burner performance periodically. Note that when performing a blow-off (without agent) check, make sure that the air flow to the nebulizer is on because it imposes a small perturbation to the flame, thus lowering the blow-off velocity somewhat. The average blow-off velocity (without agent and air flowing in the nebulizer) is 250 cm/s with a combined uncertainty of 1 cm/s and a degree of freedom of 87, compared to the average blow-off velocity (without agent but with air flowing in the

nebulizer at 0.25 L/min) of 226 cm/s with a combined uncertainty of 1 cm/s and a degree of freedom of 168.

- For the piezoelectric droplet generator, start the liquid delivery system with a *preset* liquid flow rate. For the nebulizer, initiate the atomizing air (set at 0.25 L/min) and turn on the syringe pump.
- Increase the air flow using the blower controller box by stepping up the blower frequency. When the flame is near blow-off, one side of the flame will detach from the leading edge, and caution should be used at this point not to increase the air flow air too quickly. Sudden increases in air speed will blow-off the flame at lower velocities.
- Record the blower frequency reading at blow-off. The oxidizer blow-off velocity can be obtained from the calibration curve (frequency *vs.* velocity, Figure 7).

Note: Once the flame has blown-off, it can be returned to an enveloped state by decreasing the air flow and turning off the droplet generation device.

- Set another liquid flow rate, and repeat the blow-off experiment, if desired.
- Compare the suppression effectiveness of individual agents in terms of blow-off velocity at a given liquid application rate; the higher the air blow-off velocity, the less effective the fire suppressant.

Note: Since the densities of the fluids that we have tested do not differ significantly, we express the liquid application rate in terms of volumetric flow (directly from the setting from the syringe pump) rather than mass flow for simplicity.

Sample Results with Aqueous Suppressants

Several test fluids (water, skim milk, 30 % sodium iodide, and 30 % and 60 % potassium lactate) have been used to evaluate the performance of the screening apparatus. Milk is known to be a fire suppressant [26], sodium iodide was selected because it may be more effective than sodium bromide [27], and potassium lactate has been demonstrated to be more effective than water [27]. Figure 16 shows the screening results using these test fluids. Each data point represents one test. For a given fluid, increasing the liquid application rate decreases the blow-off velocity. As expected, a mass fraction of 60 % potassium lactate is more effective than 30 % potassium lactate. Water is the least effective when compared to skim milk, 30 % sodium iodide,

and 60 % potassium acetate. Based on this set of data, the coefficient of variation from run-to-run using the liquid screening apparatus is estimated to be better than 20 %.

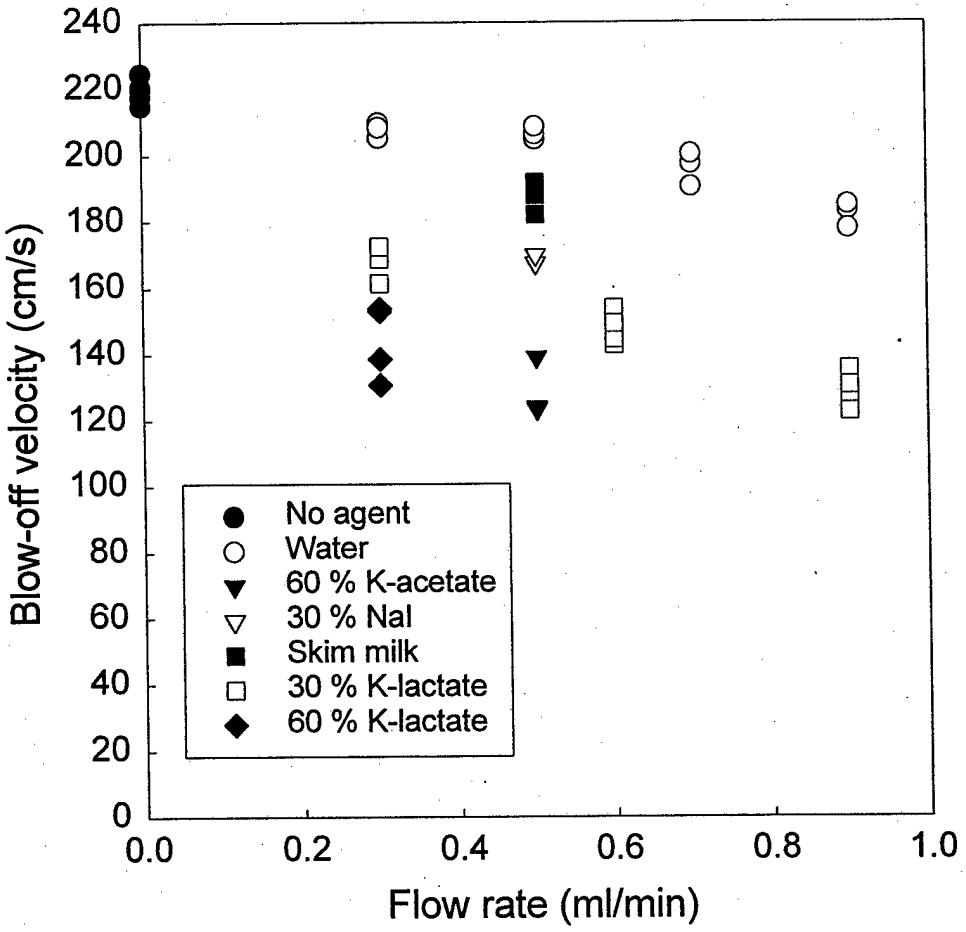

Figure 16. Screening results using different types of fluids.

Proposed Test Protocol

The above test procedure can be used for *rapid* screening. A blow-off experiment without agent is first conducted to check the burner performance, followed by a blow-off experiment with a fixed agent application rate. This process is shown schematically as the

vertical line in Figure 17. The blow-off velocities are used to provide a *relative* ranking of various liquid agents.

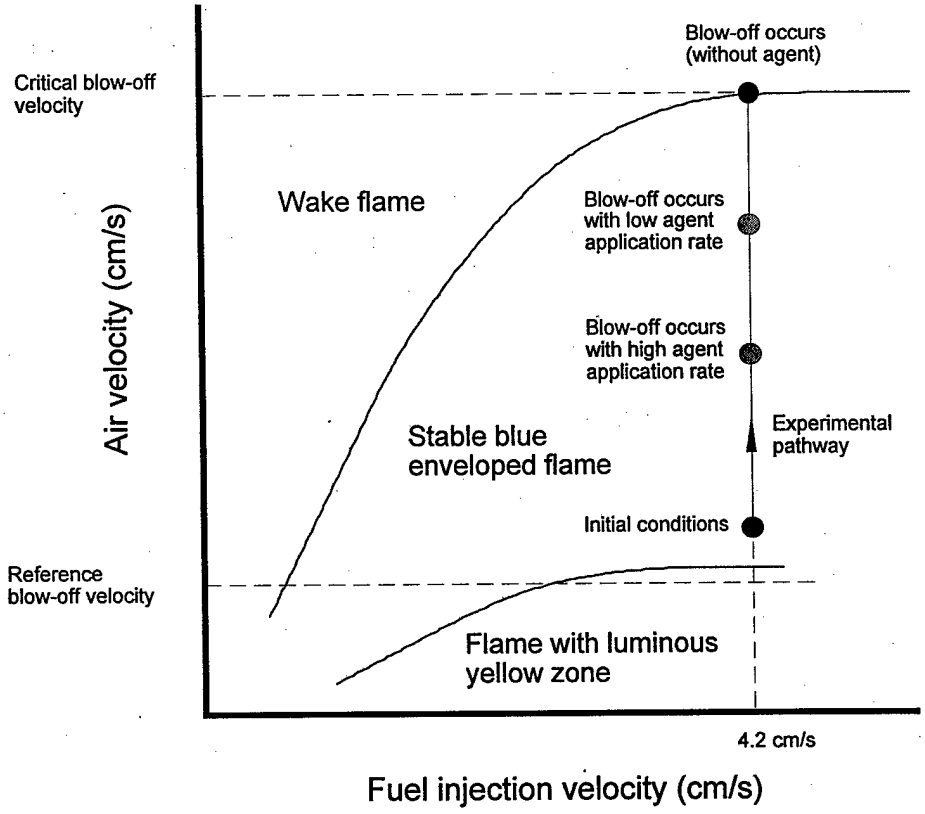

Figure 17. Schematic illustrating the experimental procedure.

Since there are many liquid delivery rates that one can use in the screening procedure, a reference delivery rate is needed to compare and interpret the fire suppression effectiveness of various liquid agents in a consistent and meaningful way. We have developed the following protocol which is based on the conditions commensurate with the cup-burner results for nitrogen.

The average propane cup burner value for nitrogen is 32 % (mass fraction) [17]. An examination of the results in Figure 10 for a propane flow of 2 L/min (selected to eliminate fuel flow effects and heat transfer to the burner) indicates that the nitrogen mass fraction (at blow-off) equivalent to the cup burner value corresponds to a $2V_o / R$ of approximately 100 s^{-1}, or a

reference blow-off velocity of ≈ 30 cm/s (see Figure 18). At this velocity and a propane flow of 2 L/min, a flame cannot be stabilized in the desired blue enveloped flame region (refer to Figure 17). In addition, the experimental protocol calls for increasing the air velocity (*i.e.*, moving away from 30 cm/s) until blow-off at a fixed fluid delivery rate. Therefore, in order to compare the results obtained from the cylindrical burner to conditions commensurate with cup-burner results, extrapolation to lower air velocity (strain rate) is required. Note that nitrogen is selected as a reference gas simply due to the availability of suppression data for the cylindrical burner (see Figure 10). Similar reference blow-off velocities will be obtained when the cup-burner results for other gases are used because at the *same* low global strain rate in a counterflow flat-flame burner, the agent extinction concentrations agree well with the measurements obtained from a cup burner [17].

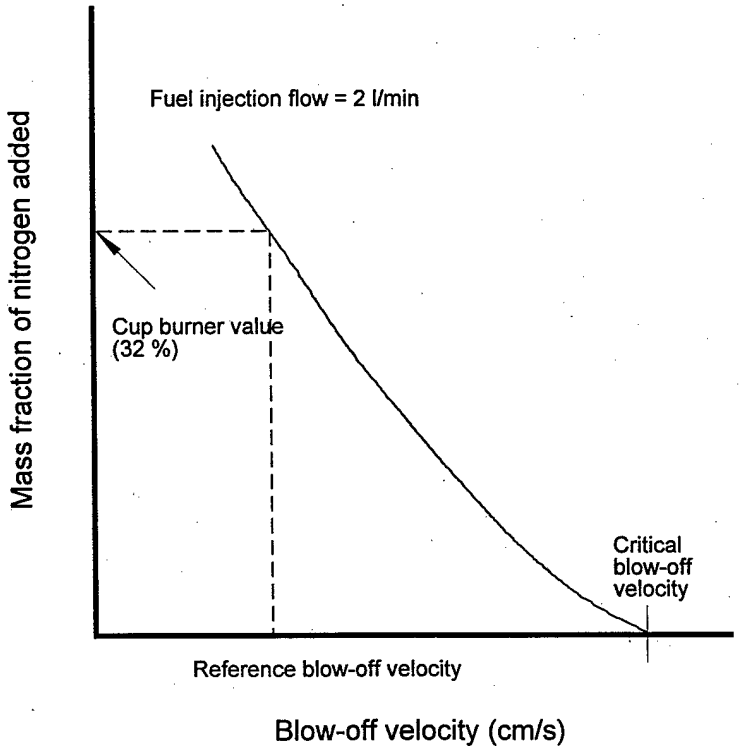

Figure 18. Schematic illustrating the definition of the reference blow-off velocity used in the proposed test protocol.

Figure 19 demonstrates the proposed extrapolation mechanism. A blow-off air velocity without fluid application (but with air in the nebulizer flowing) is obtained, followed by a blow-off experiment with a fixed fluid application rate. The fluid delivery rate at an air velocity of 30 cm/s is then deduced by linear extrapolation. Based on our experience, an application rate between 0.6 ml/min and 1 ml/min appears to be appropriate, which is a compromise between minimizing the fluid consumption for a test and attaining a blow-off velocity close to the reference blow-off velocity of 30 cm/s. Note that application rate greater than 1.3 ml/min is not recommended (see Nebulizer).

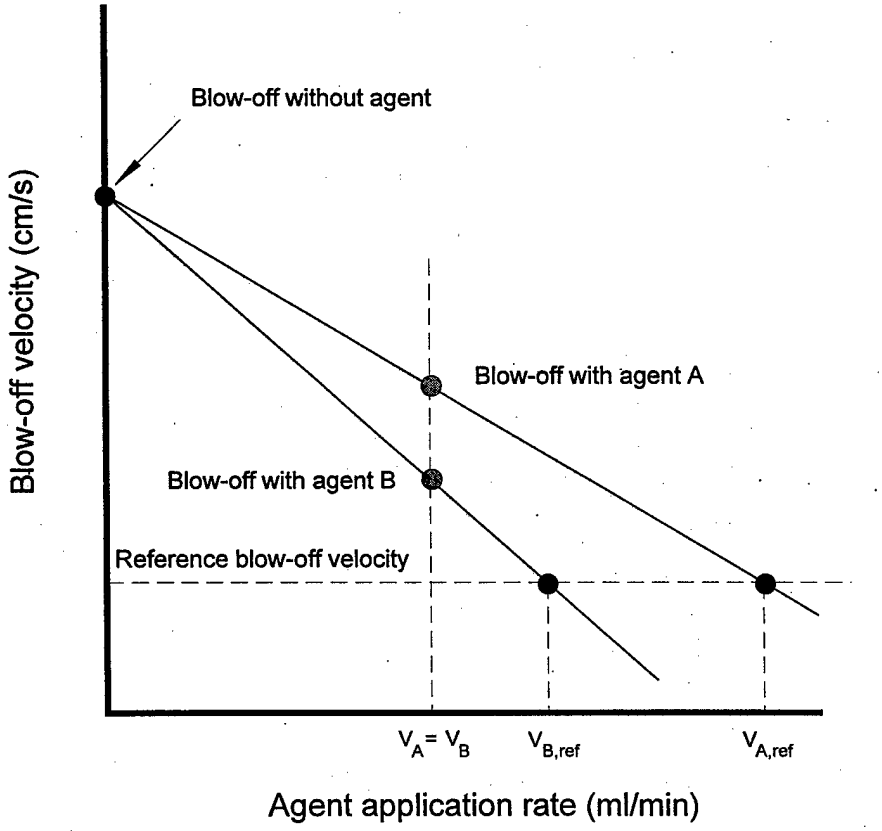

Figure 19. Schematic illustrating the extrapolation of agent application rates at the reference blow-off velocity.

Once the application rate corresponding to the reference blow-off velocity is deduced, the reference mass flow rate of the liquid agent, $\dot{m}_{agent,ref}$, can be calculated using the liquid density. The reference mass fraction of the liquid agent in the air stream is then

$$Y_{agent,ref} = \frac{\dot{m}_{agent,ref}}{\dot{m}_{agent,ref} + \dot{m}_{air,ref}} \qquad (5)$$

where $\dot{m}_{air,ref}$ is the mass flow of air, calculated based on the cross-sectional area of the test section and 30 cm/s. Note that in writing Equation (5), it is implicitly assumed that the droplets are homogeneously dispersed in the carrier phase (air).

Table 3 summarizes the calculations of the reference agent mass fraction in air using the screening results from Figure 16 and the proposed approach described above. Average values of the blow-off velocities were used in the extrapolation. For cases where blow-off velocities at more than one liquid application rates are available, linear regressions were used to extrapolate the reference blow-off velocities. When data with one application rate were available, simple linear extrapolation was applied to obtain the reference blow-off velocities.

The last column of Table 3 lists the ranking indices relative to water. For example, the 60 % K-acetate and K-lactate solutions are considered to be four times more effective than water at the reference blow-off velocity. If the droplets are not homogeneously dispersed across the total cross-sectional area, the calculated agent mass fraction will be underestimated because $\dot{m}_{air,ref}$ is overestimated. The effective area can be considered as the effective coverage area of the mist in the test section. Depending on the effective coverage area, a difference of a factor of *two* to *three* in the calculated liquid mass fraction can result. By placing a filter paper over the exit of the test section for a short duration with the wind tunnel operating (without the burner) and the nebulizer atomizing water with a dye added, the droplet-impact (color) pattern on the filter paper can be visualized and used as an indicator to determine the mist coverage area in the test section. The color pattern, which is approximately circular, indicates that the mist from the nebulizer completely covers the burner and its vicinity. The mist coverage area was estimated to be *ca.* 40

% of the total cross-sectional area of the test section for all the conditions encountered in our screening tests.

Table 3. Calculated nominal agent mass fractions at reference blow-off air velocity of 30 cm/s

Agent	$V_{agent,ref}$ (ml/min)	Agent density (g/cm^3) @ 20 °C	$\dot{m}_{agent,ref}$ (g/s)	*Nominal* agent mass percent (%)	$\frac{\dot{m}_{water,ref}}{\dot{m}_{agent,ref}}$
Water	4.62	1.00	0.08	2.6	1.0
60 % K-acetate	0.99	1.34	0.02	0.8	4.0
30 % NaI	1.76	1.29	0.04	1.3	2.0
Skim milk	2.78	1.01	0.05	1.6	1.6
30 % K-lactate	1.74	1.15	0.04	1.2	2.0
60 % K-lactate	0.71	1.33	0.02	0.6	4.0

Irrespective of the uncertainty associated with the estimated nominal agent mass concentration, water and the aqueous agents studied here are found to be more effective than CF_3Br, compared to the propane cup burner value (mass fraction of 17 % [17]) for CF_3Br. The computational study by Lentati and Chelliah [28] also demonstrates that 20 μm water droplets are more effective (mass fraction of 4.24 % *vs.* 5.9 %) in extinguishing an opposed-flow methane diffusion flame than CF_3Br at an extinction strain rate of 176 s^{-1}. Although the ratio of our calculated nominal water mass fraction to the cup burner value for CF_3Br using propane is smaller, both studies are in qualitative agreement in terms of the suppression effectiveness of water droplets.

Care should be exercised when interpreting the screening results in Table 3, which were obtained using an idealized laboratory flame and a droplet delivery system such that the transport of fine liquid droplets *to* the flames is not a factor in determining the suppression effectiveness. In the case of real fires, droplet entrainment and transport to the fire can significantly affect the liquid agent mass concentration required to suppress a fire, especially in highly obstructed enclosure fires.

CONCLUSIONS

An apparatus for screening liquid agents delivered in droplet form has been developed. The performance of the apparatus has been characterized using fluids with different thermophysical properties and fire suppression effectiveness. The apparatus is robust and easy to operate. A step-by-step test procedure is provided to facilitate the use of the apparatus. The droplet delivery system is designed to handle small quantity of liquid sample. For all the test results reported here, 10 ml of sample is needed to perform a rapid screen (with one repeat). The apparatus can also be used to screen gaseous agents. When a powder delivery system is integrated into the current apparatus, the facility, in principle, can be employed to screen powder agents.

REFERENCES

1. Tsuji, H. and Yamaoka, I., "The Counterflow Diffusion Flame in the Forward Stagnation Region of a Porous Cylinder," *Eleventh Symposium (International) on Combustion*, The Combustion Institute, Pittsburgh, PA, pp. 979-984, 1967.

2. Tsuji, H. and Yamaoka, I., "The Structure of Counterflow Diffusion Flames in the Forward Stagnation Region of a Porous Cylinder," *Twelfth Symposium (International) on Combustion*, The Combustion Institute, Pittsburgh, PA, pp. 997-1005, 1969.

3. Tsuji, H. and Yamaoka, I., "Structure Analysis of Counterflow Diffusion Flames in the Forward Stagnation Region of a Porous Cylinder," *Thirteenth Symposium (International) on Combustion*, The Combustion Institute, Pittsburgh, PA, pp. 723-731, 1971.

4. Tsuji, H., "Counterflow Diffusion Flames," *Prog. Energy Combustion Sci.*, **8**, 93 (1982).

5. Ishizuka, S. and Tsuji, H., "An Experimental Study of Effect of Inert Gases on Extinction of Laminar Diffusion Flames," *Eighteenth Symposium (International) on Combustion*, The Combustion Institute, Pittsburgh, PA, pp. 695-703, 1981.

6. Milne, T.A., Green, C.L., and Benson, D.K., "The Use of the Counterflow Diffusion Flame in Studies of Inhibition Effectiveness of Gaseous and Powdered Agents," *Comb. Flame*, **15**, 255 (1970).

7. Dixon-Lewis, G., David, T., Gaskell, P.H., Fukutani, S., Jinno, H., Miller, J.A., Kee, R.J., Smooke, M.D., Peters, N., Effelsberg, E., Warnatz, J., and Behrendt, F., "Calculation of the Structure and Extinction Limit of a Methane-Air Counterflow Diffusion Flame in the Forward Stagnation Region of a Porous Cylinder," *Twentieth Symposium (International) on Combustion*, The Combustion Institute, Pittsburgh, PA, pp. 1893-1904, 1984.

8. Dreier, T., Lange, B., Wolfrum, J., Zahn, M., Behrendt, F., and Warnatz, J., "CARS Measurements and Computations of the Structure of Laminar Stagnation-Point Methane-Air Counterflow Diffusion Flames," *Twenty-first Symposium (International) on Combustion*, The Combustion Institute, Pittsburgh, PA, pp. 1729-1736, 1986.

9. Peters, N. and Kee, R.J., "The Computation of Stretched Laminar Methane-Air Diffusion Flames Using a Reduced Four-Step Mechanism," *Comb. Flame*, **68**, 17 (1987).

10. Olson, S.L. and T'ien, J.S., "A Theoretical Analysis of the Extinction Limits of a Methane-Air Opposed-Jet Diffusion Flame," *Comb. Flame*, **70**, 161 (1987).

11. Dixon-Lewis, G. and Missaghi, M., "Structure and Extinction Limits of Counterflow Diffusion Flames of Hydrogen-Nitrogen Mixtures in Air," *Twenty-second Symposium (International) on Combustion*, The Combustion Institute, Pittsburgh, PA, pp. 1461-1470, 1988.

12. Chen, C.H. and Weng, F.B., "Flame Stabilization and Blowoff Over a Porous Cylinder," *Combust. Sci. Tech.*, **73**, 427 (1990).

13. Sick, V., Arnold, A., Dieβel, E., Dreier, T., Ketterle, W., Lange, B., Wofrum, J., Thiele, K.U., Behrendt, F., and Warnatz, J., "Two-Dimensional Laser Diagnostics and Modeling of Counterflow Diffusion Flames, " *Twenty-third Symposium (International) on Combustion*, The Combustion Institute, Pittsburgh, PA, pp. 495-501, 1990.

14. Fleming, J.W., Reed, M.D., Zegers, E.J.P., Williams, B.A. and Sheinson, R.S., "Extinction Studies of Propane/Air Counterflow Diffusion Flames: The Effectiveness of Aerosols," *Halon Options Technical Working Conference*, Albuquerque, New Mexico, May 12-14, 1998.

15. Chelliah, H.K., Krauss, R.H., Zhou, H., and A.M. Lentati, "Characterization of Physical, Thermal, and Chemical Contributions of Sodium Bicarbonate Particles in Extinguishing Counterflow Nonpremixed Flames," *Proceedings of the 5th ASME/JSME Joint Thermal Engineering Conference*, San Diego, California, March 1999.

16. Li, S.C., "Spray Stagnation Flames," *Prog. Energy Combustion Sci.*, **23**, 303 (1997).

17. Grosshandler, W.L., Gann, R.G., and Pitts, W.M., "Evaluation of Alternative In-Flight Fire Suppressants for Full-Scale Testing in Simulated Aircraft Engine Nacelles and Dry Bays," NIST SP861, U.S. Department of Commerce, April 1994.

18. Shilling, H., Dlugogorski, B.Z., and Kennedy, E.M., "Extinction of Diffusion Flames by Ultrafine Water Mist Doped with Metal Chlorides," *Proceedings of the Sixth Australasian Heat and Mass Transfer Conference*, December 9-12, 1996, Sydney, Australia, pp. 275-282.

19. Bayvel, L. and Orzechowski, Z., *Liquid Atomization*, Taylor and Francis, Washington DC, 1993.

20. Schneider, J.M. and Hendricks, C.D., "Source of Uniform-Sized Liquid Droplets," *Rev. Sci. Instrum.*, **35**, 1349 (1964).

21. Warnica, W.D., Van Reenen, M., Renksizbulut, M., and Strong, A.B., "A Piezoelectric Droplet Generator for Use in Wind Tunnels," *Rev. Sci. Instrum.*, **62**, 3037 (1991).

22. Yang, J.C., Chien, W., King, M., and Grosshandler, W.L., "A Simple Piezoelectric Droplet Generator," *Experiments in Fluids*, **23**, 445 (1997).

23. Yang, J.C., Donnelly, M.K., Privé, N.C., and Grosshandler, W.L., "Fire Suppression Efficiency Screening Using a Counterflow Cylindrical Burner," *Proceedings of the 5th ASME/JSME Joint Thermal Engineering Conference*, San Diego, California, March 1999.

24. *ISO, Guide to the Expression of Uncertainty in Measurement*, International Standards Organization, Geneva, Switzerland, 1993.

25. Crowe, C., Sommerfeld, M., and Tsuji, Y., *Multiphase Flows with Droplets and Particles*, CRC Press, Boca Raton, Florida, 1998.

26. Rossotti, H., *Fire*, Oxford University Press, Oxford, 1993.

27. Finnerty, A.E., McGrill, R.L., and Slack, W.A., "Water-Based Halon Replacement Sprays," ARL-TR-1138, U.S. Army Research Laboratory, Aberdeen Proving Ground, July 1996.

28. Lentati, A.M. and Chelliah, H.K., "Physical, Thermal, and Chemical Effects of Fine-Water Droplets in Extinguishing Counterflow Diffusion Flames," *Twenty-Seventh Symposium (International) on Combustion*, The Combustion Institute, Pittsburgh, PA, pp. 2839-2846, 1998.

APPENDIX I

Drawings of the transition duct

Drawing: Wind52

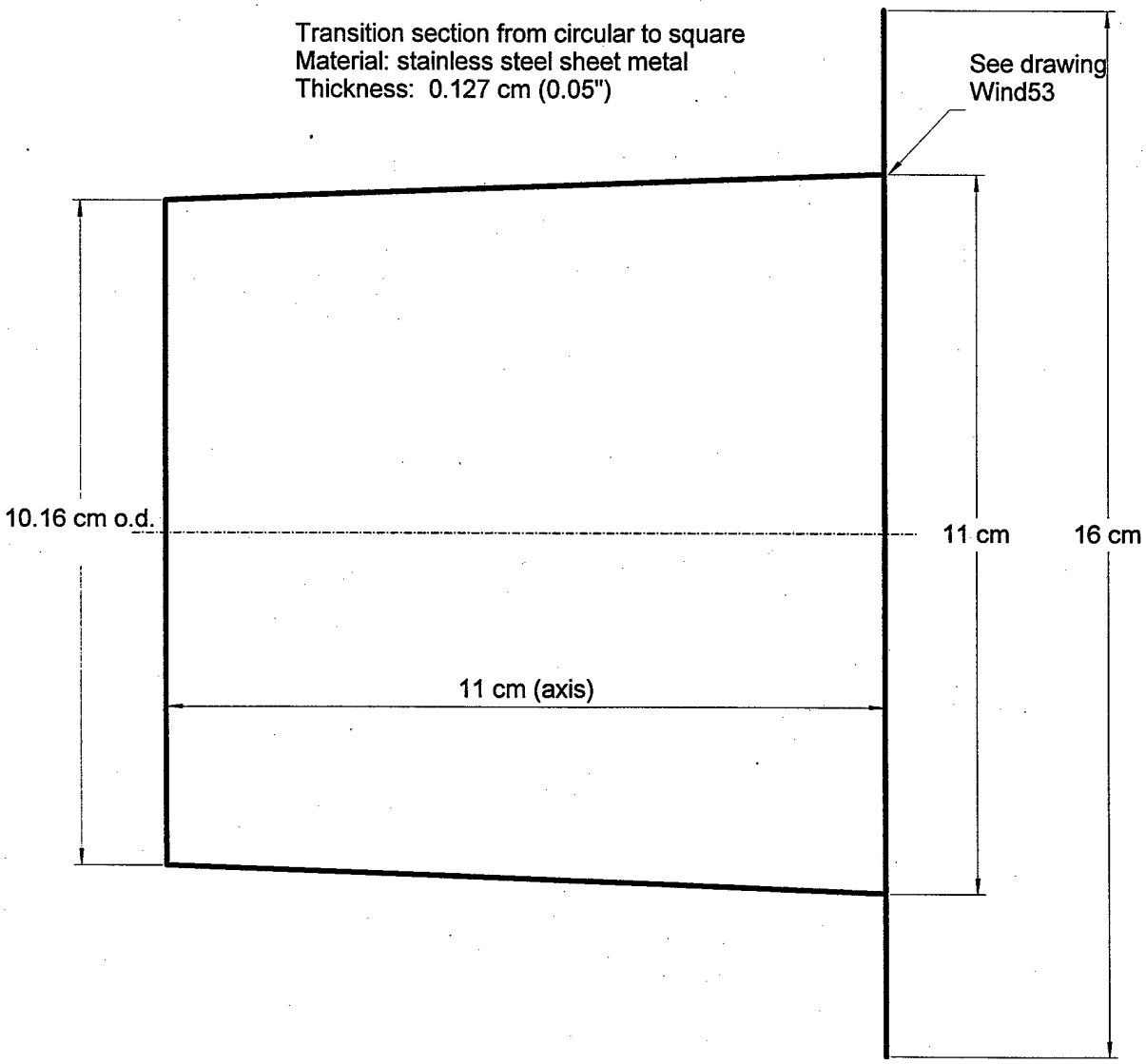

APPENDIX I (continued)

Flange (downstream of transition section)
Material: stainless steel sheet metal
Thickness: 0.127 cm (0.05")

Drawing: Wind53

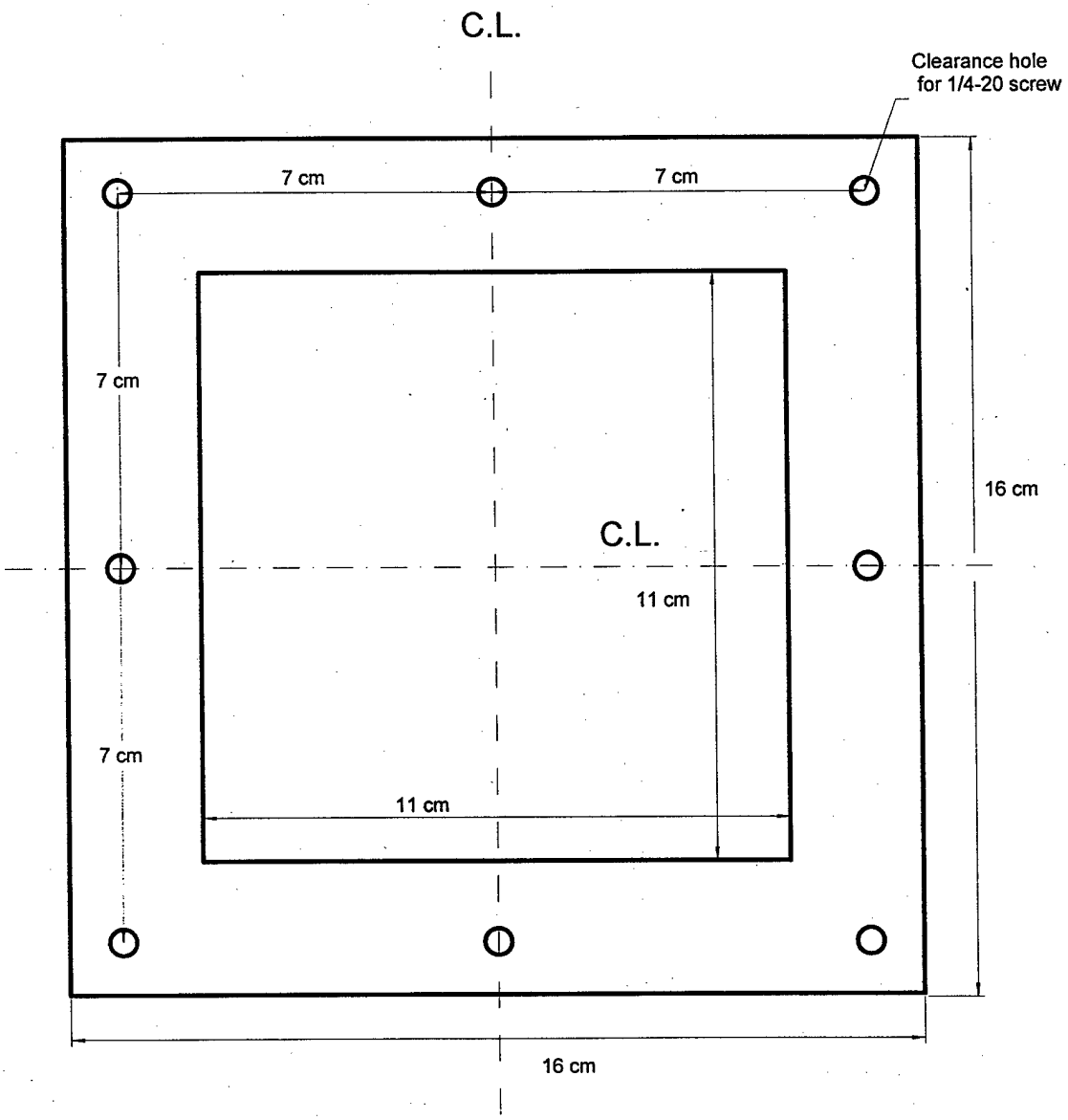

APPENDIX II

Drawing of the damper plate for the blower

Damper plate for blower
Material: Aluminum
Thickness: 0.318 cm (1/8")

Drawing: Wind62

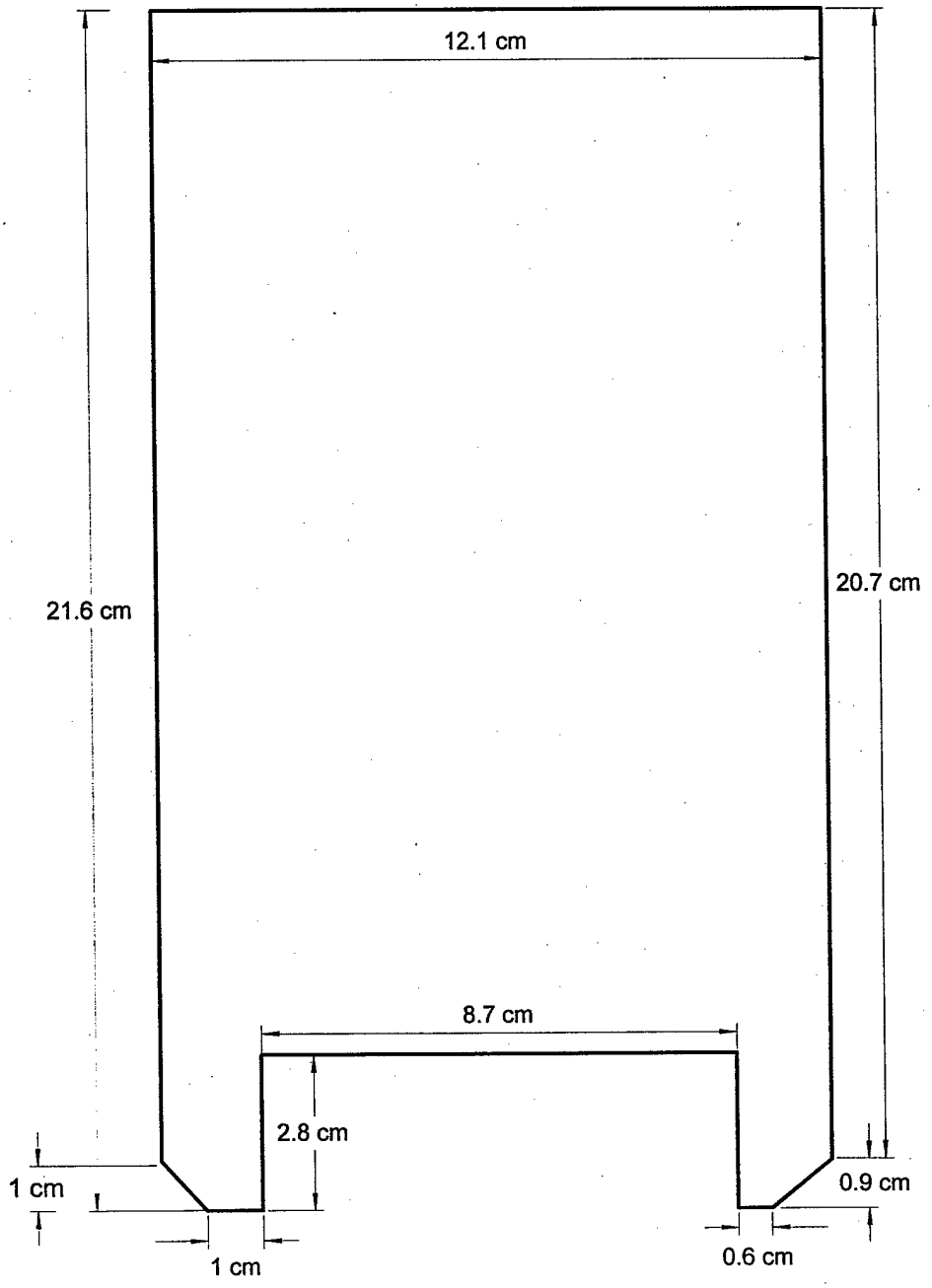

APPENDIX III

Drawings of the diffuser

Schematic showing how the four sides of the diffuser are connected

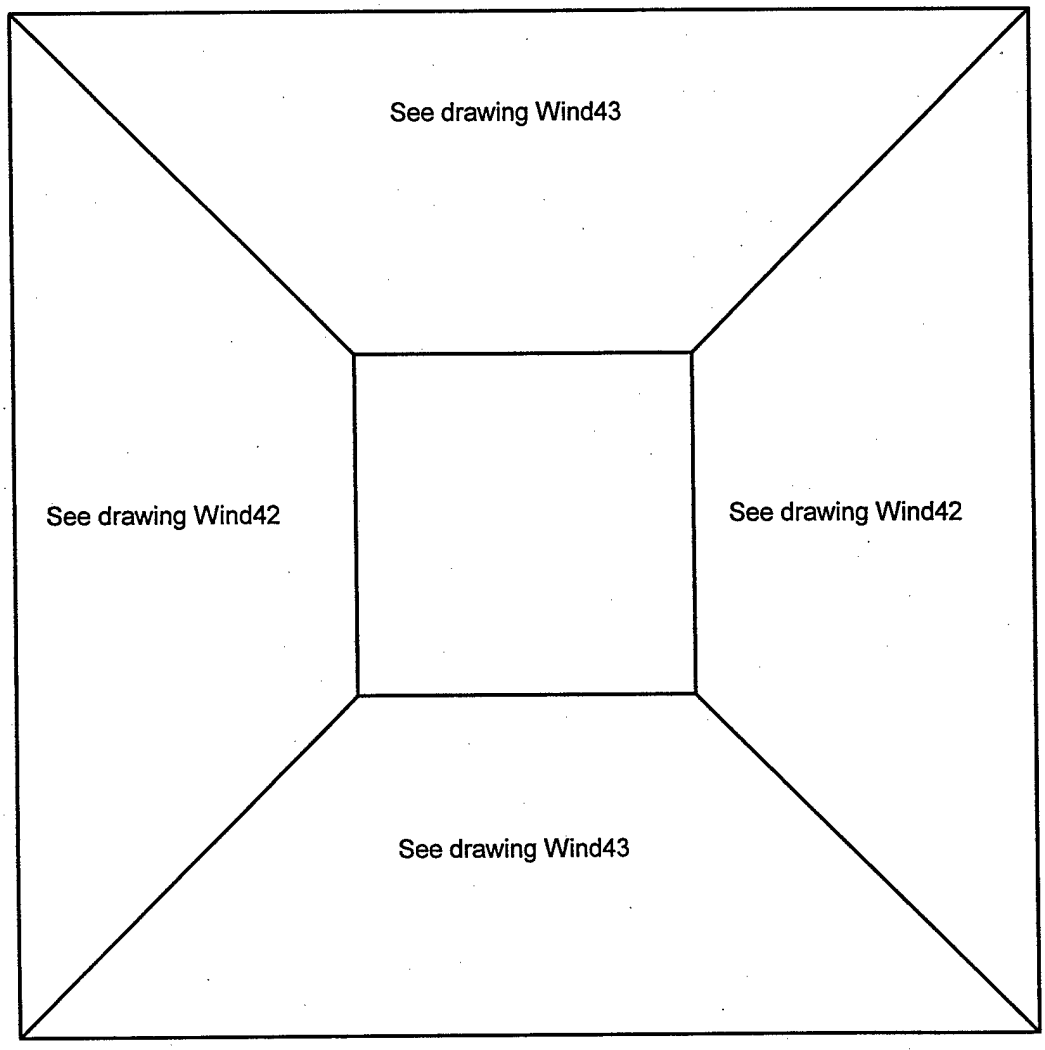

APPENDIX III (continued)

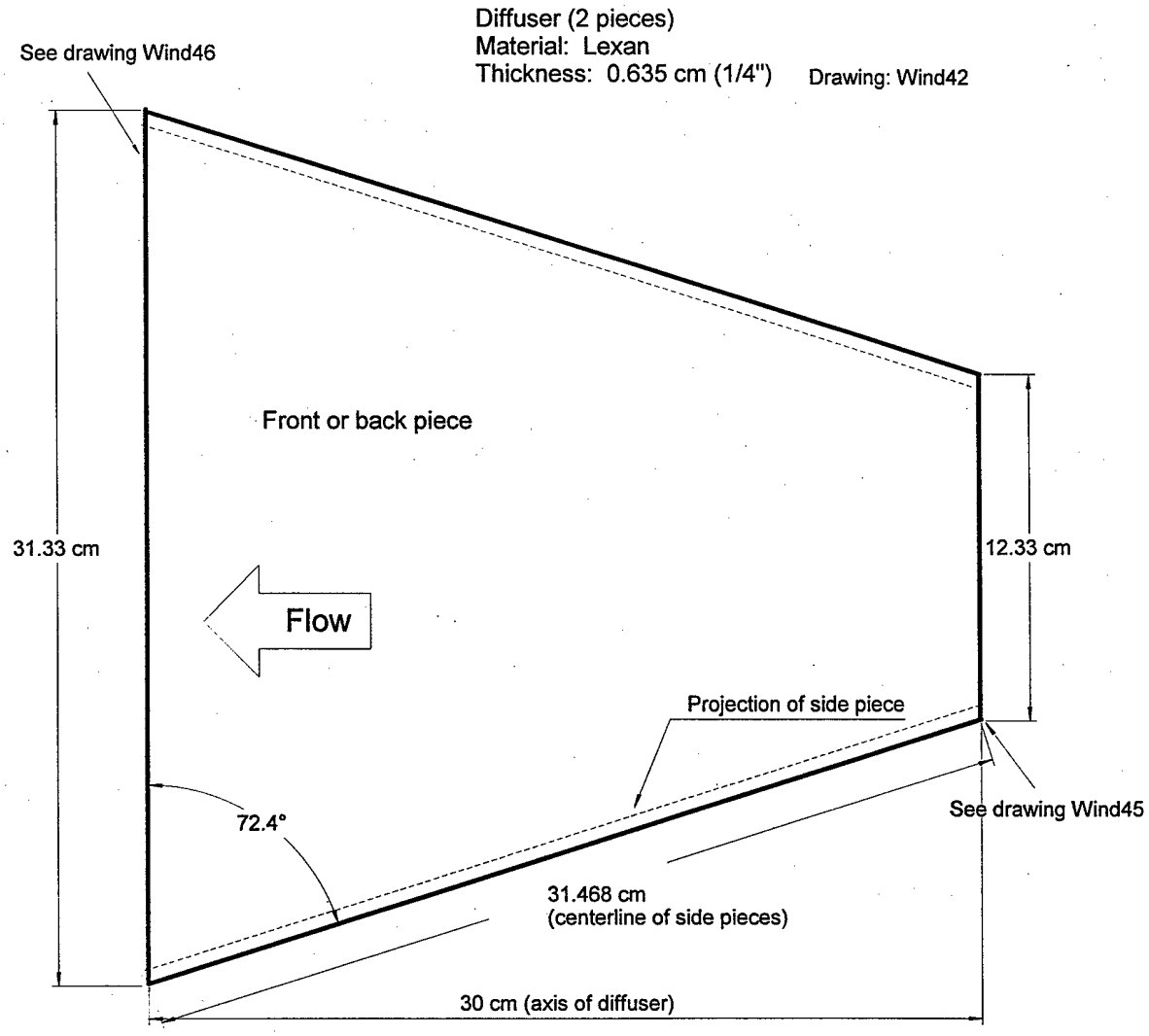

APPENDIX III (continued)

Diffuser (2 pieces)
Material: Lexan
Thickness: 0.635 cm (1/4")

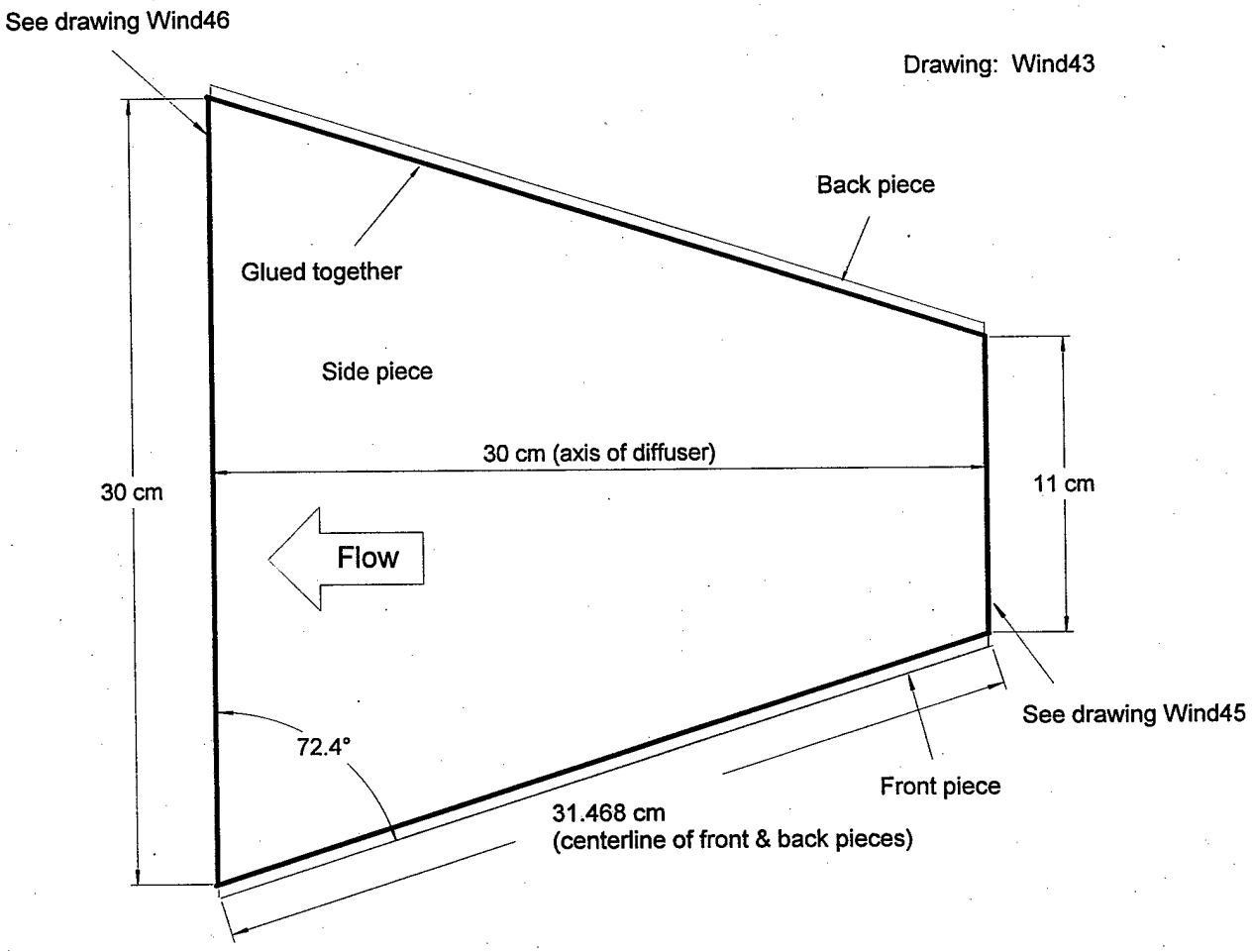

APPENDIX III (continued)

Flange (upstream of diffuser)
Material: Lexan
Thickness: 1.27 cm (1/2")

Drawing: Wind45

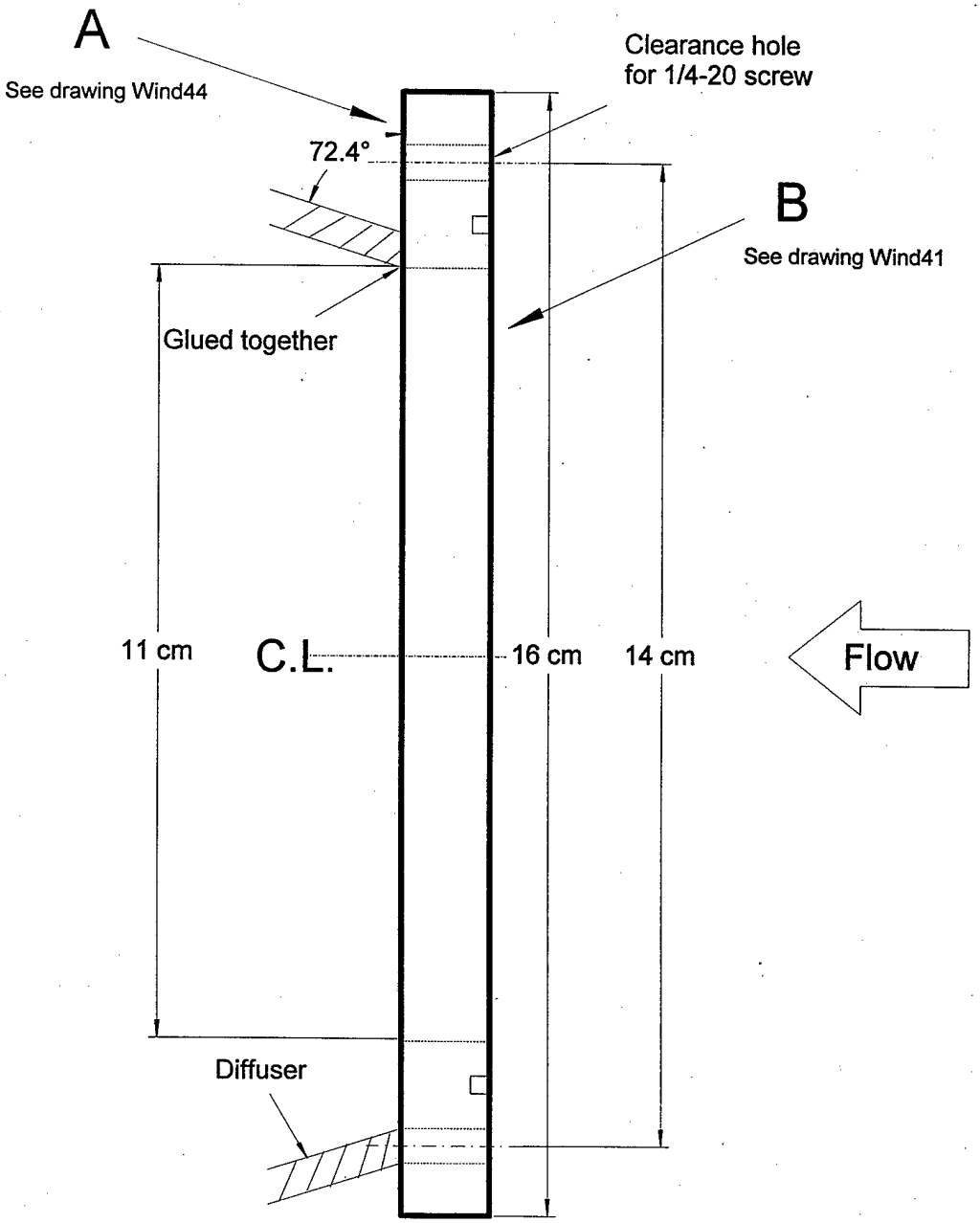

APPENDIX III (continued)

Flange (upstream of diffuser)
Material: Lexan
Thickness: 1.27 cm (1/2")

Drawing: Wind44

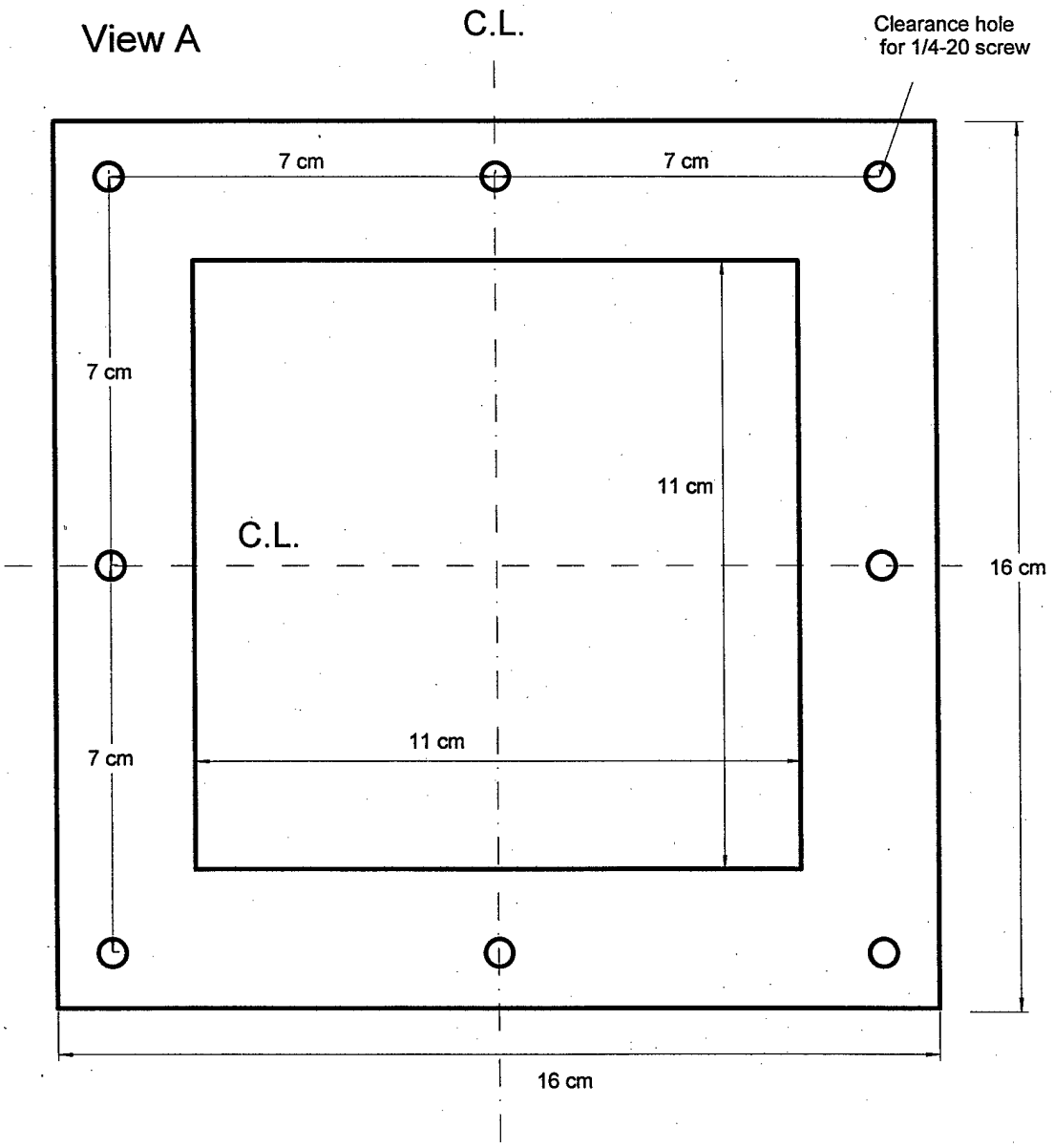

APPENDIX III (continued)

Flange (upstream of diffuser)
Material: Lexan
Thickness: 1.27 cm (1/2")

Drawing: Wind41

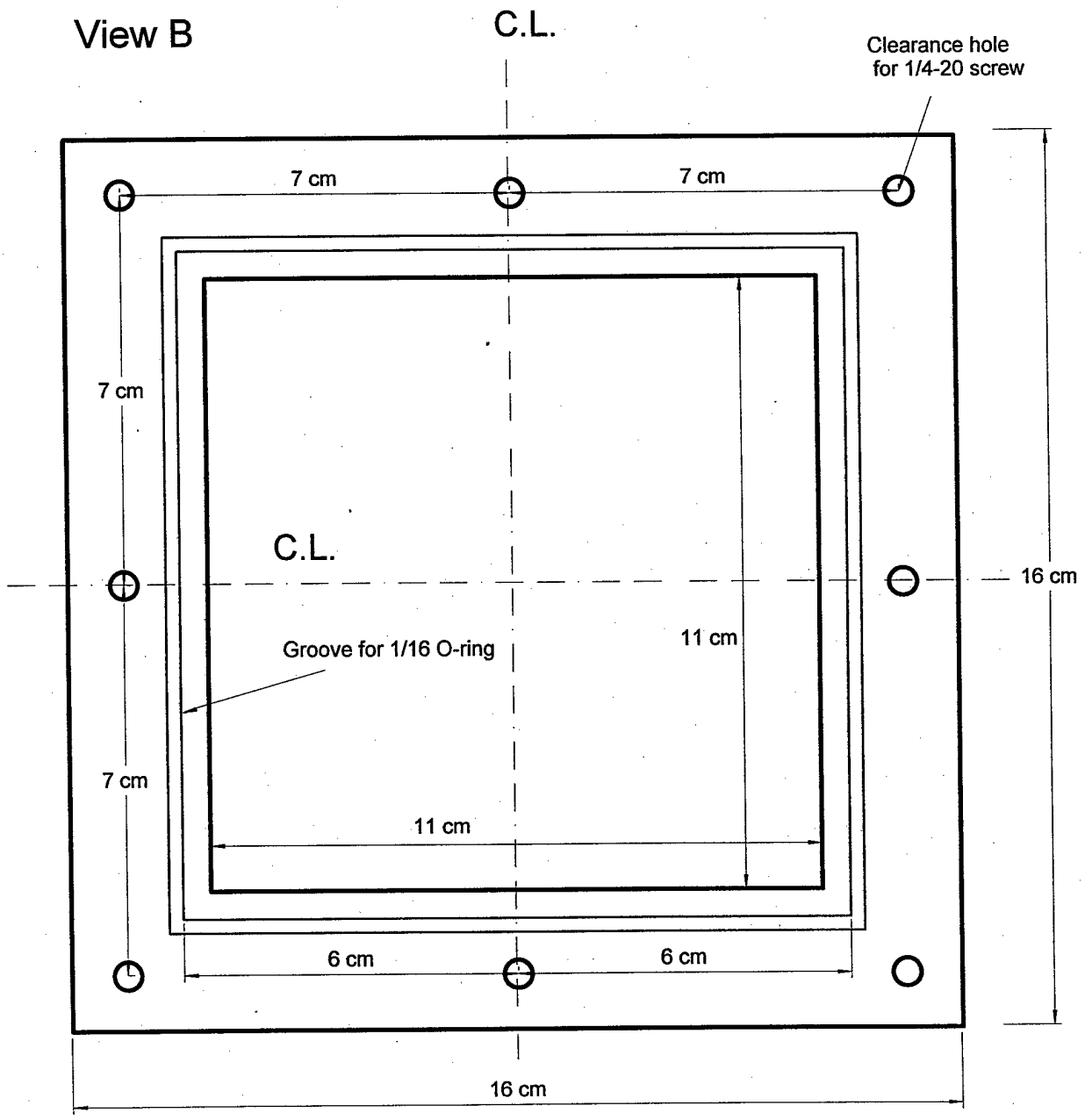

APPENDIX III (continued)

Flange (downstream of diffuser)
Material: Lexan
Thickness: 0.95 cm (3/8")

Drawing: Wind46

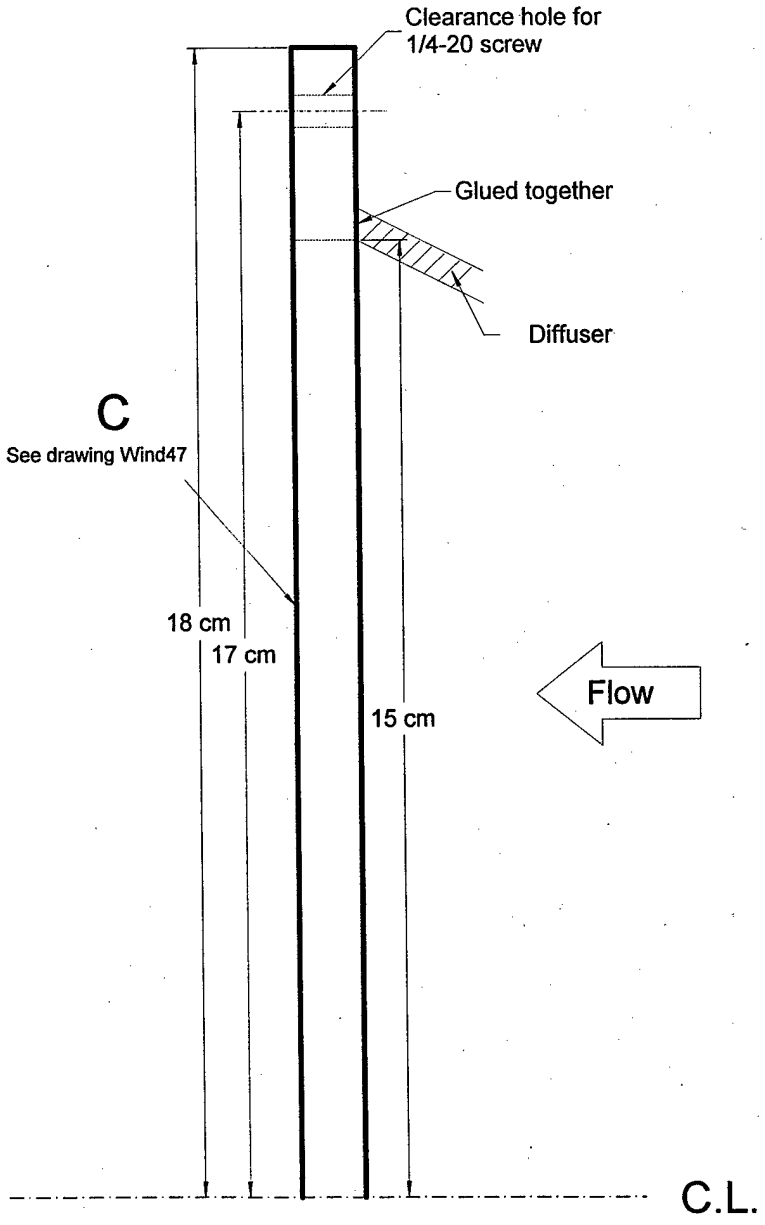

APPENDIX III (continued)

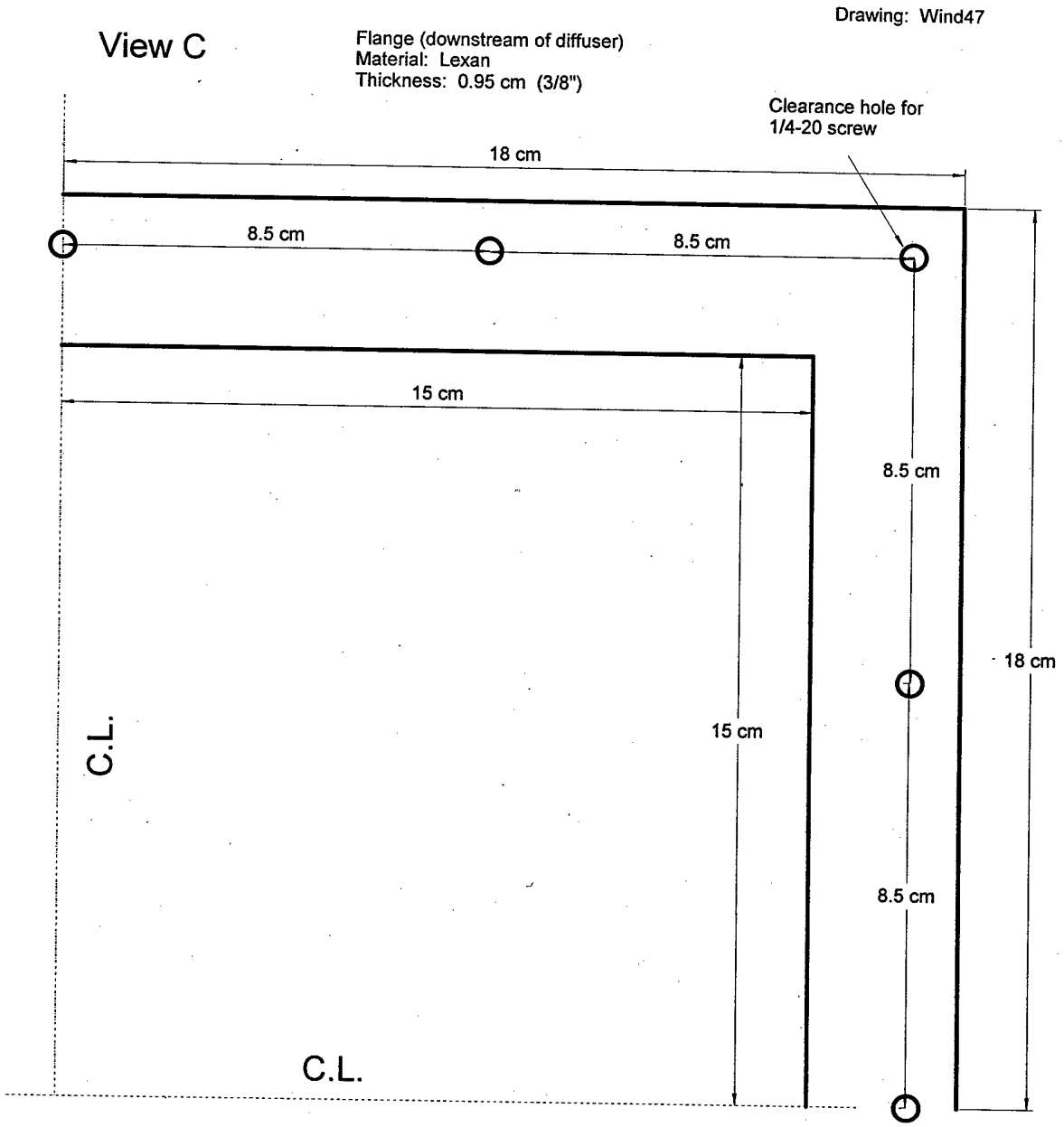

APPENDIX IV

Drawings of the honeycomb housing

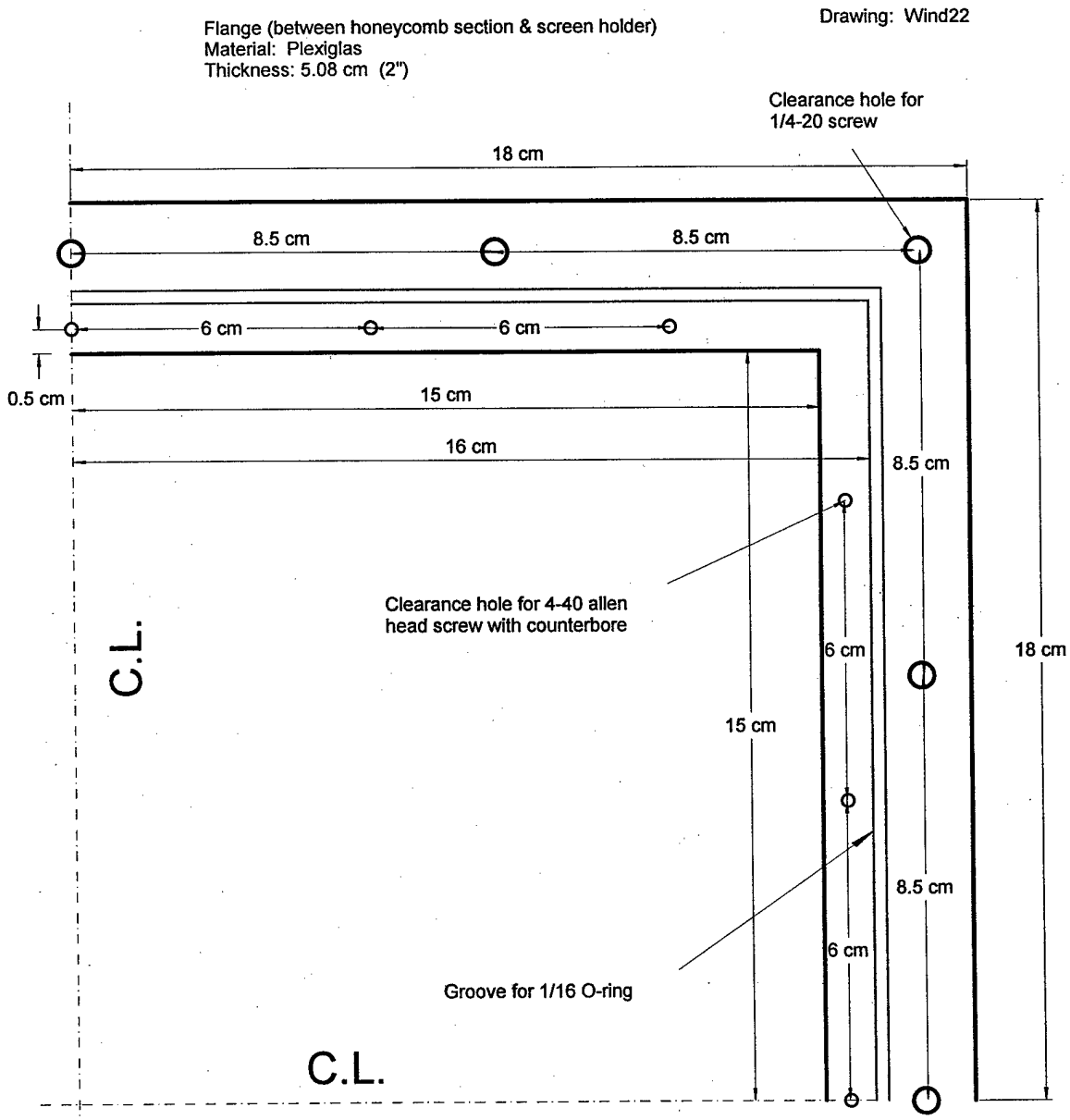

APPENDIX IV (continued)

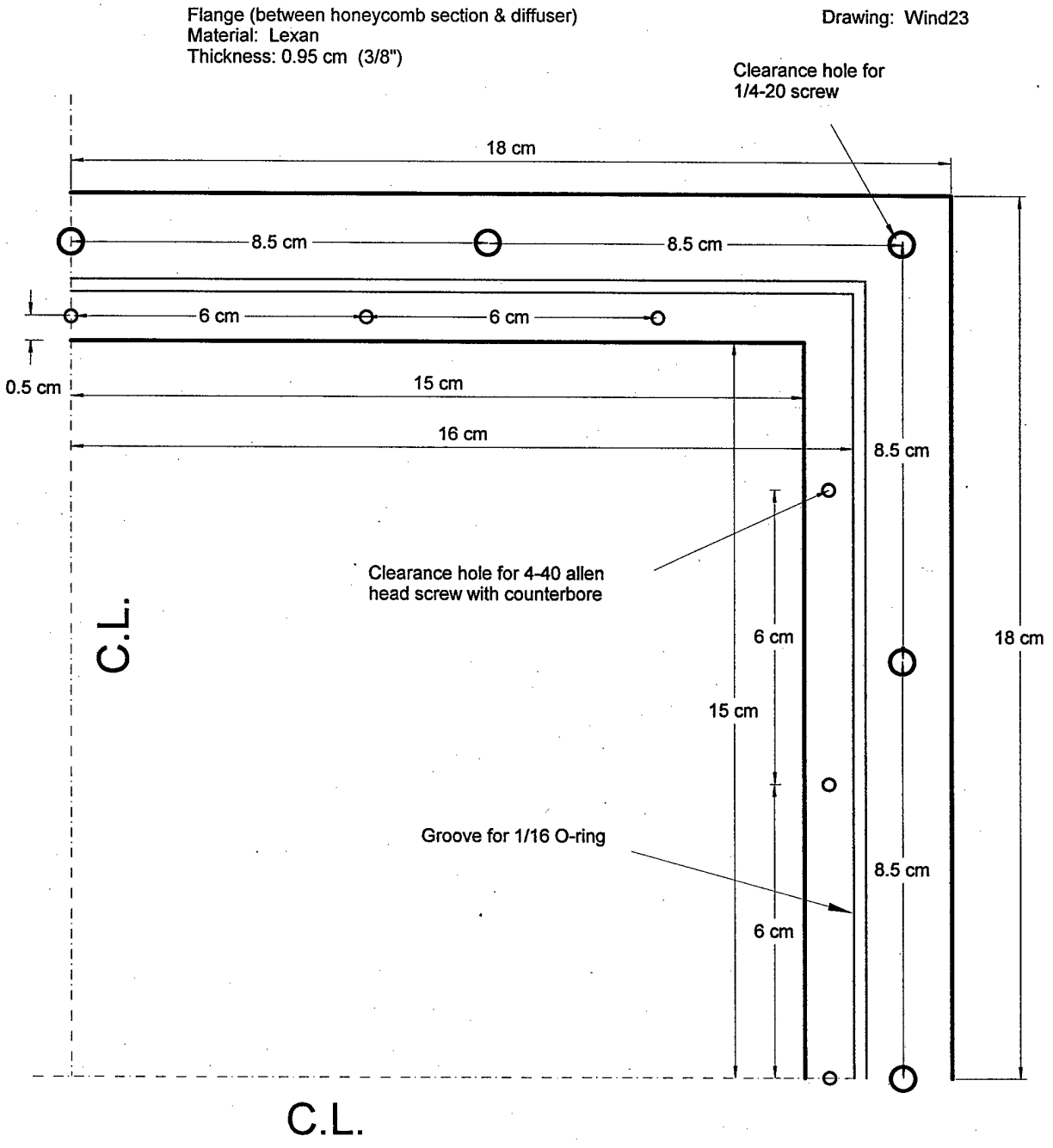

APPENDIX IV (continued)

Honey comb chamber
Material: Lexan
Thickness: 0.635 cm (1/4"); 2 pieces

Drawing: Wind24

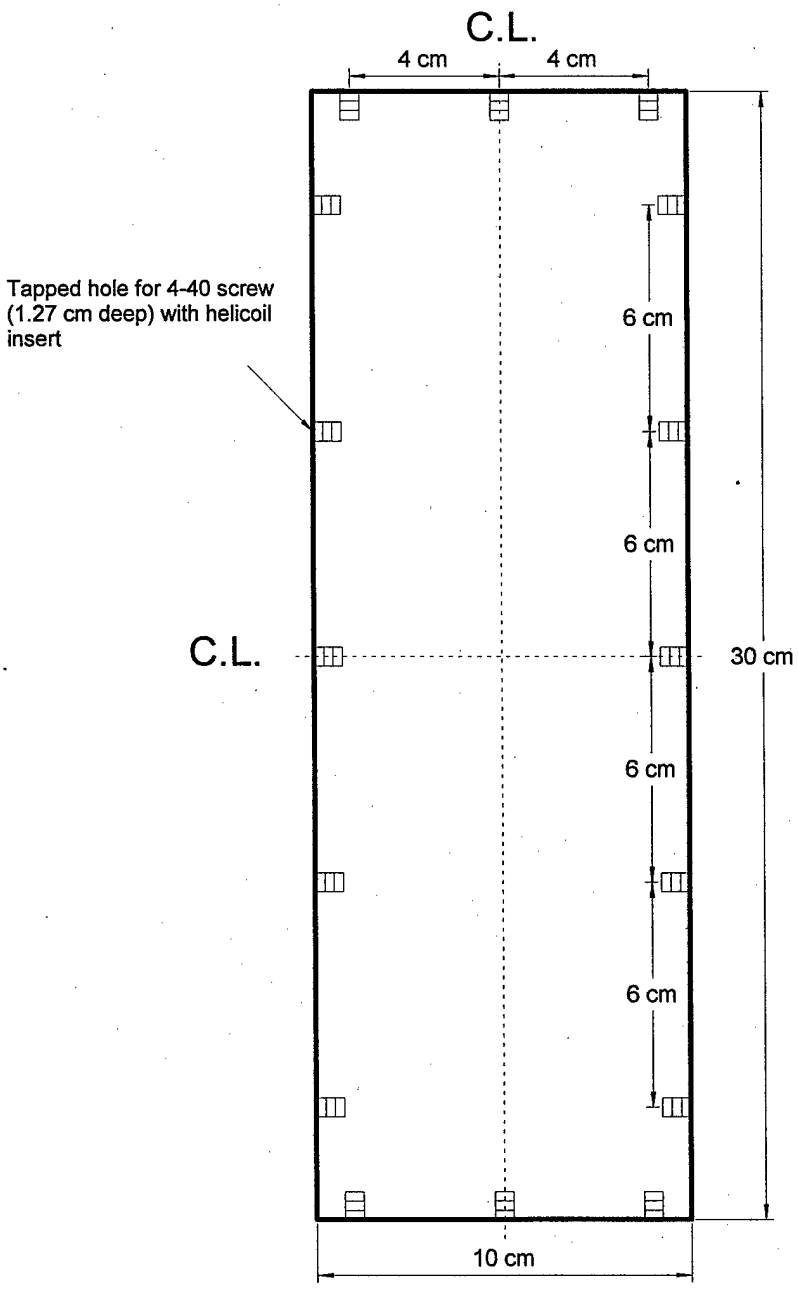

APPENDIX IV (continued)

Drawing: Wind25

Honey comb chamber
Material: Lexan
Thickness: 0.635 cm (1/4"); 2 pieces

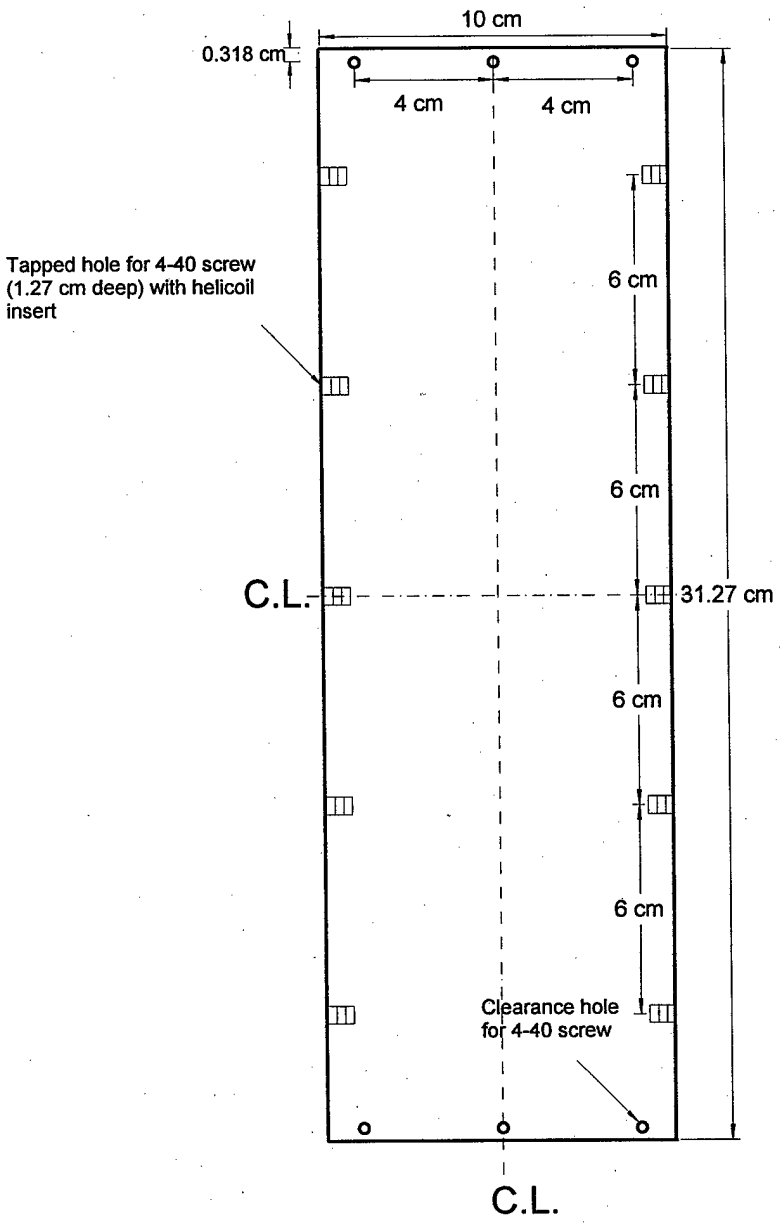

APPENDIX V

Drawings of the screen holder

Screen holder 1
Material: Aluminum
Thickness: 0.476 cm (3/16")

Drawing: Wind39

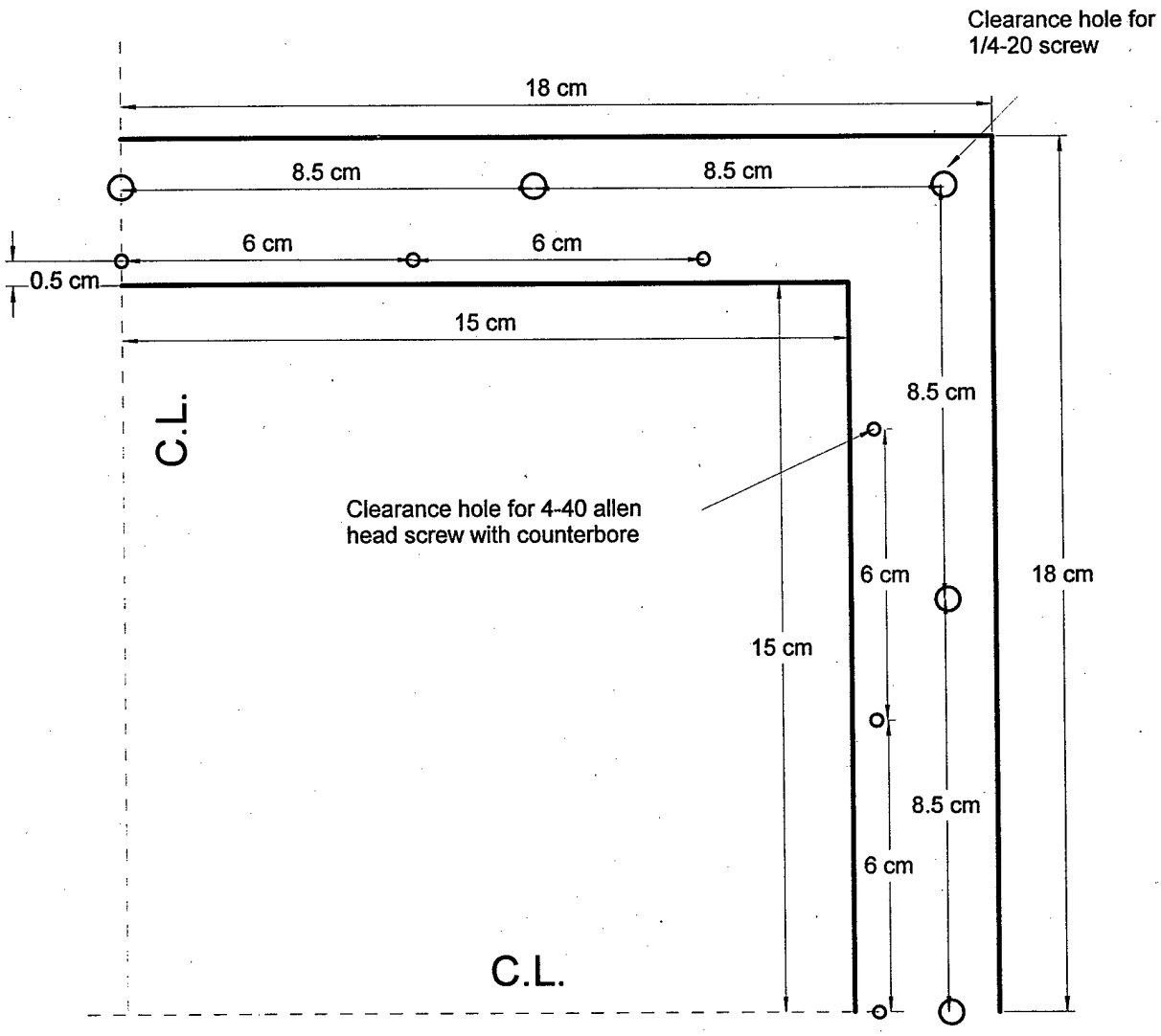

APPENDIX V (continued)

Screen holder 2
Material: Aluminum
Thickness: 0.318 cm (1/8")

Drawing: Wind40

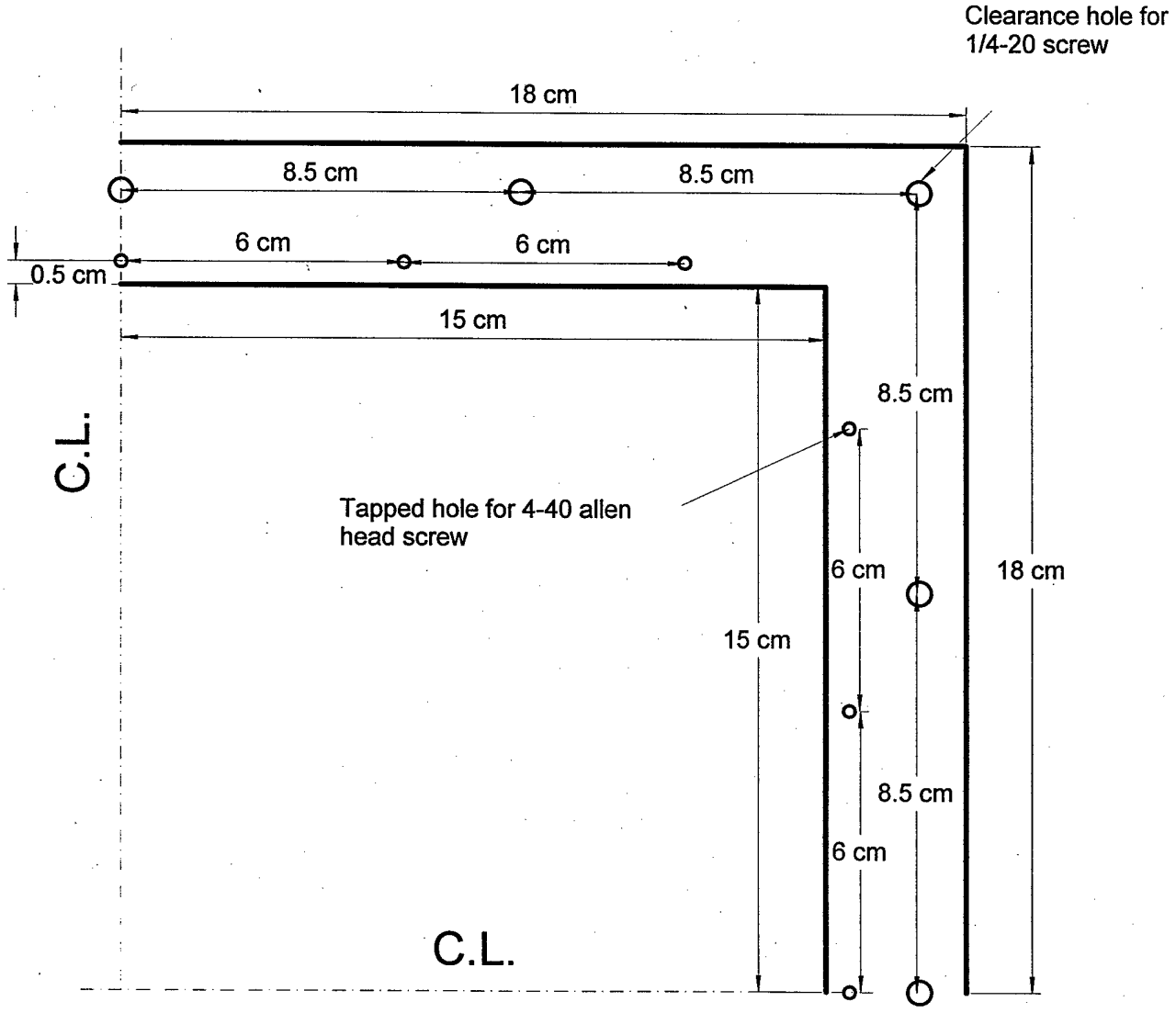

APPENDIX VI

Drawings of the settling chamber

Settling chamber (A)
Material: Lexan
Thickness: 0.635 cm (1/4")

Drawing: Wind19

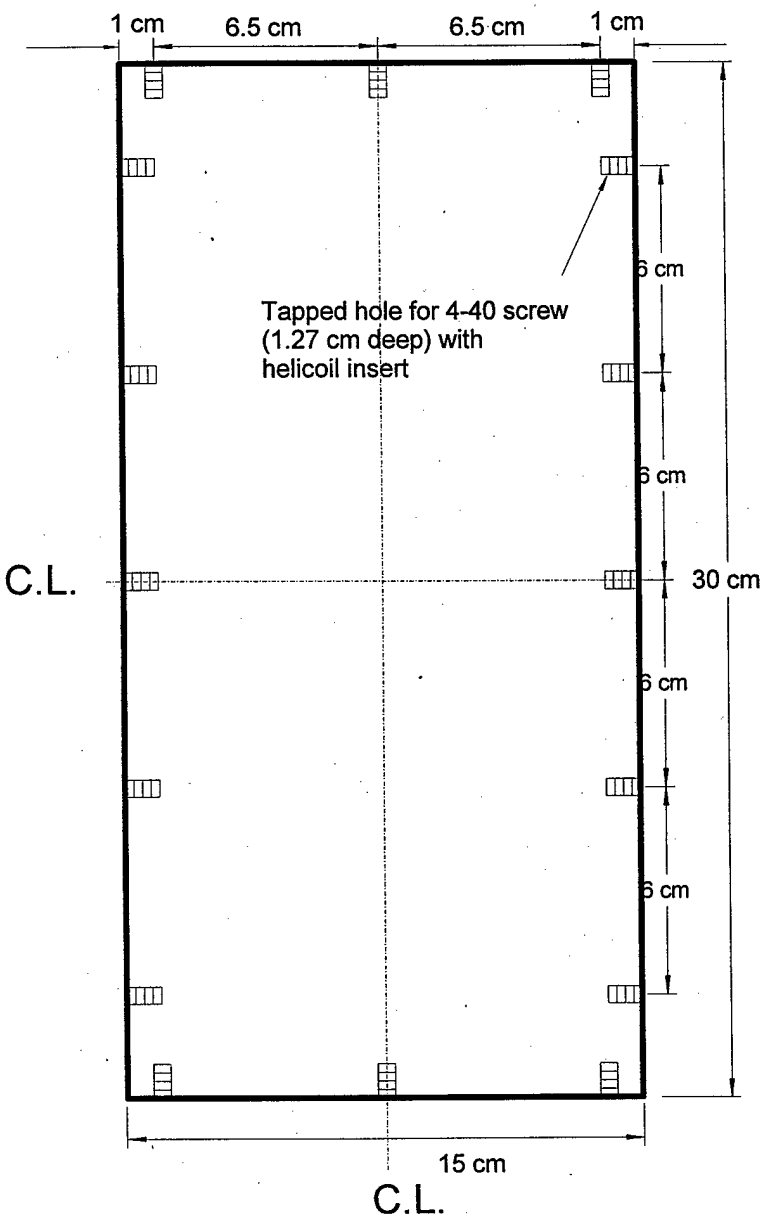

APPENDIX VI (continued)

Settling chamber (B) Drawing: Wind20
Material: Lexan
Thickness: 0.635 cm (1/4"); 2 pieces

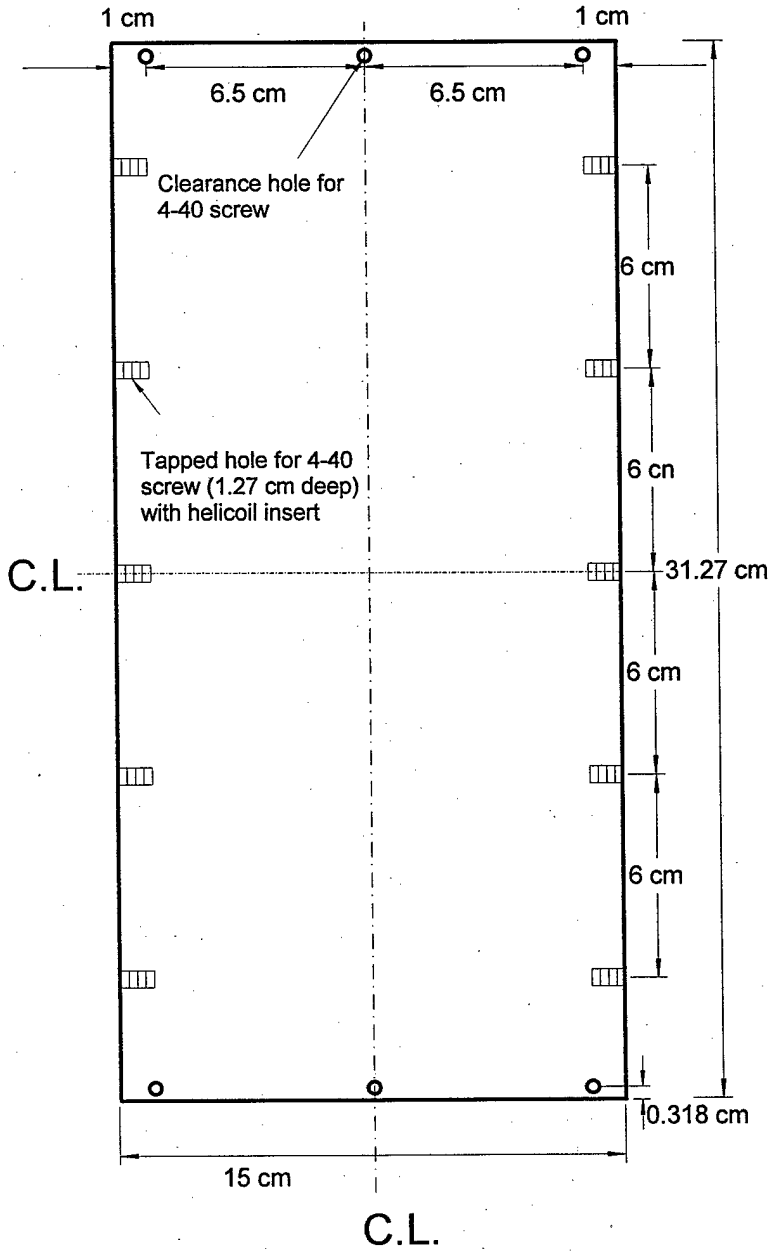

APPENDIX VI (continued)

Settling chamber (C)
Material: Lexan
Thickness: 0.635 cm (1/4")

Drawing: Wind17

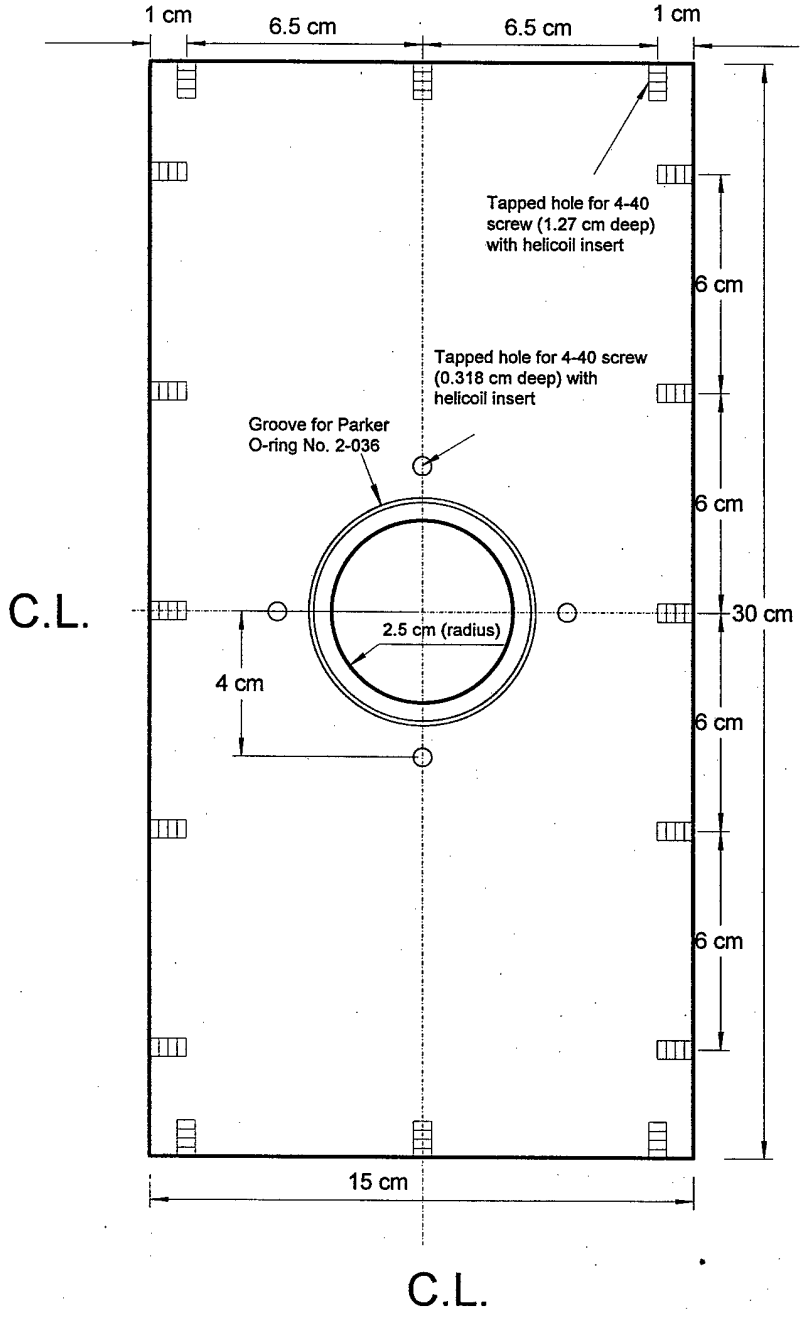

APPENDIX VI (continued)

Settling chamber (flange)
Material: Lexan
Thickness: 0.95 cm (3/8") ; 2 pieces

Drawing: Wind21

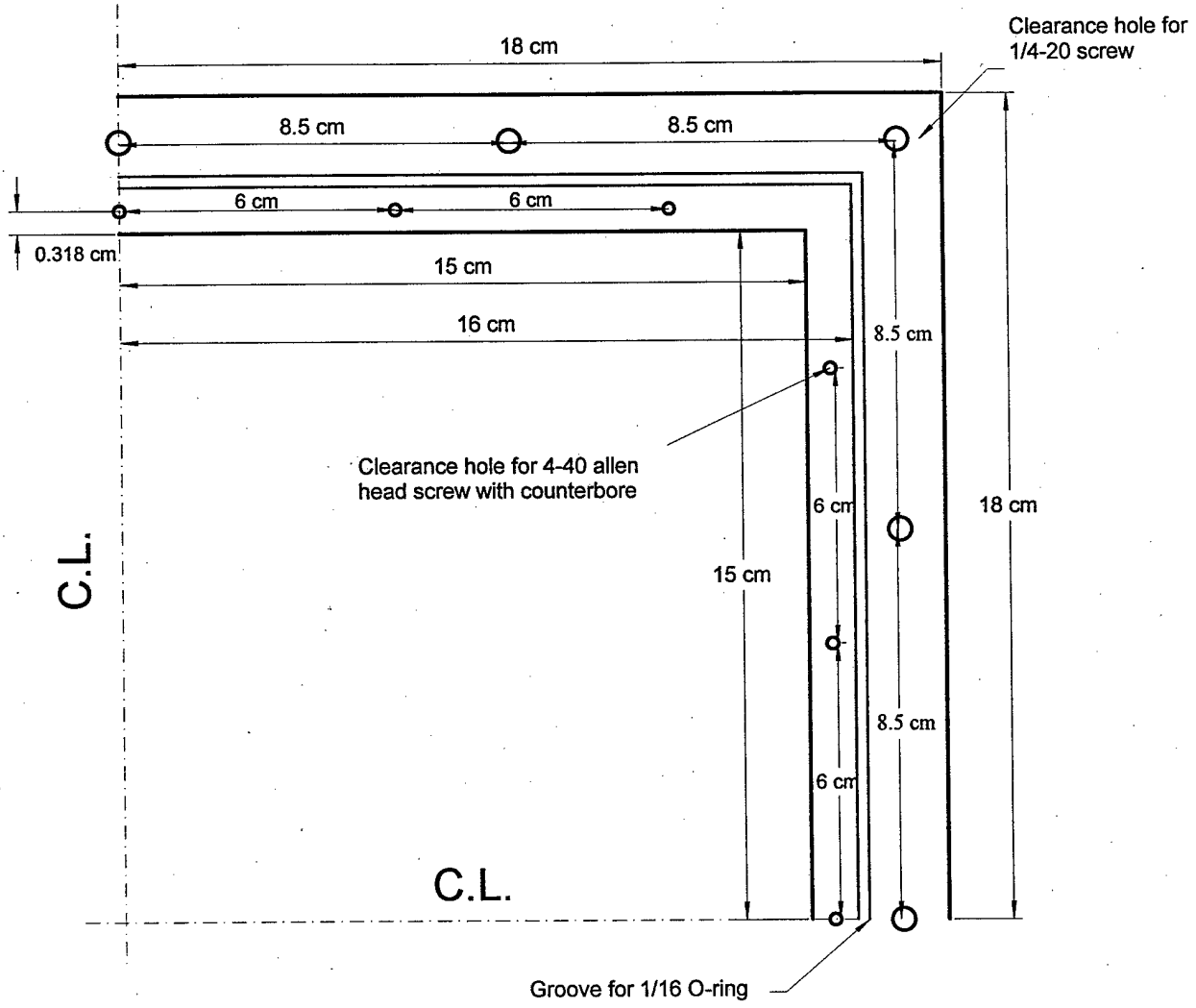

APPENDIX VII

Drawings of the contraction section

Schematic showing how the four sides
of the contraction section are connected

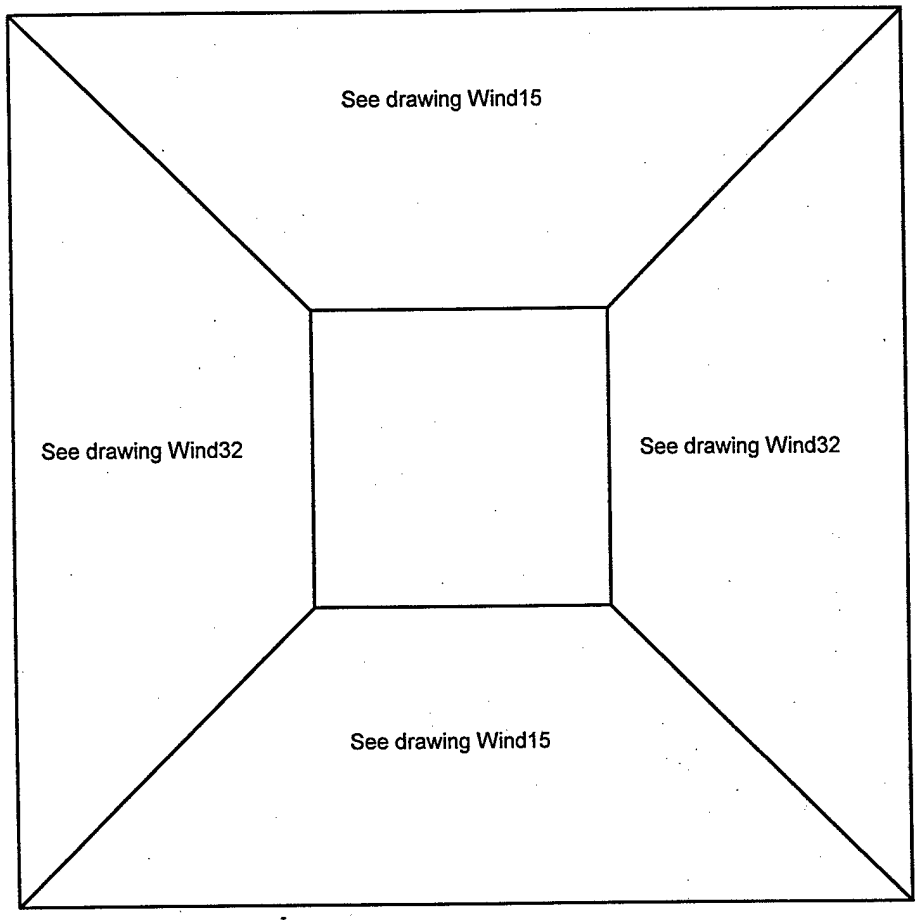

APPENDIX VII (continued)

Drawing: Wind15

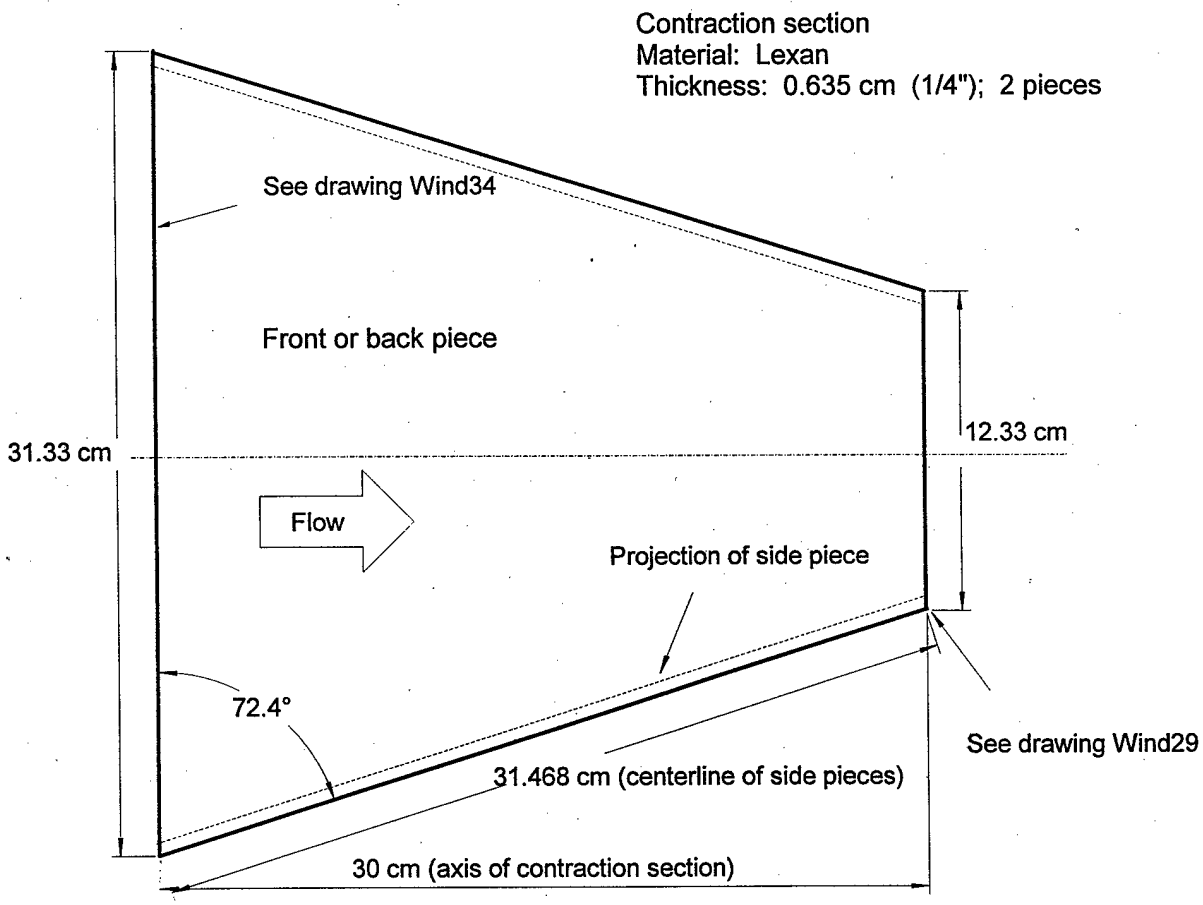

APPENDIX VII (continued)

Contraction section
Material: Lexan
Thickness: 0.635 cm (1/4"); 2 pieces

Drawing: Wind32

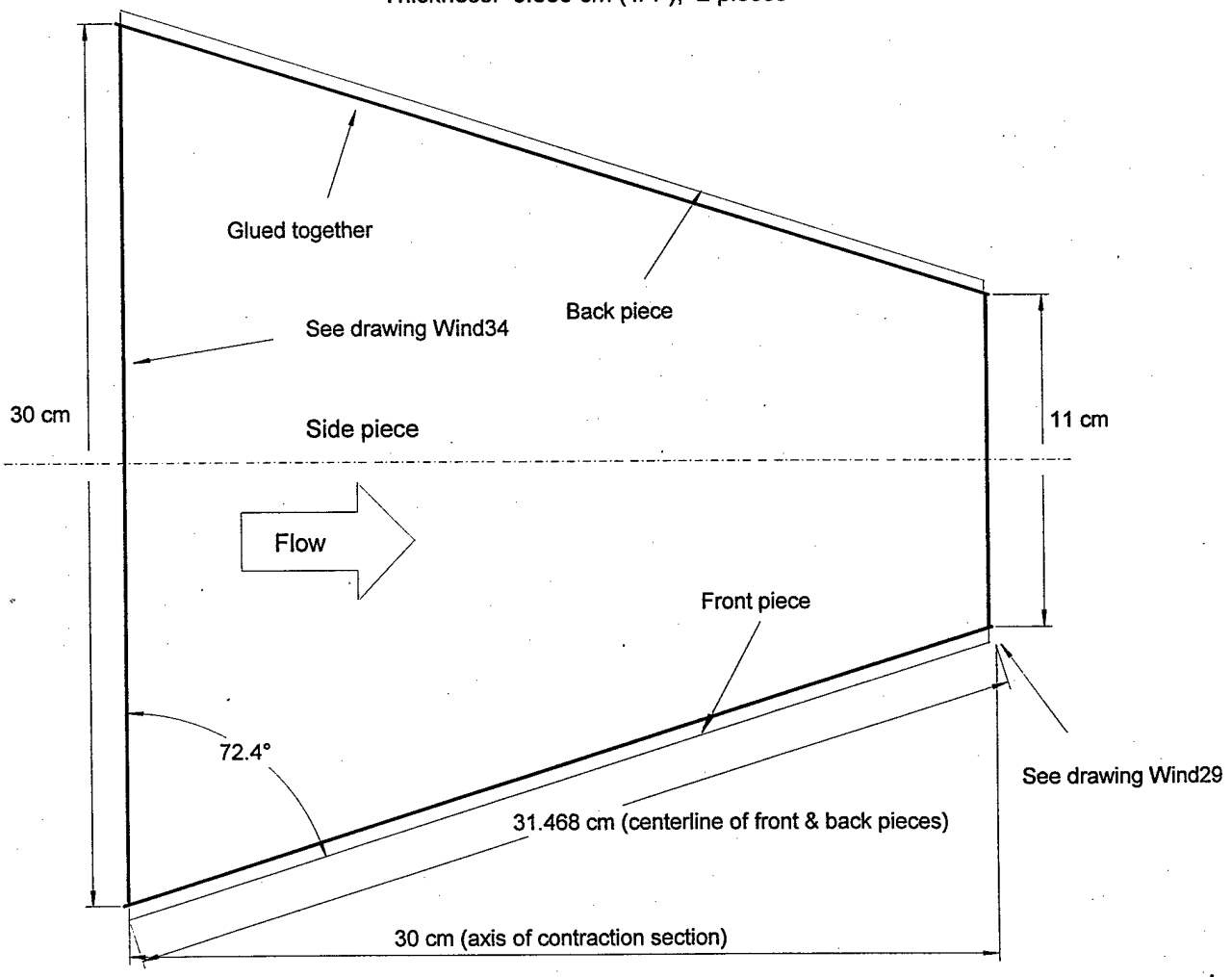

APPENDIX VII (continued)

Flange (upstream of contraction section)
Material: Lexan
Thickness: 0.95 cm (3/8"); 2 pieces

Drawing: Wind33

View C

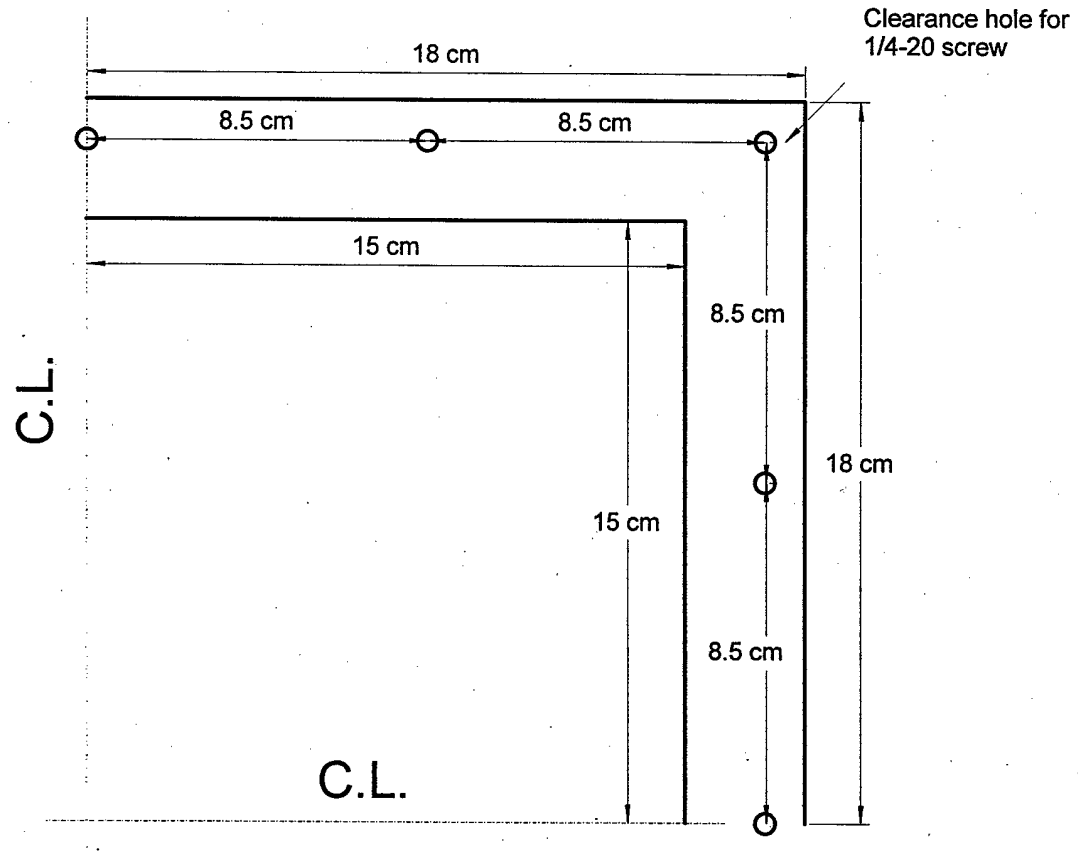

APPENDIX VII (continued)

Flange (upstream of contraction section) Drawing: Wind34
Material: Lexan
Thickness: 0.95 cm (3/8")

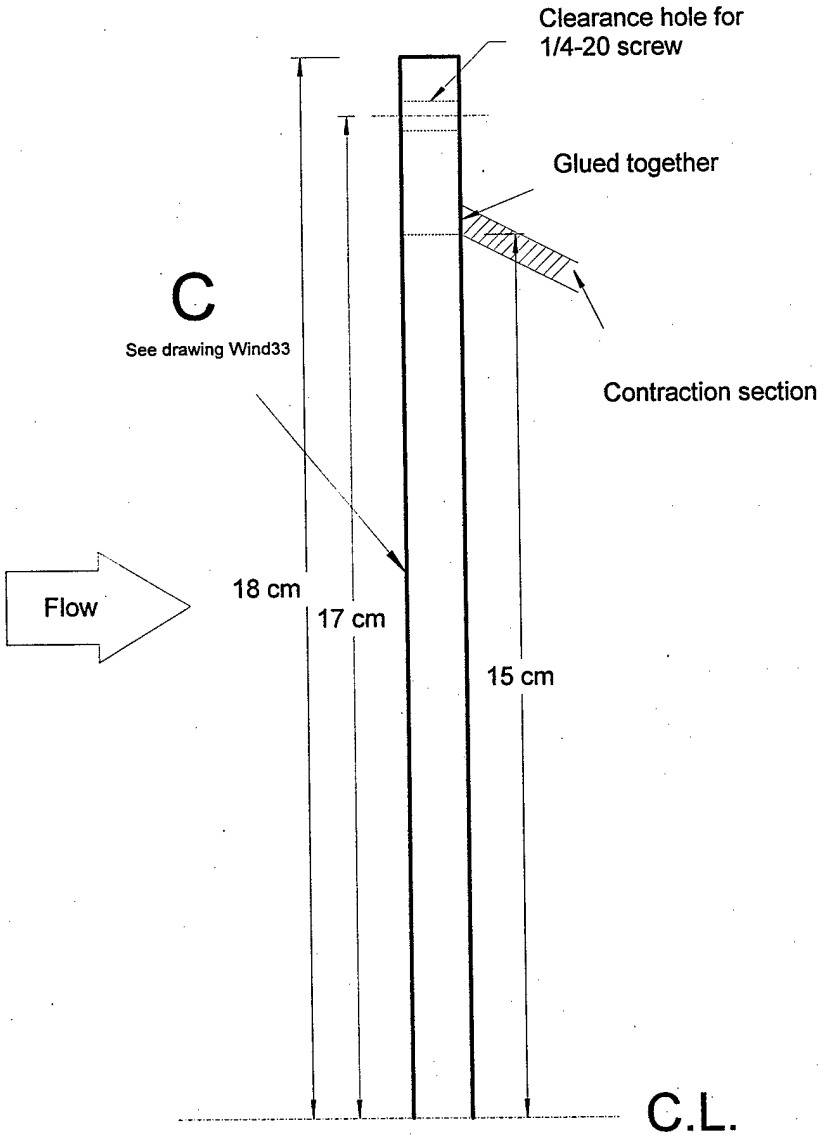

APPENDIX VIII

Drawings of the transition flange

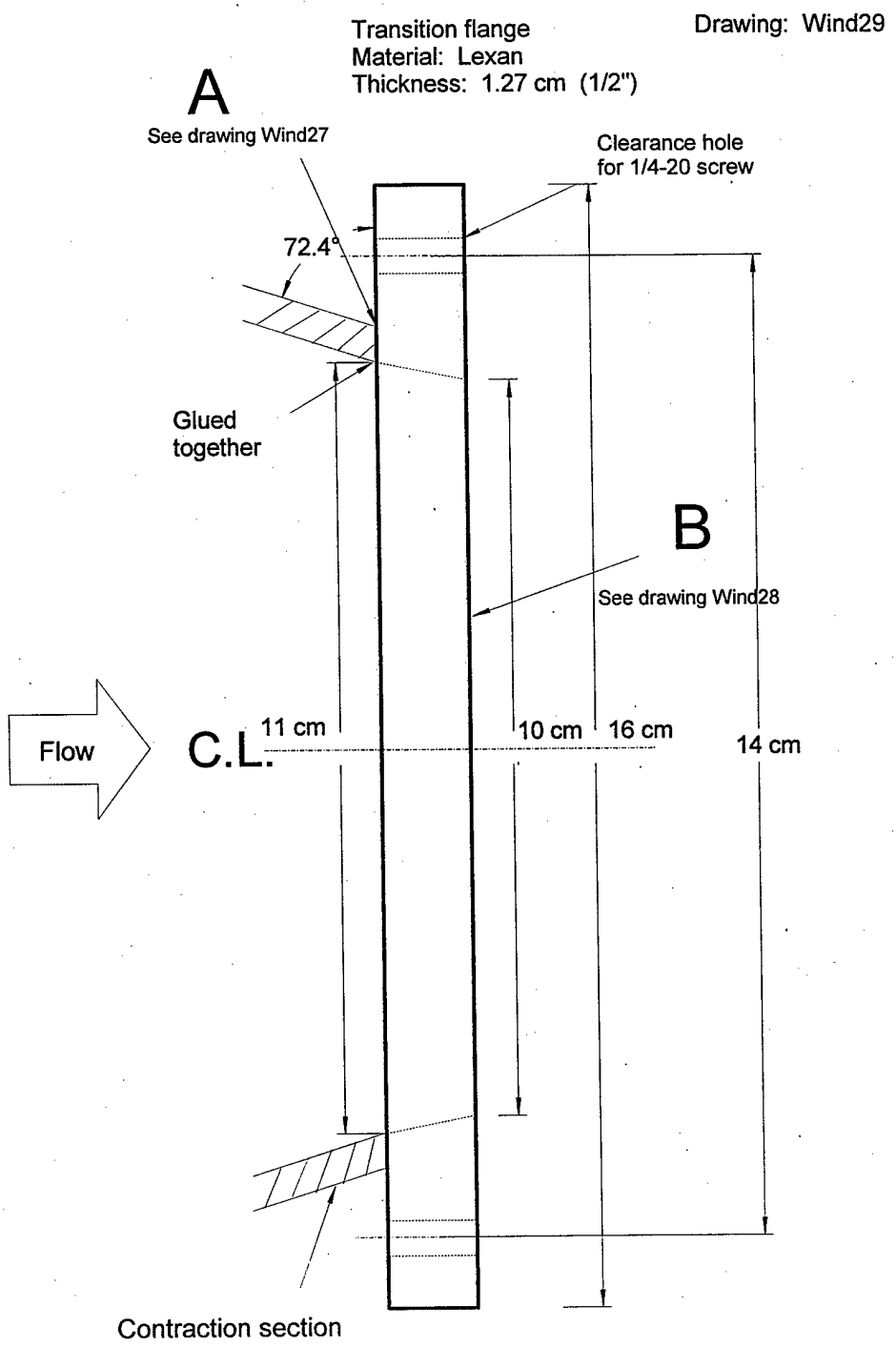

APPENDIX VIII (continued)

Transition flange
Material: Lexan
Thickness: 1.27 cm (1/2")

Drawing: Wind27

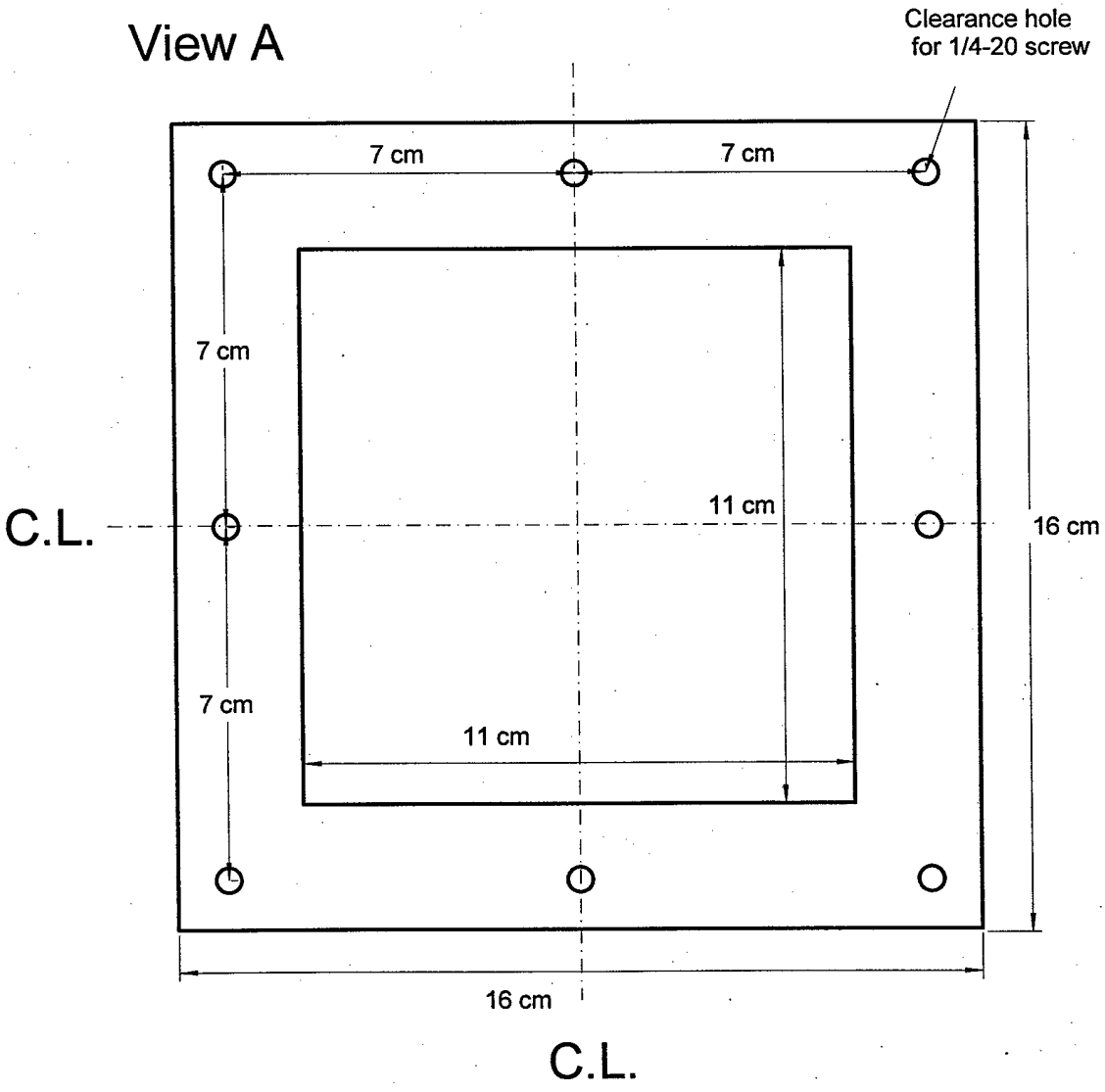

APPENDIX VIII (continued)

Transition flange
Material: Lexan
Thickness: 1.27 cm (1/2")

Drawing: Wind28

Clearance hole
for 1/4-20 screw

View B

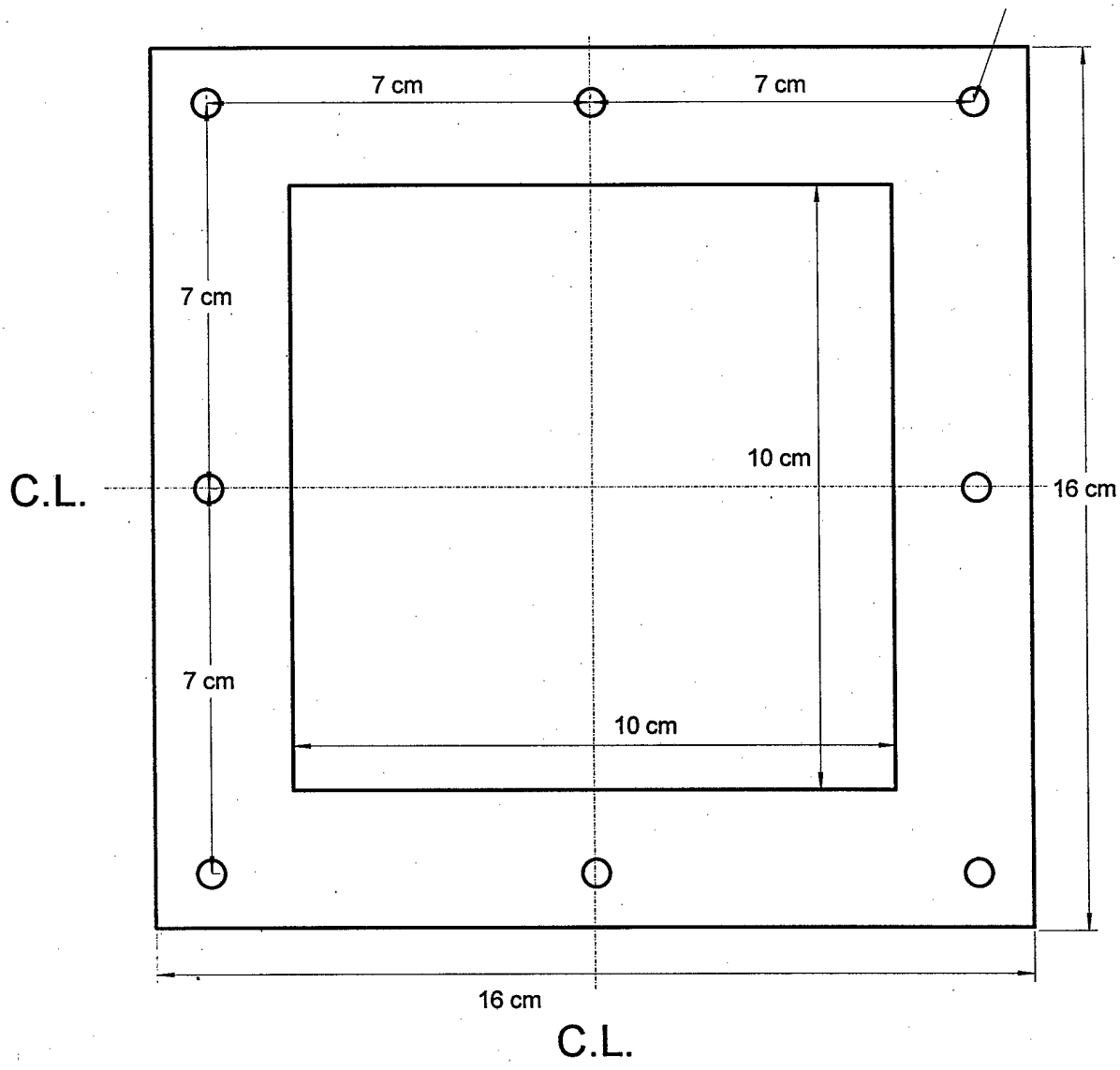

APPENDIX IX

Drawings of the test section

Test Section
Material: Aluminum
Thickness: 0.635 cm (1/4")

Drawing: Wind54

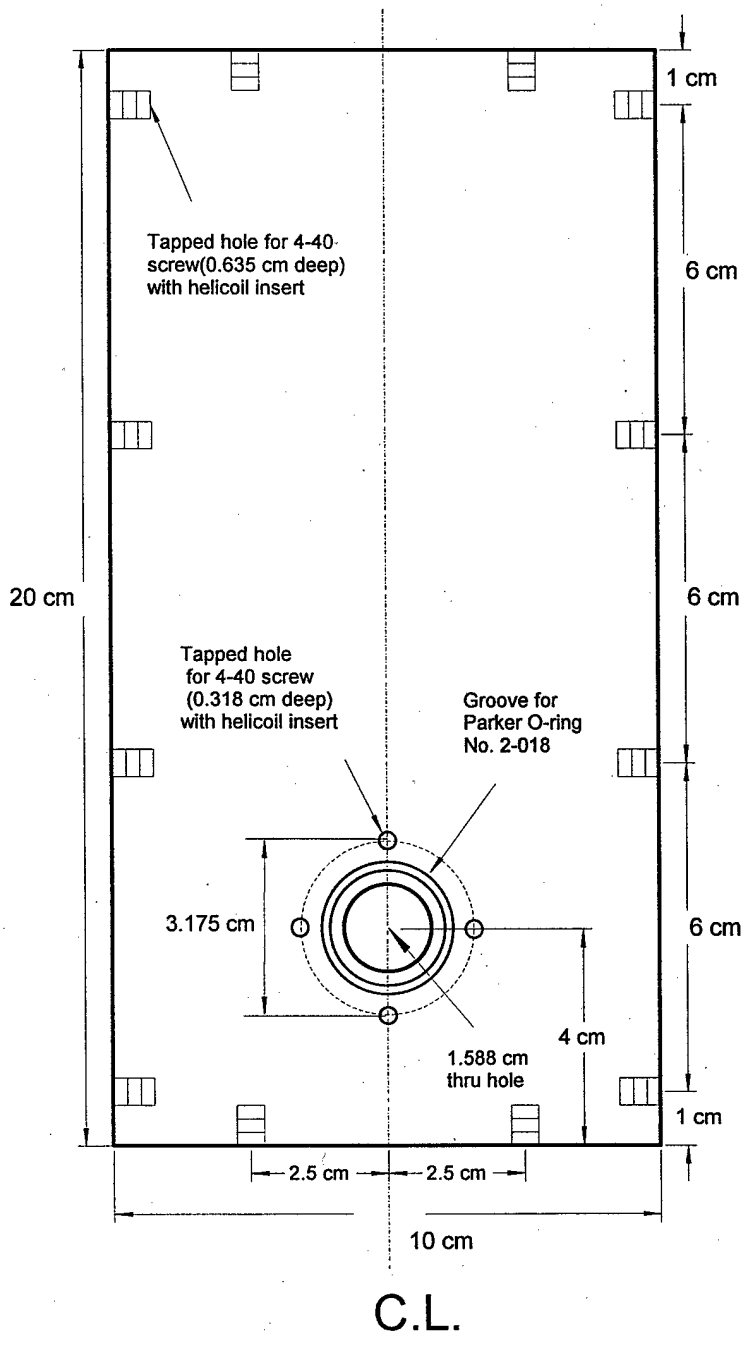

APPENDIX IX (continued)

Test Section (2 pieces)
Material: Aluminum
Thickness: 0.635 cm (1/4")

Drawing: Wind 55

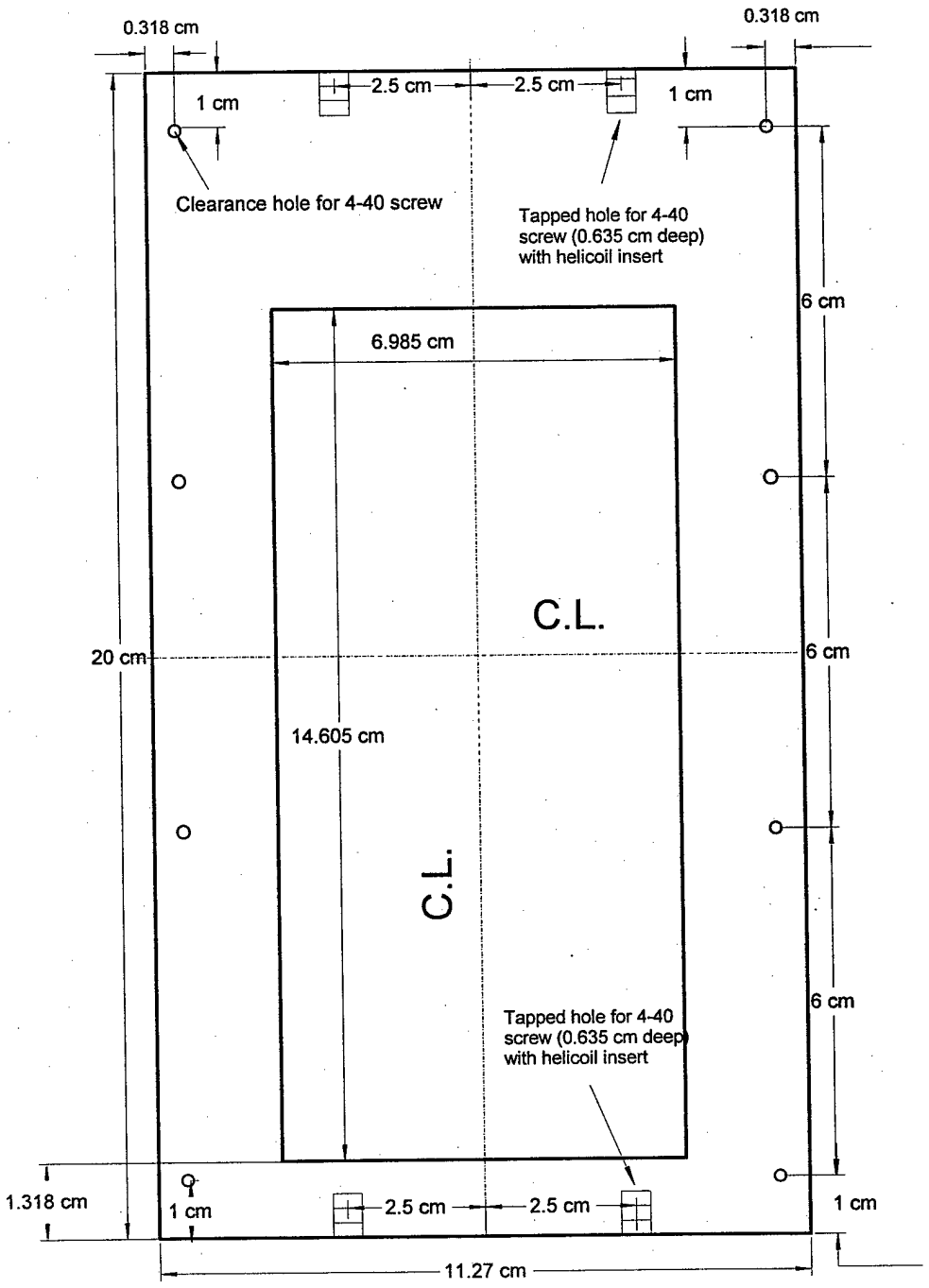

APPENDIX IX (continued)

Test Section
Material: Aluminum
Thickness: 0.635 cm (1/4")

Drawing: Wind 57

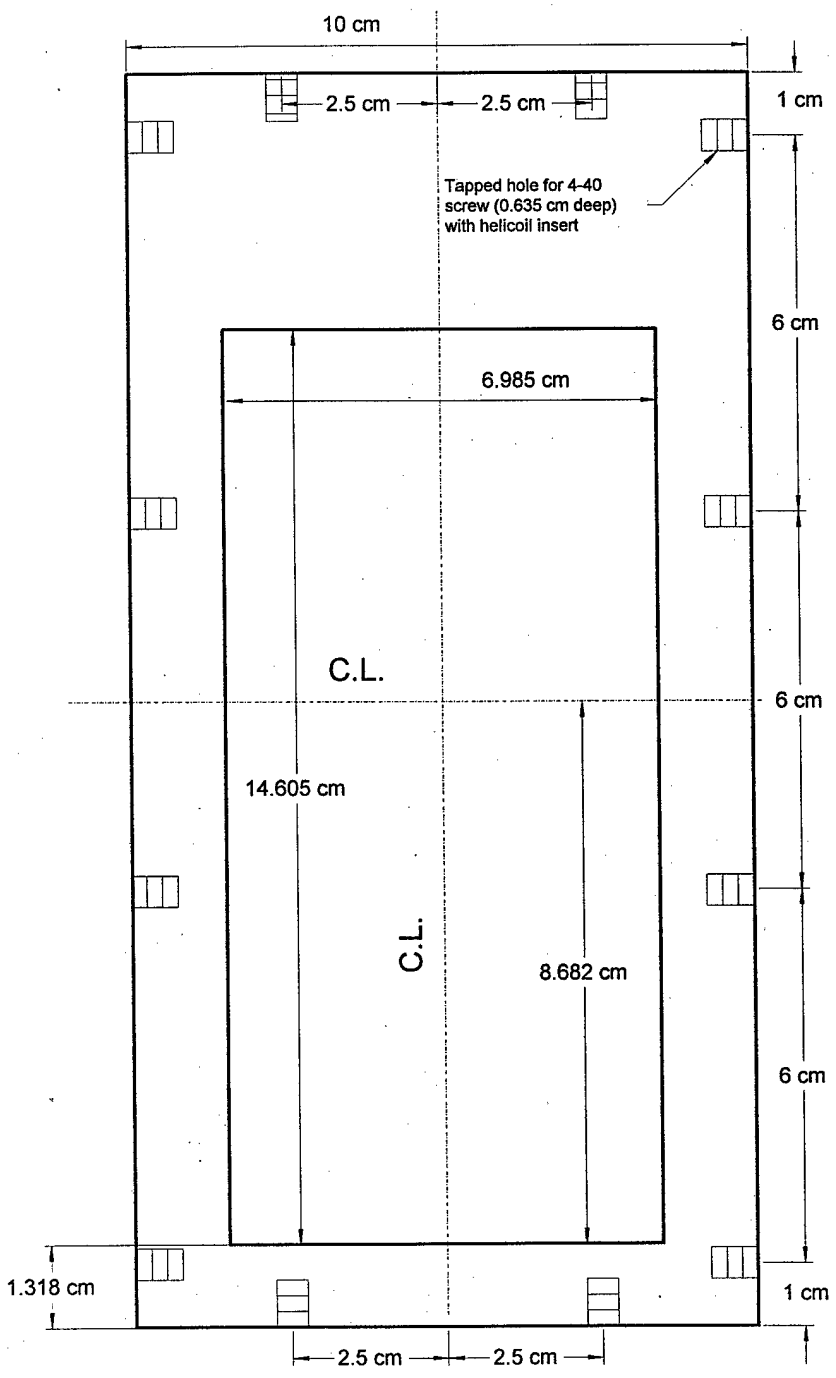

APPENDIX IX (continued)

Test section (window for drawing Wind57)
Material: Pyrex
Thickness: 0.635 cm (1/4")

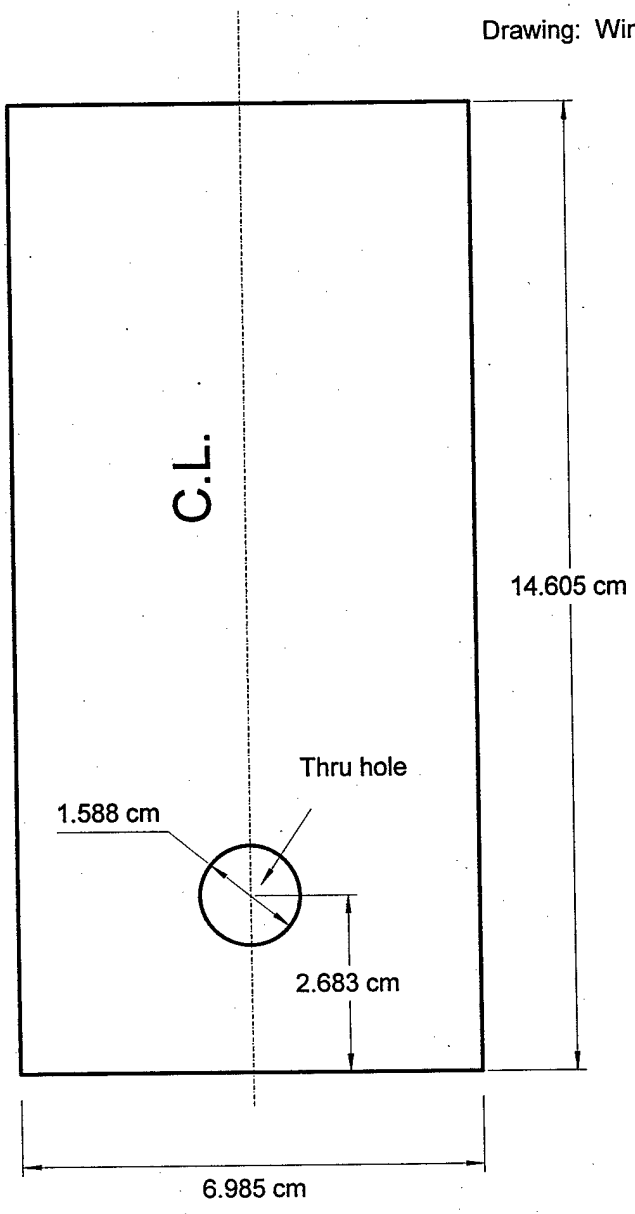

APPENDIX IX (continued)

Test section (window for drawing Wind55)
Material: Pyrex
Thickness: 0.64 cm (1/4"); 2 pieces

Drawing: Wind 61b

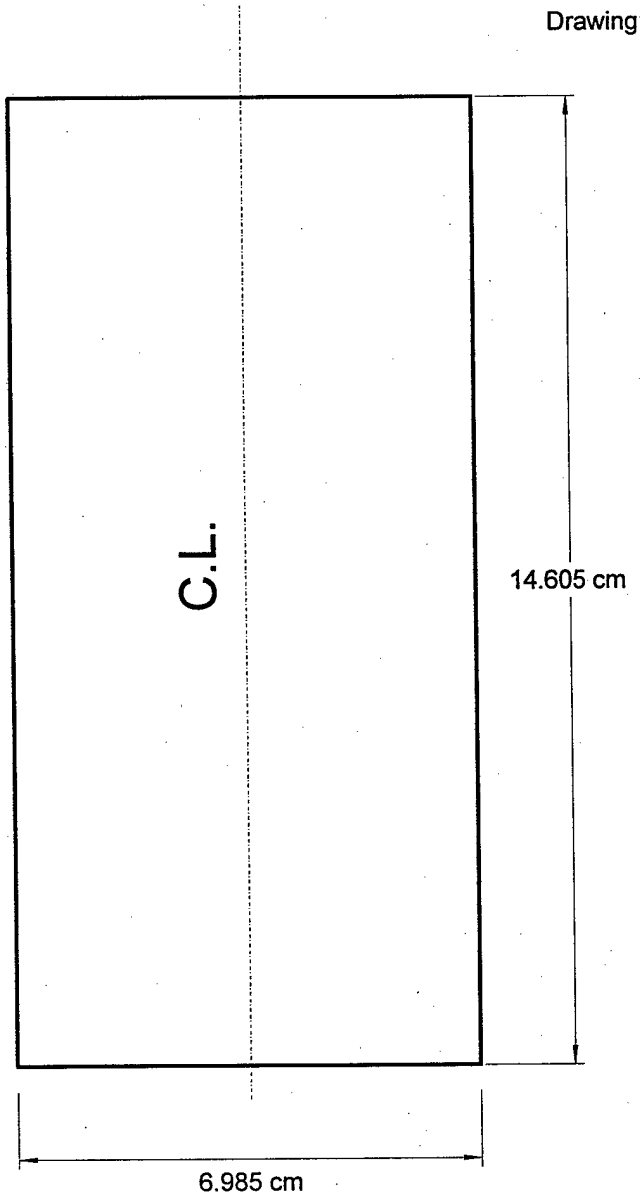

APPENDIX IX (continued)

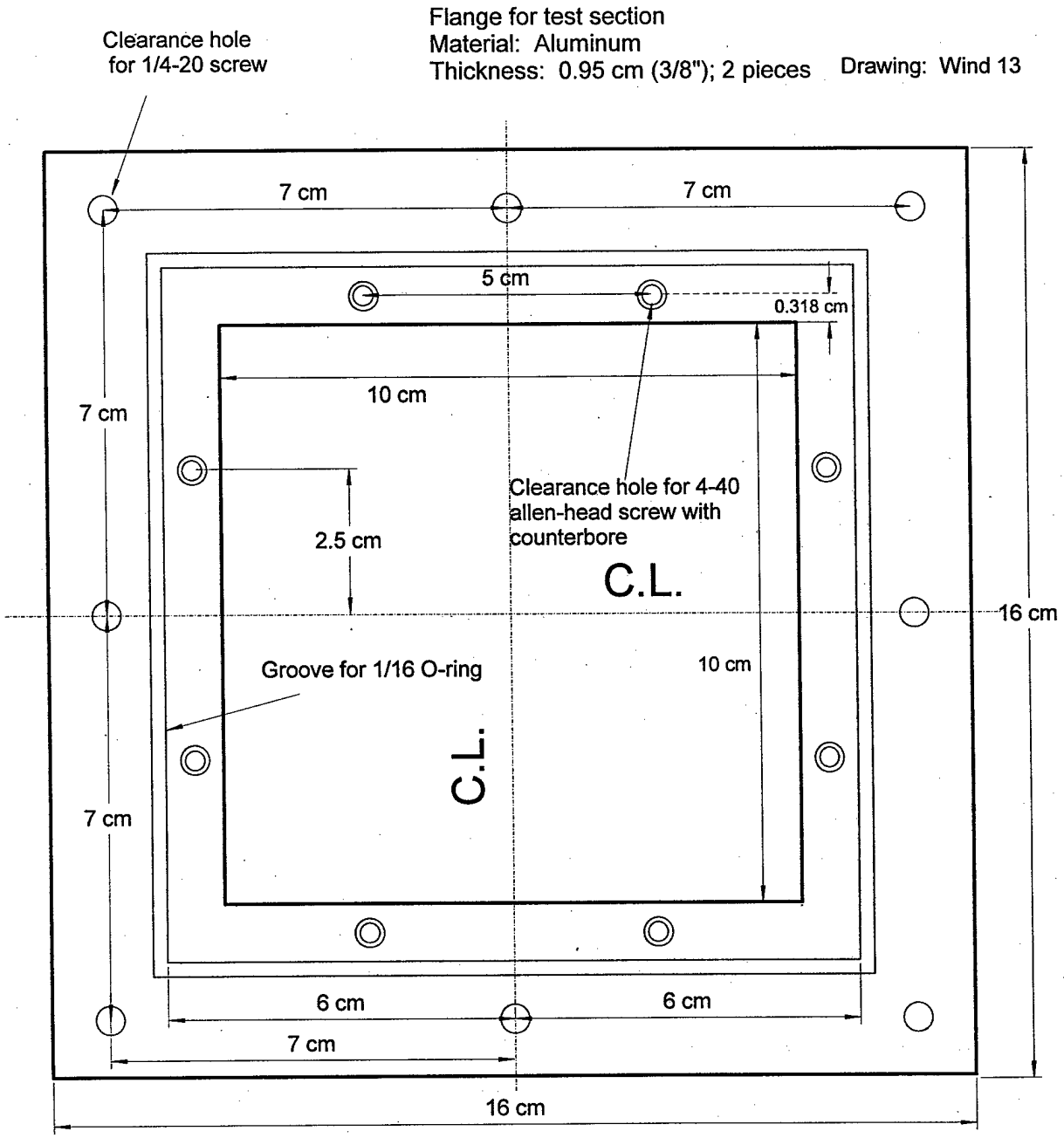

APPENDIX X

StepperBASIC™ program listing

```
10 RUN.SPEED = 800
20 PRINT "TRAVEL DIRECTION? (U)P OR (D)OWN"
25 INT1 =0
30 WHILE INT1 = 0
40 INT1 = INKEY()
50 WEND
60 IF INT1 = 85  THEN 70 ELSE 80
70 DIR = 0
75 GOTO 90
80 DIR = 1
90 PRINT "TRAVEL DISTANCE? (mm)"
100 INPUT INT1
140 INT2 = INT1*12500/2.54
145 IF DIR = 0 THEN 150 ELSE 155
150 INDEX.DIST = INT2
153 GOTO 160
155 INDEX.DIST = -INT2
160 PRINT "(G)O OR (S)TOP?"
170 INT4 = 0
180 WHILE INT4 = 0
190 INT4 = INKEY()
200 WEND
210 IF INT4 = 71 THEN 310 ELSE 350
310 GO.INCR
320 GOTO 160
350 GO.HOME
360 END
```

Note: Details of StepperBASIC can be found in the StepperBASIC Programming Reference Manual (MA6445-SW, Pacific Scientific, Motion Technology Division).

APPENDIX XI

Drawings of the burner assembly

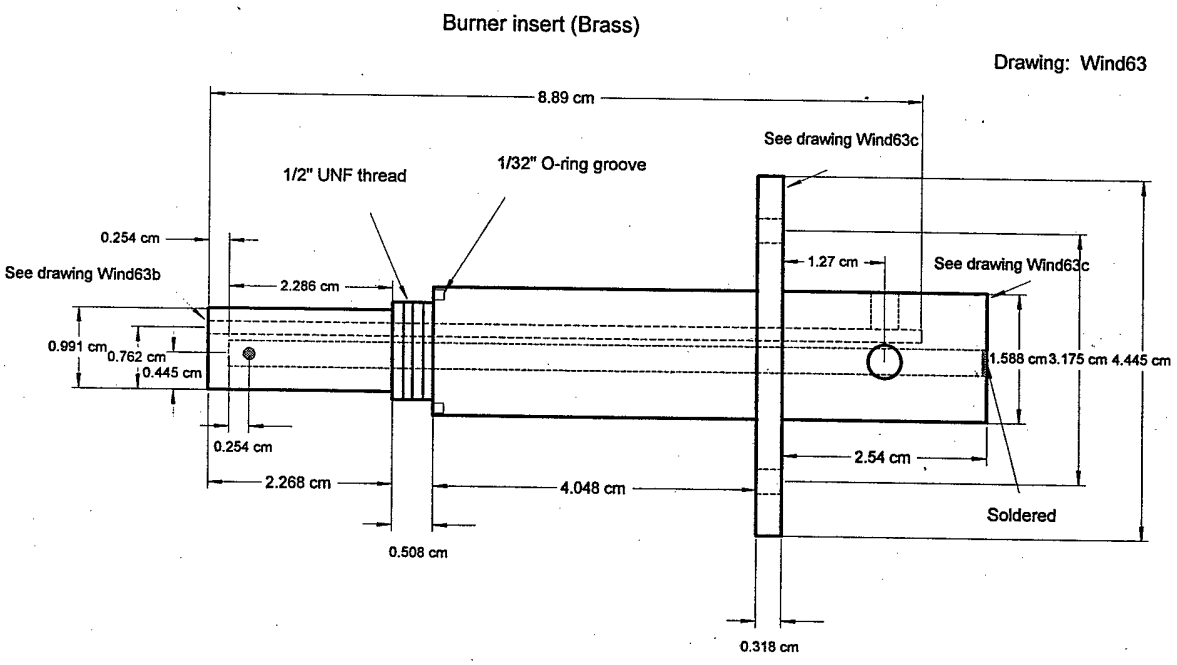

APPENDIX XI (continued)

Burner insert (Brass)

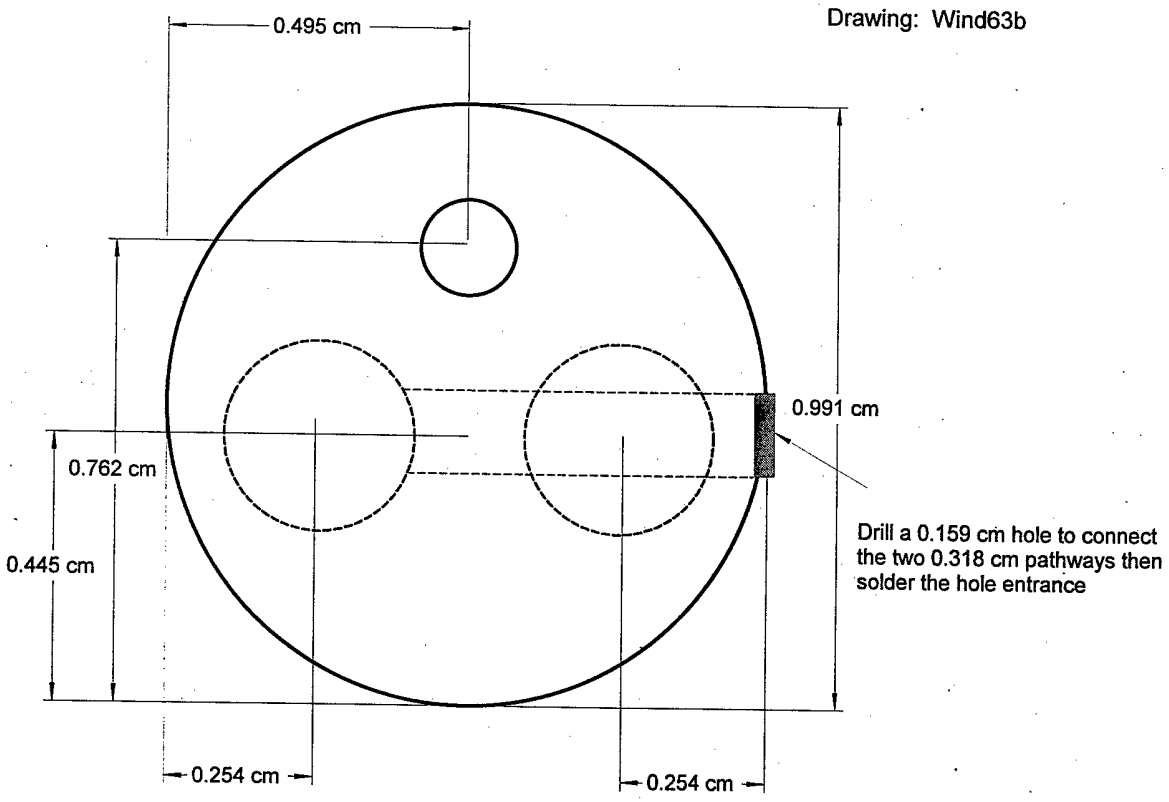

APPENDIX XI (continued)

Burner insert (Brass)

Drawing: Wind63c

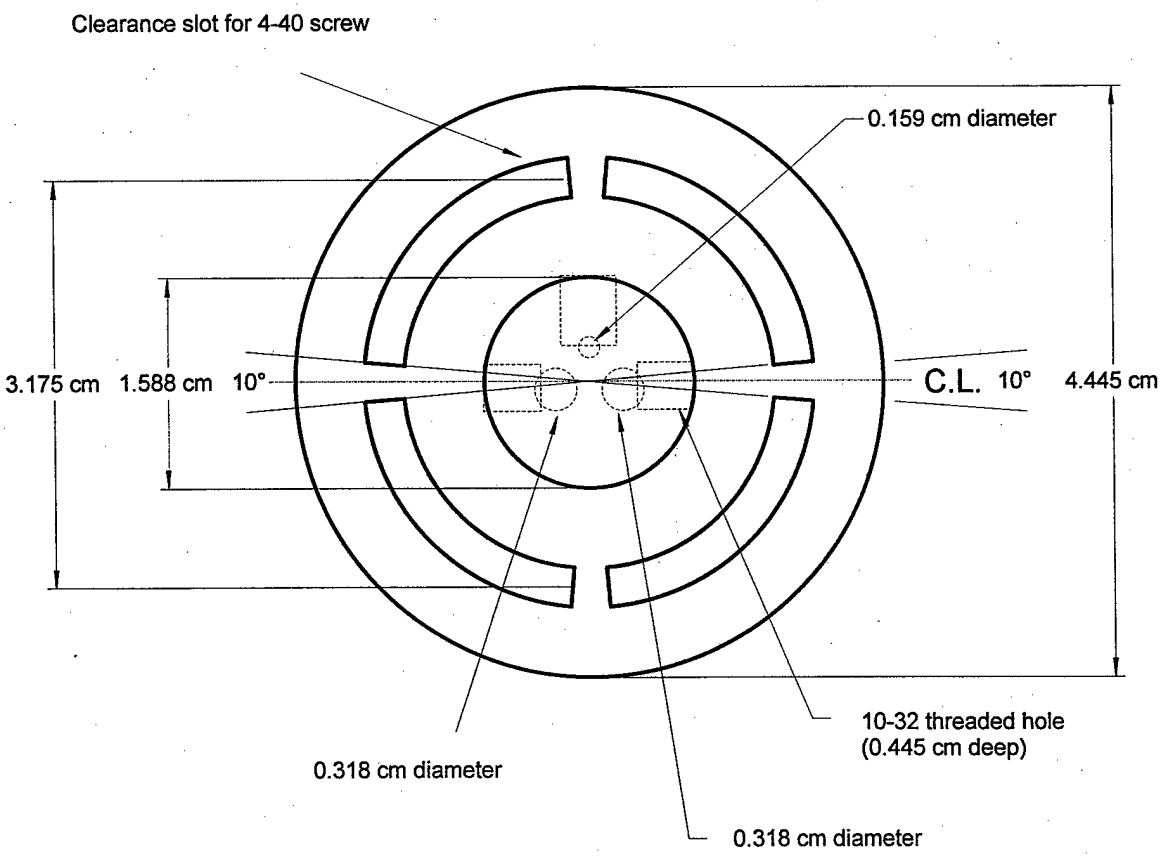

APPENDIX XI (continued)

Cylindrical extension
Material: Brass

Drawing: Wind 50

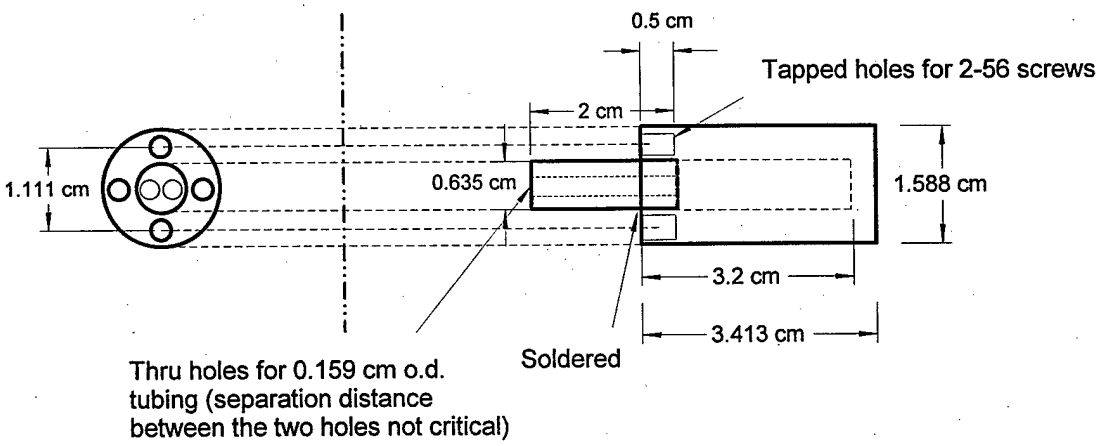

APPENDIX XI (continued)

For mounting of the cylindrical extension to the Pyrex window
Material: Aluminum
Thickness: 0.635 cm

Drawing: Wind 58

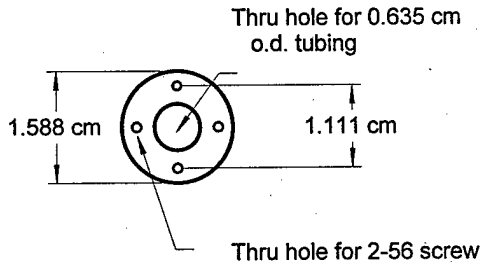

APPENDIX XII

Drawings of piezoelectric droplet generator

Orifice plate
Material: SS 303

Drawing: Drop 19

1 of 4

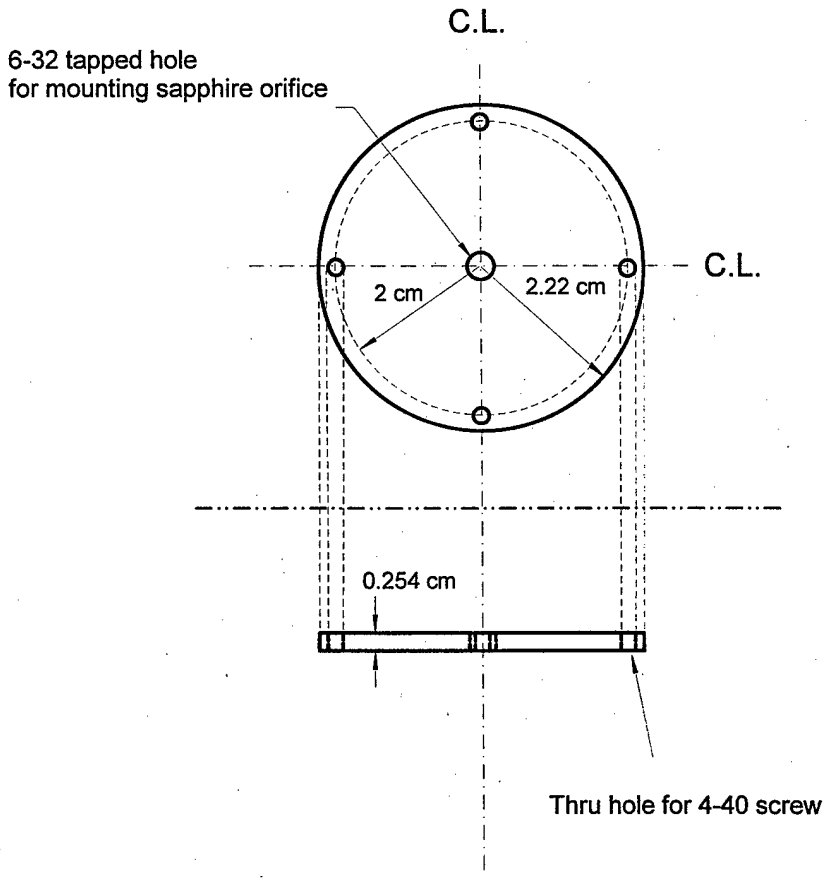

APPENDIX XII (continued)

Droplet generator body
Material: SS 303

Drawing: Drop 16

2 of 4

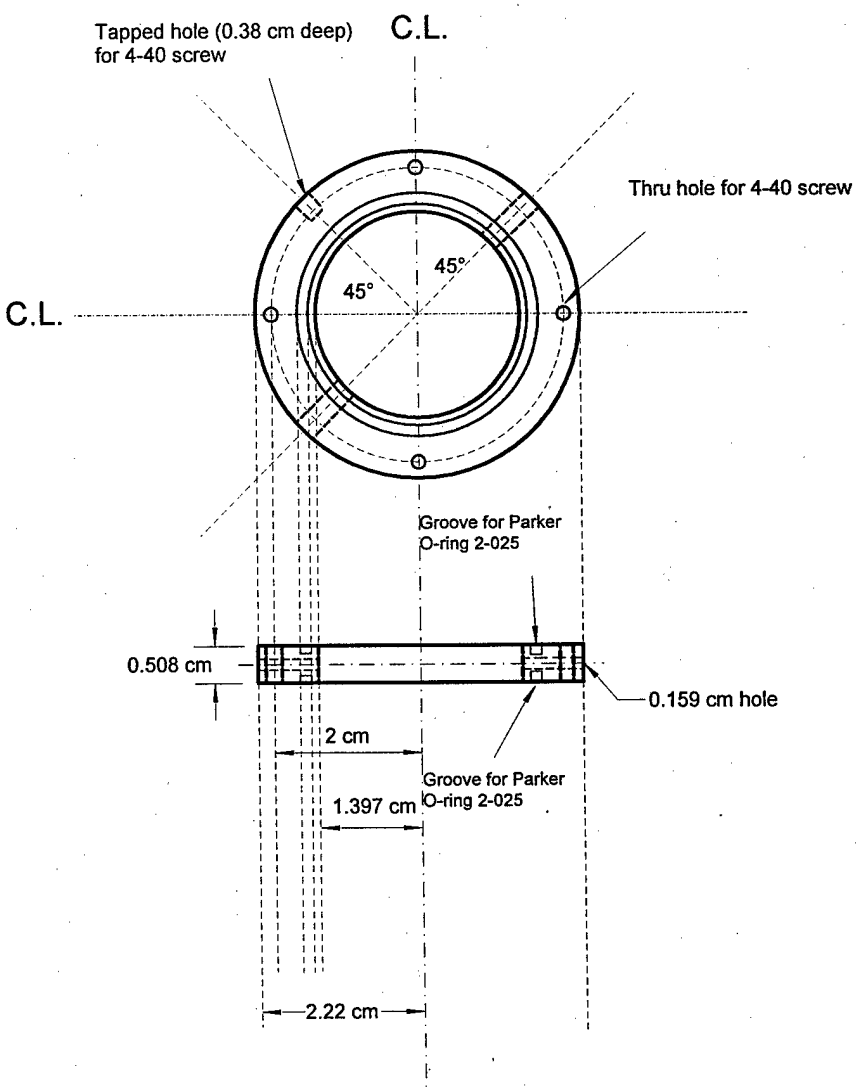

3 of 4

Drawing: Drop 20

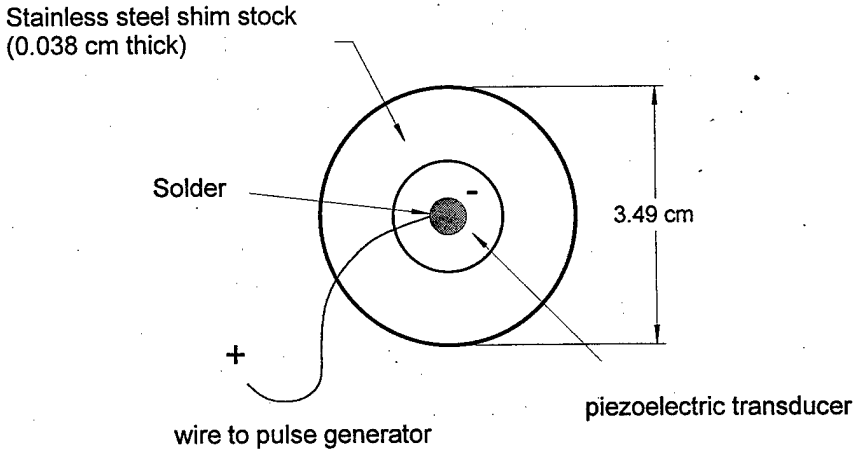

APPENDIX XII (continued)

Droplet generator flange
(for holding piezoelectric transducer)
Material: SS 303

4 of 4

Drawing: Drop 9

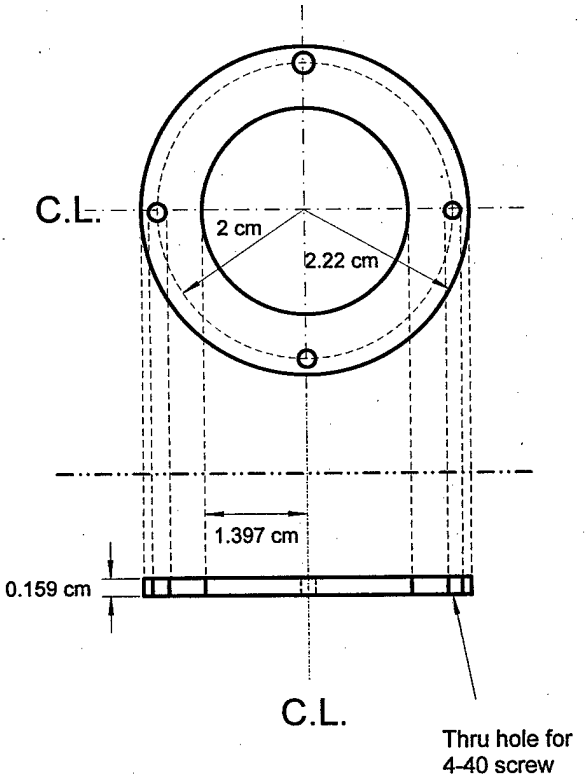

APPENDIX XIII

DIGITAL Fortran program listing for calculating droplet trajectory

The following Fortran program, which solves Equations (3) and (4), is run using DIGITAL Fortran and its IMSL libraries.

```
program fallingdrop

!this program calculates the trajectory of a liquid droplet in a convective air flow
!m dV/dt = 3*pi*muc*D*f*(U - V) + m*G - rhoc*G*Vd
!f = 1 + 0.15*Rer**0.687 + 0.0175/(1 + 4.25e+4*Rer**-1.16)

use numerical_libraries
implicit none

integer mxparm, n
parameter (mxparm=50, n=2)

integer ido, nout
real istep, param(mxparm), t, tend, tol, v(n)

external dropfn

real rhoc, muc, uair, vinit, dia, rhod, tmax
common /vars/rhoc, muc, uair, vinit, dia, rhod

rhoc = 1.00                                   !density of air (kg/m3)
muc = 0.000017                                !viscosity of air (N s/m2)
rhod = 1000.00                                !density of water (kg/m3)

call UMACH (2,nout)

open(2, file = 'c:\program\dropdata.dat')
print *, "What is the velocity of the air (m/s)?"
read *, uair

print *, "What is the initial droplet velocity (m/s)?"
read *, vinit

print *, "What is the diameter of the droplet (m)?"
read *, dia
```

```
print *, "How long (s)?"
read *, tmax

t = 0.0
! set initial conditions
v(1) = vinit
v(2) = 0.0

tol = 0.0005

call SSET(mxparm, 0.0, param, 1)

param(4) = 10000
param(10) = 1.0

ido = 1
istep = 0

write (2, *) istep, v          !print initial conditions

10 continue
 istep = istep + 0.001
 tend = istep

 call IVPRK(ido,n,dropfn,t,tend,tol,param,v)
   print *, "t = ", tend, " vel = ", v(1), "    dist = ", v(2)
   write (2,*) tend, v
if (v(2) .GT. 0.375) then
 goto 20
end if

t = tend
 if (istep .le. tmax) then
   if (istep .eq. tmax) ido = 3
   goto 10
 end if

20 continue
 end program fallingdrop

subroutine dropfn(n,t,v,vprime)

integer n
real t,v(n),vprime(n)
real reyn, f, mass, velair
```

```
real uair, rhod, rhoc, muc, dia
common /vars/rhoc, muc, uair, vinit, dia, rhod

mass = rhod*3.1415926*4*((dia/2.0)**3.0)/3.0
velair = findvel(v(2),uair)
reyn = rhoc*dia*abs(velair-v(1))/muc          !Reynolds number

f = 1.0 + 0.15*(reyn**0.687) + (0.0175/(1.0+42500.0*(reyn**-1.16)))

vprime(1) = (3.0*3.141593*muc*dia*f*(velair-v(1))-9.81*mass+rhoc*9.81*mass/rhod)/mass

vprime(2) = v(1)

return
end subroutine dropfn

real function findvel(dist,uair)
real uair,dist

if (dist .LE. 0.075) then
 findvel = uair
else
 findvel = uair*.09/((0.30-(19.0/30.0)*(dist-0.075))**2.0)
end if

end function findvel
```

APPENDIX XIV

List of vendors for the components used in the apparatus

Wind tunnel

Cincinnati Fan
Pressure blower Model PB-9
Slide gate damper, Model FG-5

LEESON Electric Corporation,
2 HP, 1750 rpm, TEFC, 56 C Frame Motor, 208-230/460/3/60, Model 101780
Micro Series Inverter Drive, Model 174931

Pacific Scientific
Stepper Motor, Model E22NC-LTLNN-NS50
Microstepping Indexer/Drive, Model MA6445-001-K-N

JOYCE/DAYTON
Worm-gear screw jacks, Model WJ-1000-6UPT1KFTN

S.S. White Technologies, Inc.
Flexible connector shafts, Model #187SMX15.00EE

80/20, Inc.
T-slotted aluminum structural extrusions, Part No. 1010
2-hole Slotted Corner Brackets, Part No. 4265

F.P. Smith Wire Cloth Co.
50-mesh center-to-center stainless steel screen with 30.3 % open area and wire diameter of 0.23 mm

Loctite Corporation
High temperature silicone RTV, Permatex HI-TEMP RTV

Burner

Bill Hirsch Automotive Products
High-Temperature Space Age 1800 Black Paint

MKS, Inc.
Mass-flow controller, 1359C-10000SN

Humonics
Bubble flow meter, #730

Sinter Metals-Krebsoge Filters, Inc.
Sintered cup filter, 1/2" UNF

Olympian
Flexible tip butane lighter, Gas-match-3X

Droplet Generation Device

Piezoelectric droplet generator components

American Piezo Ceramics
Piezoelectric transducer, Part. No. D-0.750-0.040-850

Hewlett Packard
Pulse generator, Model HP 8114A

Brockton Jewel Bearing Co., Inc.
Sapphire orifices

O'Keefe Controls Co.
Precision sapphire orifices

Chemtronics, Inc.
Conductive epoxy, CircuitWorks, Part No. CW2400

McMaster-Carr Supply Co.
Stainless Steel Shim Stock, Cat. No. 9011K91

Swagelok
40 ml Stainless Steel Resevoir, 30L-HDF2-40

Nebulizer components

Kent Scientific Corporation
Programmable syringe pump, GENIE

J.E. Meinhard Associates, Inc.
ICP nebulizer, HEN-170-AA

Data Acquisition and Control

Strawberry Tree
Data acquisition control board, Flash-12
WorkBench 4.0 Software